Brno University of Technology
Faculty of Mechanical Engineering
Institute of Machine and Industrial Design

Vysoké učení technické v Brně
Fakulta strojního inženýrství
Ústav konstruování

SEMI-ACTIVELY CONTROLLED SUSPENSION SYSTEM OF RAILWAY VEHICLE

SEMIAKTIVNĚ ŘÍZENÝ SYSTÉM VYPRUŽENÍ ŽELEZNIČNÍHO VOZIDLA

Ing. Filip Jeniš
Author
Autor práce

doc. Ing. Ivan Mazůrek, CSc.
Supervisor
Školitel

Dissertation Thesis
Dizertační práce

Brno 2024

ABSTRACT

It is well known that semi-actively controlled dampers can significantly improve the running behaviour of road or rail vehicles, mainly in terms of vehicle stability or passenger comfort. The effectiveness of semi-actively controlled damping is strongly dependent on the dynamic behaviour of the dampers. It means the speed at which the damper states change (time response) and the ratio between the maximum and minimum damping force (dynamic range). The dynamic behaviour of the damper is negatively influenced by the eddy currents in the piston core. In the first part, the thesis describes the material and the shape approach to eliminate these currents. Several variants of the magnetorheological (MR) valve were designed, their properties were simulated using a magnetic model, and the results were verified by measuring the magnetic properties of the manufactured cores. The dynamic behaviour of the assembled dampers was also measured. The shortest force response time is obtained when the valve's magnetic circuit is made of ferrite (iron oxide) or SMC (soft magnetic composites) due to the high electrical resistance of these materials. The highest dynamic range can be achieved by using the Vacoflux material due to its high magnetic saturation. A valve with grooves can reduce the force response time to 1/6. Attention is also paid to the dynamic behaviour of the fail-safe MR damper with a permanent magnet. The permanent magnet in the MR valve provides a permanent magnetic field in the case of a power failure. Such an MR damper has been designed and tested, and it has been found that the magnet in the damper core does not degrade the dynamic behaviour of the damper. The next part of the dissertation thesis deals with the influence of the damper force response time and dynamic force range on the effectiveness of semi-active control of the railway vehicle suspension. One new algorithm has been proposed in the thesis. A real MR damper was tested in the hardware-in-the-loop simulation to get closer to reality. It has been shown that the highest control efficiency is achieved with the force response time of 8 ms and that the response time for the force drop is more important than the response time for the force rise. The ideal dynamic range of the damper should be around 10. In the ideal case, a 34% reduction in lateral vibration was achieved. These results must be taken into account when designing MR dampers for a railway vehicle, both for high-speed and conventional vehicles currently in service.

KEYWORDS

semi-active, magnetorheological, damper, response time, dynamic range, eddy currents, fail-safe, railway vehicle, lateral vibration, comfort

ABSTRAKT

Je všeobecně známo, že semiaktivně řízené tlumiče mohou podstatně vylepšit jízdní vlastnosti silničních nebo kolejových vozidel, a to především stabilitu vozidla a komfort posádky. Efektivita semiaktivně řízeného tlumení je silně závislá na dynamických vlastnostech tlumičů. Tím je myšlena rychlost přepínání stavů tlumiče (časová odezva), a poměr mezi maximální a minimální tlumící silou (dynamický rozsah). Dynamické vlastnosti tlumiče nepříznivě ovlivňují vířivé proudy v jádru pístu. V první části dizertační práce je popsán materiálový a tvarový přístup k eliminaci těchto proudů. Bylo navrženo několik variant magnetoreologického (MR) ventilu, jejich vlastnosti byly simulovány pomocí magnetického modelu a výsledky byly ověřeny měřením magnetických vlastností vyrobených jader. Také byly naměřeny dynamické vlastnosti sestavených tlumičů. Nejkratší časové odezvy je možné dosáhnout při výrobě magnetického obvodu ventilu z feritu (oxid železa) nebo SMC (soft magnetic composites), díky jejich vysoké elektrické rezistivitě. Nejvyššího dynamického rozsahu je možné dosáhnout užitím materiálu Vacoflux, díky jeho vysoké magnetické saturaci. Drážkování ventilu dokáže časovou odezvu zkrátit na 1/6. Pozornost je věnována také dynamickým vlastnostem fail-safe MR tlumiče s permanentním magnetem. Permanentní magnet v MR ventilu zajišťuje stálé magnetické pole v případě výpadku napájení. Takový MR tlumič byl navržen a otestován přižemž se ukázalo, že přítomnost magnetu v jádru tlumiče dynamické vlastnosti tlumiče nezhorší. Další část dizertační práce se zabývá vlivem časové odezvy a dynamického rozsahu tlumiče na účinnost semiaktivního řízení odpružení železničního vozidla. Jeden nový algoritmus byl v práci navržen. Pro přiblížení realitě byl použit reálný magnetorheologický tlumič v simulaci hardware-in-the-loop. Ukázalo se, že nejvyšší účinnosti řízení je dosaženo s časovou odezvou 8 ms, a že časová odezva pro pokles síly je důležitější než časová odezva pro její nárůst. Ideální dynamický rozsah tlumiče by měl být kolem 10. V ideálním případě bylo dosaženo snížení příčných vibrací skříně o 34%. Tyto výsledky je třeba vzít v úvahu při návrhu MR tlumičů pro železniční vozidla, a to jak pro vysokorychlostní, tak pro konvenční vozidla, která jsou v současné době v provozu.

KLÍČOVÁ SLOVA

semiaktivní, magnetoreologický, tlumič, časová odezva, dynamický rozsah, vířivé proudy, fail-safe, kolejové vozidlo, příčné vibrace, komfort

BIBLIOGRAPHICAL REFERENCE

JENIŠ, Filip. *Semi-actively controlled suspension system of railway vehicle*. Brno, 2024. Available at: https://www.vut.cz/studenti/zav-prace/detail/154762. PhD thesis. Brno University of Technology, Faculty of Mechanical Engineering, Institute of Machine and Industrial Design. Supervisor doc. Ing. Ivan Mazůrek, CSc.

ACKNOWLEDGEMENT

In this place, I would like to thank the people who have supported me. First, to my supervisors doc. Ing. Ivan Mazůrek, CSc., Ing. Zbyňek Strecker, Ph.D. and doc. Ing. Michal Kubík, Ph.D., for their support and advice. Also, to colleagues from my research group, Ing. Jiří Žáček and others. I would also like to thank my colleagues from the Faculty of Transportation University Pardubice, Ing. Tomáš Michálek, Ph.D. and others for their help in the field of railway vehicles. And, of course, I can't forget to thank my family, especially my wife and children, for their support.

The article *Insight into the response time of fail-safe magnetorheological damper* published in the journal *Smart Materials and Structures* is reproduced with permission from IOP Publishing.

STATEMENT

I hereby declare that I have written the PhD thesis *Semi-actively controlled suspension system of railway vehicle* on my own according to the advice of my supervisor doc. Ing. Ivan Mazůrek, CSc., and using the sources listed in the references.

……..…

Ing. Filip Jeniš

CONTENT

1 INTRODUCTION

High-speed rail is currently developing in Europe. Compared to air transport, trains are slower, but this disadvantage is compensated by the location of the station: train stations are mainly located in city centres, while airports are located on the outskirts. Compared to road transport, rail transport achieves higher speeds and transport capacities. Environmental friendliness is also an important advantage of rail.

Currently, there are a number of new issues that need to be addressed. Safety, comfort, and economy are the main areas of increased demand. Safety is mainly related to vehicle stability. Higher speeds increase the probability of unwanted bogie oscillation, which increases the risk of derailment. At the same time, unwanted bogie oscillation reduces passenger comfort and increases wear on the running gear components and track superstructure, resulting in higher maintenance costs. The suspension system is primarily responsible for the passenger comfort. Of course, these problems affect not only high-speed trains but also conventional trains currently in service.

Conventional passive dampers are becoming unable to meet the increased demands for stability and comfort. The solution may be to use a semi-active damping system, where the damping force is adjusted based on the actual vehicle kinematic parameters. Magneto-rheological (MR) dampers are commonly used for semi-active control. Virtual simulations show that reducing railway vehicle body vibration by about 30-40% should be possible using semi-actively controlled damping.

However, the effectiveness of a semi-active control strategy depends largely on the dynamic behaviour of the MR damper. For effective control, the damper must be able to change the damping force from minimum to maximum and vice versa very quickly, and the ratio between the maximum and minimum damping force must be as large as possible. However, the vibration frequency of the rail vehicle body is quite low. Therefore, S/A control could work even with a relatively long force response time. It is necessary to find acceptable values of force response time and dynamic range for S/A controlled damping of the railway vehicle. The material and shape of the magnetic circuit of the MR valve have a great influence on the damper dynamic behaviour. It is, therefore, necessary to investigate this influence on different materials and shapes before designing MR dampers for railway vehicles.

As the MR damper is an electronically controlled component, it is necessary to ensure the safety of the vehicle in the case of damper power failure. This could be a problem because, without power, a conventional MR damper produces only minimal damping force, which could be potentially dangerous from a vehicle stability point of view. It is possible to use fail-safe MR dampers that contain a permanent magnet in the valve core that generates a permanent magnetic field. Therefore, it is necessary to investigate the effect of the permanent magnet on the dynamic behaviour of the MR damper.

2 STATE OF THE ART

2.1 Railway vehicle damping system and requirements for it

The spring and damping system of the railway vehicle provides the connection between the wheelsets, bogies and carbody and their mutual movement. In particular, it must ensure the safety of the vehicle, low wear of the track superstructure and low vibration of the carbody.

2.1.1 Brief description of railway vehicle suspension system

First of all, it is necessary to briefly describe the design of railway vehicle suspension. We can divide it into three different masses:

- wheelset (unsprung mass),
- bogie frame (primarily sprung mass),
- carbody (secondarily sprung mass).

Between these masses, there are two levels of springs and dampers:

- primary – between wheelset and bogie frame, it protects the bogie from vibration damage caused by hard wheel-rail contact,
- secondary – between the bogie frame and carbody, it benefits mainly the carbody vibration isolation and the associated passenger comfort.

Railway vehicle suspension components can move in all six degrees of freedom, but they are sprung and damped only in some directions. In other directions, the connections between the elements are rigid and are realized, for example, by silent blocks. However, it is important to note that even these bonds have certain flexibility and damping properties.

Springs are only used in the vertical direction. Coil springs are often used in primary suspension, although leaf springs can still be seen on older vehicles. Vertical secondary suspension is usually provided by adjustable air bellows or flexi-coil type coil springs, which, in addition to vertical suspension, also provide lateral and longitudinal stiffness [1], see Fig. 2-1.

The primary dampers between the wheelset and the bogie frame are used only in the vertical direction on standard railway vehicles. However, longitudinal dampers are also beginning to appear in research and literature [2–5]. The secondary dampers between the bogie frame and the carbody can be divided into vertical, lateral and yaw dampers, see Fig. 2-1.

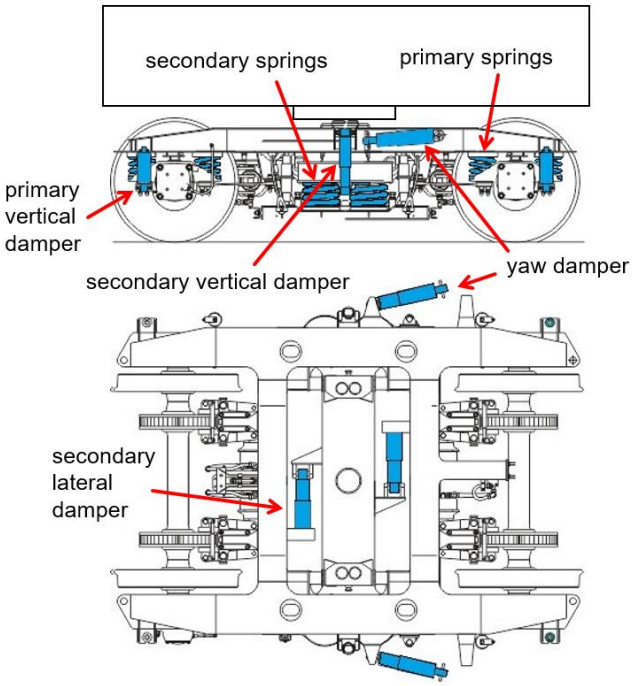

Fig. 2-1 A basic view of the springs and dampers of a railway vehicle [6]

The most commonly used dampers today are hydraulic. In the past, friction dampers were also widely used, and more recently, controlled damping systems, either active or semi-actively controlled systems, are beginning to be used.

2.1.2 Carbody vibration (comfort) requirement

At higher speeds, more vibrations are transmitted from the bogie to the carbody, both vertically and horizontally, which has a negative effect on passenger comfort. This fact places higher demands on the vehicle damping system, especially the secondary vertical and lateral dampers. Increased body vibration can also be related to poor stability of the railway vehicle, which will be discussed in the next chapter. The unstable running of the vehicle leads to increased vibrations in the body. Too high comfort requirements may not be solved by conventional passive dampers, because passive damper settings are always about a some compromise. In the literature, the problem is solved by replacing passive dampers with semi-actively controlled dampers [7–13], which will be discussed below. This problem is also relevant to today's inferior railways.

2.1.3 High safety requirement

The main factor affecting the safety of a vehicle is its stability. The main influence on vehicle stability is the unwanted wheelset oscillation that occurs when the critical speed is exceeded [14, 15]. This phenomenon, called Hunting oscillation, is caused by the wheel conicity [14].

Conical wheels allow the wheelset to negotiate curves. The outer wheel reaches a larger rolling radius in the curve; therefore, it begins to move faster than the other wheel and begins to rotate the wheelset around the vertical axis, which allow a smooth negotiation curve. It also creates a typical sinusoidal motion of the wheelset (see Fig. 2-2). The phenomenon of this kinematic motion was already described mathematically in 1883 by Klingel [16].

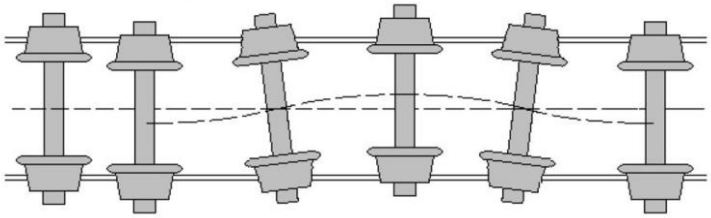

Fig. 2-2 Wheelset oscillation [14]

On a small scale, this movement is normal and unavoidable. At low speeds, the lateral and angular deviations reach small values; therefore, the oscillation of the wheels does not cause any problems. However, when the critical speed is exceeded, the lateral displacement of wheelsets begins to increase rapidly, and the amplitude of its oscillation stabilizes at a value corresponding to the clearance of the wheelset between the rails. At the same time, there is a significant increase in the lateral forces of the wheels on the rails, which is associated with greater damage to the rails, wear of bogie components, a higher risk of derailment and a reduction in running comfort due to vibrations. Unwanted oscillation quickly stops when the speed is reduced below the critical value as illustrated Fig. 2-3. The maximum allowable speed of the vehicle must be 10% below its critical speed to ensure safe running.

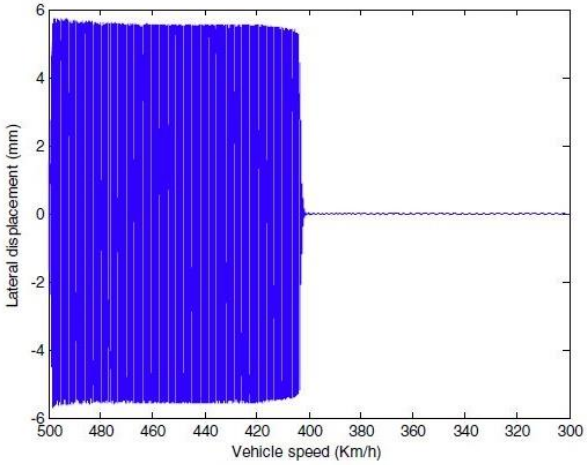

Fig. 2-3 Dependence of the wheelset lateral displacement on the vehicle speed. [15]

There are two different approaches to reducing unwanted wheelset oscillation:

- control the movement of the wheelset using the primary suspension [2–5, 17–19]
- control the movement of the bogie using the secondary suspension [20–25]

2.1.4 Low wear requirement

One way to solve the problem of vehicle stability is to increase the torsional stiffness between the bogie and the carbody, but this leads to another problem: increased stiffness makes it difficult to turn the bogie into a curve. If there is not a transition curve between the straight track and the curve with a small radius, there will be large forces between the wheel and the rail when entering the curve, which will cause the rails to wear out, see Fig. 2-4 [1]. A typical problem example is an S-curve with a switch. Track wear has a major impact on maintenance costs. Higher fees are charged in Western Europe for trains, which causes more wear of track [26].

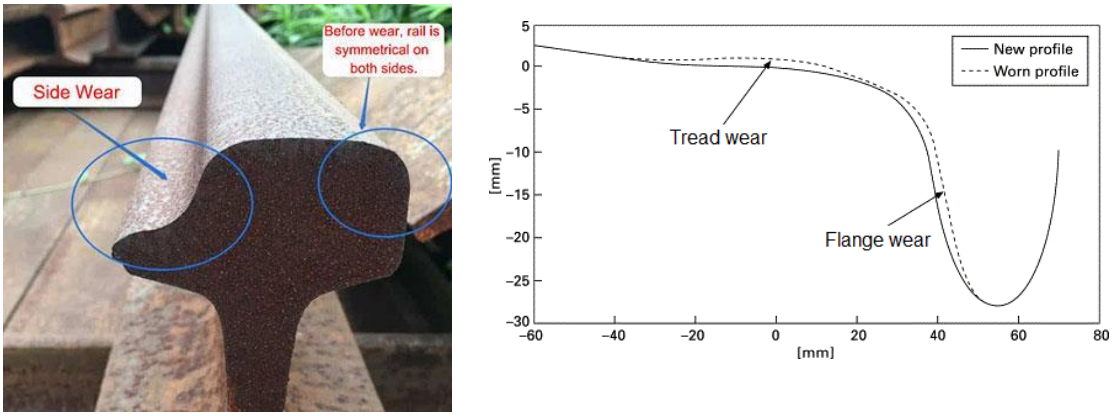

Fig. 2-4 Worn rail [27] (left), worn wheel [28] (right)

The same two approaches as in the previous case lead to a reduction in wheel-rail contact wear:

- control the movement of the wheelset using the primary suspension [2–5, 17–19]
- control the movement of the bogie using the secondary suspension [20–25]

2.2 Advanced damping systems

It is obvious that these increasing requirements on damping systems will be a problem to satisfy with classical passive dampers. It is necessary to look for an alternative in the form of controlled damping systems, either active or semi-actively controlled systems.

2.2.1 Passively damped systems

But first, about the common passive damping systems that are most commonly used today. They contain dampers with a fixed F-v curve, and the setting of the F-v curve is always a compromise. Fig. 2-5 shows that different damping coefficients are suitable for low-vibration transmission at different excitation frequencies. A damper with high damping

prevents the sprung mass from vibrating at its natural frequency but transmits high frequency vibrations to it. Conversely, a low damping damper will not transmit high frequency vibrations to the mass, but will not be able to damp the sprung mass at its natural frequency. In practice, this contradiction means finding a compromise between safety (high damping) and comfort (low damping).

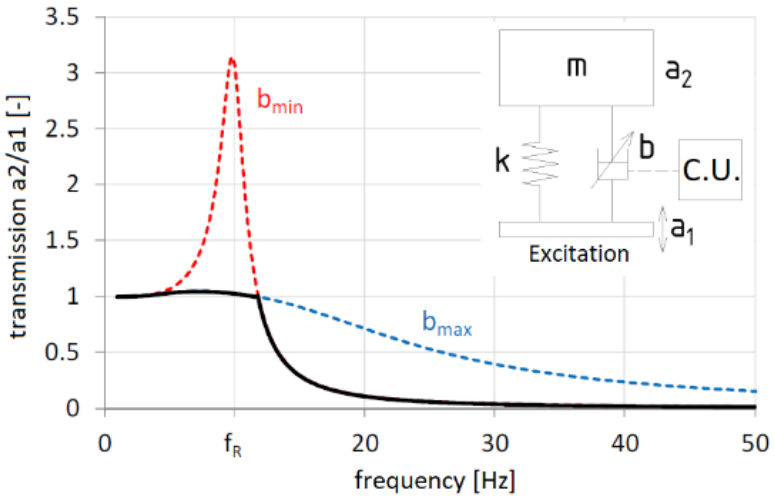

Fig. 2-5 Transfer function for differently damped systems

2.2.2 Active suspension systems

The second and most advanced systems are active systems. They contain actuators instead of springs and dampers (see Fig. 2-6). The actuator can precisely generate the force required to damp the sprung mass. However, these systems are relatively complex, expensive and energy-intensive, and they also pose difficulties in implementing a fail-safe system [29], [30].

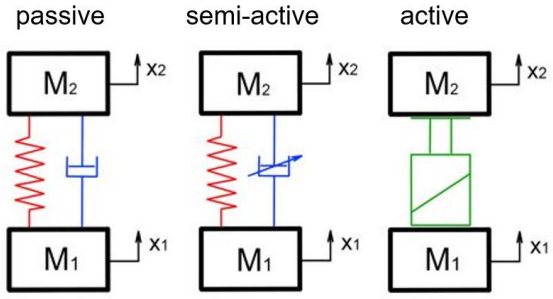

Fig. 2-6 Schemas of damping systems

2.2.3 Semi-actively controlled damping systems

The third type of damping systems are semi-actively controlled systems. They should combine the advantages of both previous types, and they would therefore be a suitable alternative to active systems. These damping systems regulate the damping force level based

on the requirements of the control unit (Fig. 2-6), even many times per second. This feature makes it possible to use the advantages of high damping to reduce vibrations at the resonant frequency and, simultaneously, the advantages of low damping to isolate vibrations at supra-resonant frequencies, see the black curve in Fig. 2-5. The most common types of semi-actively controlled dampers are CDC dampers (Continuously Damping Control) [31] and MR dampers (Magnetorheological) [32]. CDC dampers use an electromagnetically controlled valve to change its cross-section and the associated hydraulic resistance, thereby changing the damping force. MR dampers use the magnetorheological effect.

Except for railway vehicles, it is possible to use MR dampers in road vehicles [33–38], for the suspension of driver seats in trucks [39–43], for damping of vibration for seismic activity protection [44–47] or the damping of cable bridge vibrations caused by wind and rain [48, 49].

2.2.4 MR damper function

MR dampers work based on MR fluid, which is a suspension of ferromagnetic particles several micrometres in size in a carrier fluid. When the MR fluid is exposed to an external magnetic field, the ferromagnetic particles chain together in the direction of the magnetic field, rapidly increasing the apparent viscosity of the fluid.(Fig. 2-7). In an MR damper, this increase in the apparent viscosity of the MR fluid causes an increase in the hydraulic resistance of the piston and an increase in damping forces. A coil located in the core of the damper piston is used to generate the magnetic field.

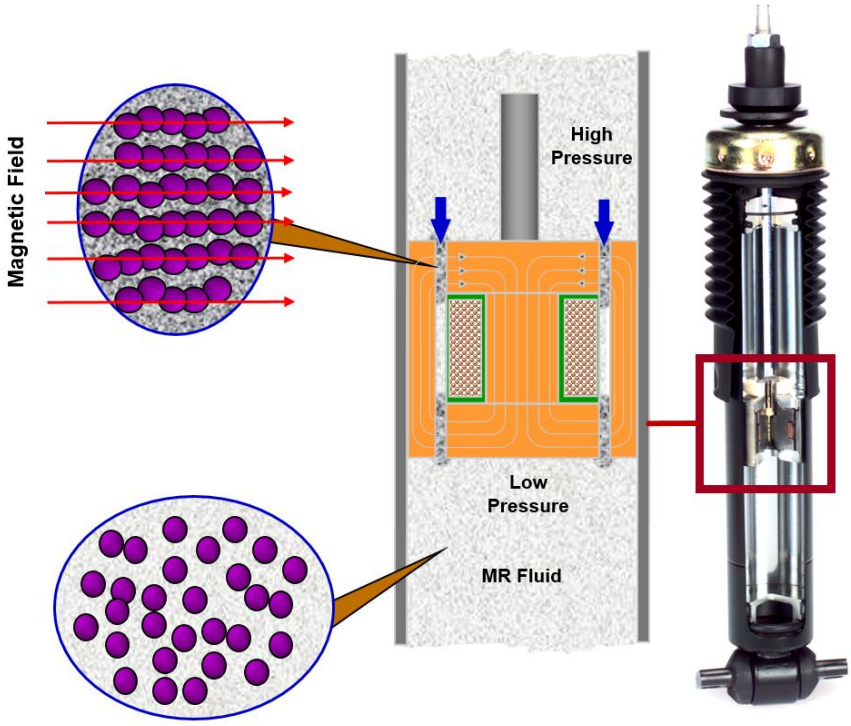

Fig. 2-7 MR damper function schema

2.2.5 Damper force response time and dynamic force range definition

The electric current in the coil controls the size of the magnetic field and the associated damping force (Fig. 2-8). The ratio between the fully activated and unactivated damping force expresses the dynamic force range of the damper. The dynamic range of the damper is not constant but depends on the damper piston velocity, see Fig. 2-9.

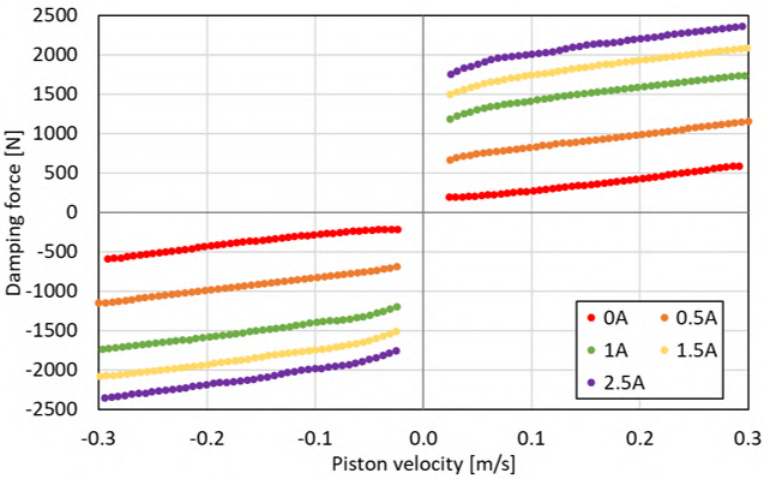

Fig. 2-8 Damper F-v curves

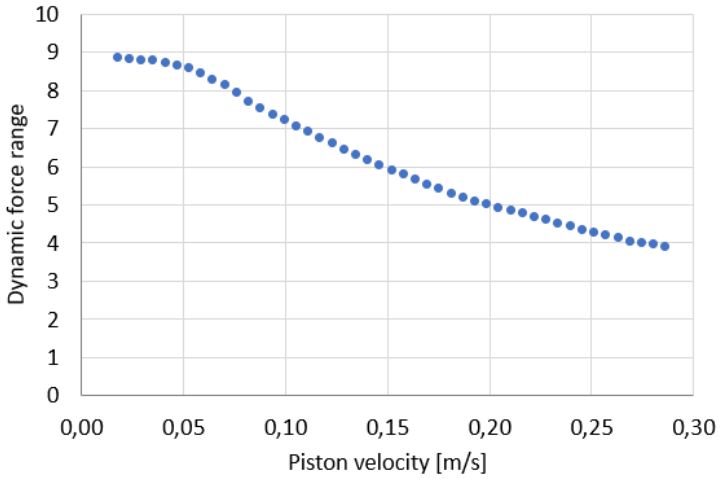

Fig. 2-9 Dependence of damper dynamic force range on piston velocity

The transient behaviour of the MR damper is usually considered as a first-order system, where the response time is defined as the time from the change in control signal for the damping force to reach 63.2% of the steady-state force value. (Fig. 2-10) [50–55].

The force in time can then be described by the equation:

$$F(v,t) = F_0(v) + \left(F_1(v) - F_0(v)\right) \cdot \left(1 - \mathrm{e}^{-\frac{t}{\tau_{63}}}\right) \qquad (1)$$

where:

$F_0(v)$ [N] force at $t = 0$, for the given velocity

$F_1(v)$ [N] desired force for the given velocity

v	[ms^{-1}]	piston velocity
t	[s]	time from the change of the control signal
τ_{63}	[s]	time constant – primary response time

Similarly, the time constant for the force drop τ_{36} is the time it takes for the force to drop back to 36.8 % of the initial force.

However, in many publications, the response time of MR damper is described as 90 % [56, 57] or 95 % [58, 59] of the steady-state force value. The 90 % criterion is often used to describe the dynamic behaviour of actuators in industrial applications [60]. The effectiveness of semi-actively controlled damping is highly dependent on the damper response time [61].

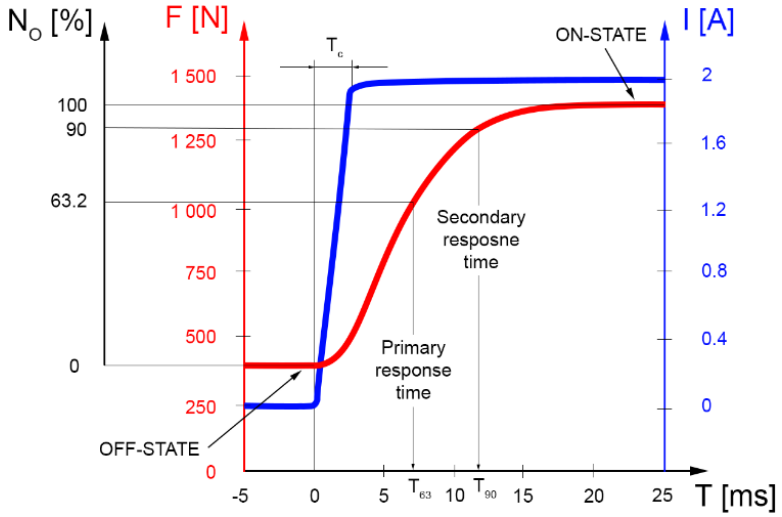

Fig. 2-10 Definition of MR damper force response time

The papers [62–64] deal with the optimal design of an MR valve using finite element analysis (FEA), but they focus only on maximizing the static magnetic field range in the valve gap and do not evaluate the response time of the damper force. Papers [65, 66] show that damper force response time is essential for the performance of semi-actively controlled damping systems. The shorter the response time, the better the S/A control performance. The paper [58] shows that the time response is also dependent on the piston velocity, the magnitude of the electric current change, the stiffness of the damper mounting and the control electronics. The response time is negatively affected by the formation of eddy currents in the piston core [59, 67]. Response time also depends on the dwell time of Fe particles in the active magnetic zone and the concentration of Fe particles in the carrier fluid [58]. Paper [8] shows that the force response time differs for force rise and drop. The damper dynamic range (the ratio of the damping force in the activated and non-activated state) is also essential for the efficiency of the S/A control [68]. The damper dynamic force range is influenced by the magnetic properties of the material used, mainly by the magnetic saturation, then the shape of the magnetic circuit and the width of the gap in the piston [55, 59].

2.3 Approaches to reducing carbody vibration

2.3.1 Semi-active control of secondary lateral damper

Passenger comfort, which becomes more important as the speed of railway vehicles increases, can be ensured by semi-actively controlled lateral secondary dampers.

Lau et al. [9] studied the effect of the lateral secondary damper on ride comfort. They used an MR damper with a maximum damping force of 12 kN and a dynamic force range of 6. The semi-active algorithm is very simple, switching between Low and High modes according to the lateral velocity of the body. The damper switches to High mode when the body exceeds the critical velocity. The simulations were performed on a complex dynamic railway vehicle model with two bogies. Semi-active control of dampers reduces lateral body vibration by up to 39% compared to passive damping, see Fig. 2-11.

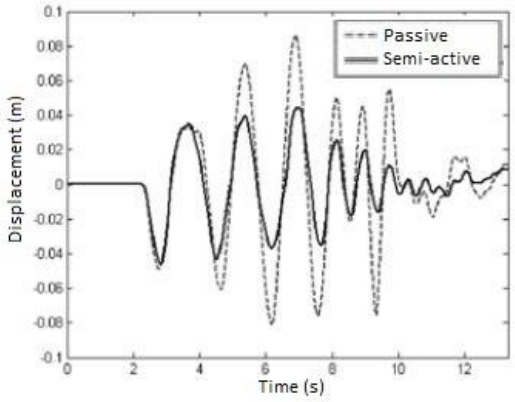

Fig. 2-11 Lateral displacement of railway carbody for Passive and Semi-active mode [9]

Spelta, Codeca et al. [7, 8] experimentally tested the effect of a semi-actively controlled lateral secondary damper on the body vibration on a realistic laboratory stand Fig. 2-21. They used ISOCOMP electro-hydraulic dampers specially designed for this application. These dampers have a maximal damping force of 6000 N (piston velocity of 0.08 ms^{-1}), with a dynamic range of about 10, and a response time of 100 ms for damper activation and 30 ms for damper deactivation. The stand was excited by a signal reproducing a real measurement on the track at high speed. The best results were achieved by combination of the Skyhook and Acceleration Driven Damping algorithms – MIX-SH-ADD, reducing vibrations by 34 % compared to a passive damper, see Fig. 2-12.

Hudha et al. [13] introduced two types of Skyhook algorithm: the body-based and bogie-based Skyhook:

$$C_{body} = \begin{cases} C_{body,max} & if \quad V_{body} \cdot V_{rel} \geq 0 \\ C_{body,min} & if \quad V_{body} \cdot V_{rel} < 0 \end{cases} \tag{2}$$

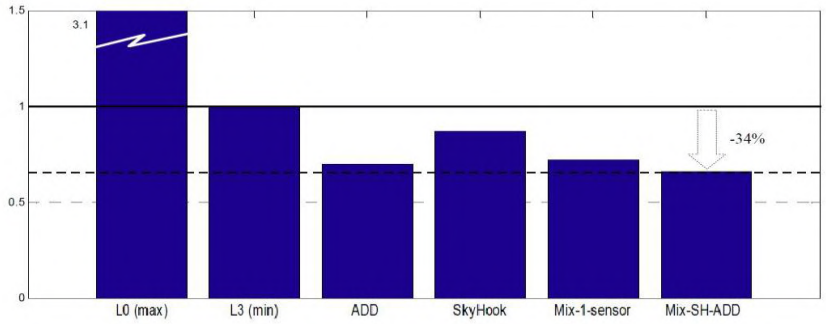

Fig. 2-12 Comparison of the semi-active strategies' effect on the car body lateral movement [7]

$$C_{bogie} = \begin{cases} C_{bogie,max} & if \quad V_{bogie} \cdot V_{rel} \geq 0 \\ C_{bogie,min} & if \quad V_{bogie} \cdot V_{rel} < 0 \end{cases} \tag{3}$$

where:

C_{body}	[Nsm^{-1}]	damping coefficient for body-based Skyhook
C_{bogie}	[Nsm^{-1}]	damping coefficient for bogie-based Skyhook
V_{body}	[ms^{-1}]	carbody lateral velocity
V_{bogie}	[ms^{-1}]	bogie lateral velocity
V_{rel}	[ms^{-1}]	relative velocity between body and bogie

These algorithms controlled the lateral secondary MR dampers. The simulations were performed on a vehicle model with 17 degrees of freedom. Three criteria were evaluated: lateral deviation, yaw, and rolling motion of the carbody. Both algorithms performed well and improved all three criteria, see Fig. 2-13.

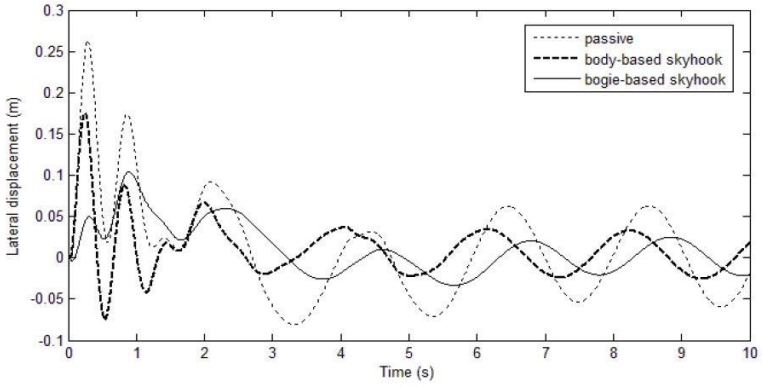

Fig. 2-13 Lateral displacements of the railway carbody for passive mode, body-based and bogie-based Skyhook [13]

Shin et al. [10, 11] also dealt with the simulation and experimental verification of the effect of semi-active control of the secondary lateral damper. A half-vehicle model with 9 degrees of freedom was used for the simulation. A 1:5 scale model was used for experimental verification (Fig. 2-22). For this purpose, the author developed a small damper with a maximum force of 150 N (0.04 ms^{-1}) but with a dynamic force range of 20 (Fig. 2-25). The Skyhook algorithm was used for control. In the simulation, vibrations were reduced by

77% compared to passive damping, when the model was excited at a frequency of 4 Hz. In the experiment, it was 67 %. See Fig. 2-14.

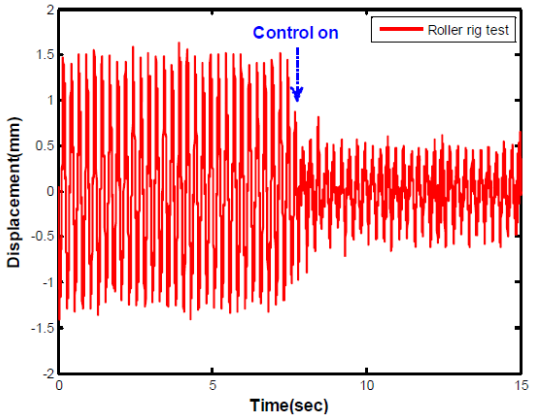

Fig. 2-14 Effect of Skyhook algorithm on the lateral displacement of 1:5 scale roller rig tester [12]

2.3.2 Simulation approaches

Virtual simulation

Different dynamic models could be used to verify the function of damper semi-active control on railway vehicle – different levels of simplification. Models from one to several tens of degrees of freedom are used. Simple verification of semi-active control can be performed on a simple dynamic model with one or two degrees of freedom (Fig. 2-15 – left).

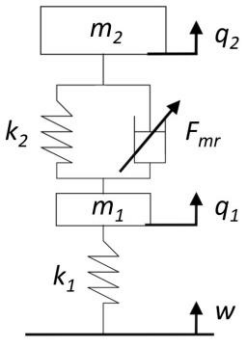

Fig. 2-15 Simple dynamic model of two degrees of freedom

However, if it is necessary to simulate the advanced motion of a railway vehicle, hunting motion, for example, is necessary to simulate more degrees of freedom. Lee et al. [69] used a bogie dynamic model with 10 degrees of freedom, which means lateral displacement y_i, the vertical displacement z_i, the roll angle φ_i, and the yaw angle ψ_i of wheelsets and lateral displacement y_t and the yaw angle ψ_t of bogie frame. Wei et al. [3] used a dynamic model of a whole vehicle with 17 degrees of freedom. It means lateral displacement y and yaw angle ψ of all wheelsets, both bogie and carbody and a roll angle θ of both bogie frame and carbody (Fig. 2-16). This model neglects the vertical movements of all masses.

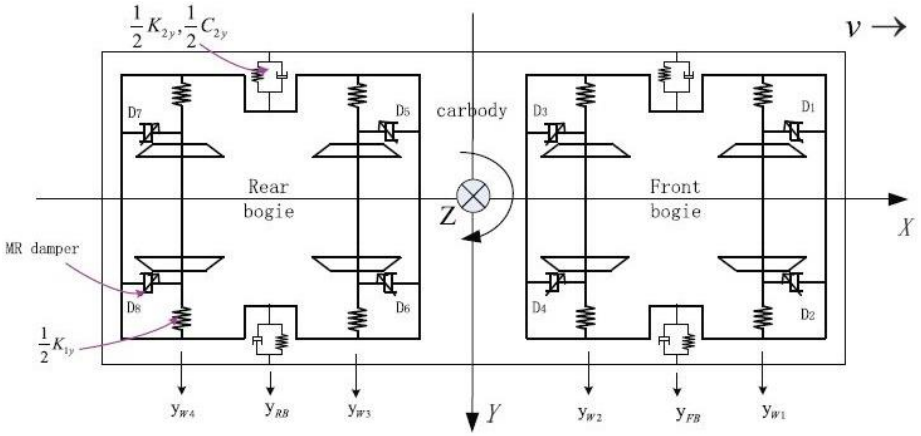

Fig. 2-16 Top view of bogie dynamic model with 17 degrees of freedom [3]

Michálek et al. [1] used a complex railway vehicle model with 58 degrees of freedom. The model consists of 15 rigid bodies: 4 wheelsets, 8 axle boxes, 2 bogie frames, and the carbody (Fig. 2-17)

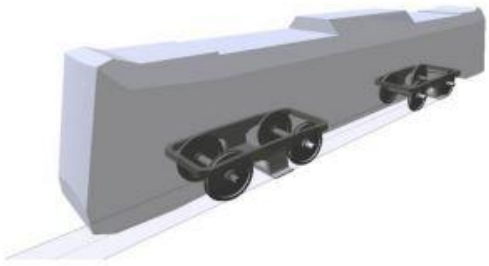

Fig. 2-17 Visualisation of SJKV model of 58 degrees of freedom [70]

The dynamic model must be described using differential equations and programmed in Matlab/Simulink, Python or other software. Or it is possible to use more advanced software such as Vampire [9], Adams (Fig. 2-18) [71] or others, in which a vehicle model can be created without knowledge of the relevant equations of motion.

Fig. 2-18 Railway vehicle model in Adams software [71]

Hardware-in-the-loop simulation

The MR dampers exhibit highly non-linear behaviour, which is very difficult to model properly. It is necessary to include hysteresis (magnetic, hydraulic, etc.), temperature dependence, etc., in the model. The MR damper models used in simulations are always simplified and often do not correspond to the force generated by the real MR damper for given operating conditions, which degrades the results of simulations of semi-active suspension. It is difficult to say how significant this degradation is.

To avoid this problem, many teams use an advanced simulation approach called Harware-in-the-loop simulation (HILS). With HILS, replacing one or more virtual elements with real ones is possible. In the case of semi-active or active damping, a damping element is usually replaced. The damper is mounted on a pulsator (Fig. 2-19) whose position is controlled in real time by a virtual model running on an appropriate platform. The damping force of the real damper excited by the pulsator is measured, and it serves as an input signal for the dynamic model to calculate the next step (Fig. 2-20).

Choi et al. [41] used HILS to design a semi-active control seat for a truck vehicle (Fig. 2-20). Lee et al. [72] used it to study the S/A control of a car suspension. Misselhorn et al. [73] successfully tested HILS usability in suspension design, comparing HILS with a virtual simulation on a single corner model and a simplified physical model of motorcycle suspension. Kwak et al. [74] used HILS to verify the benefit of the Skyhook algorithm for the lateral movement of the railway vehicle body (Fig. 2-19). Oh et al. [75] studied the active control of tramcars independently rotating wheels in HILS.

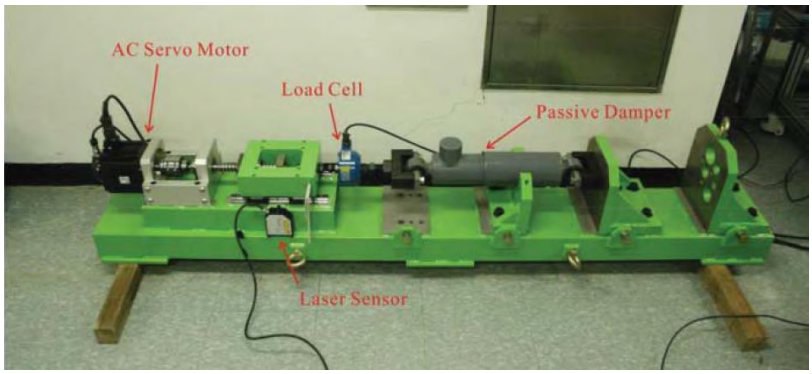

Fig. 2-19 Damper mounted on pulsator for the Hardware-in-the-loop simulation [74]

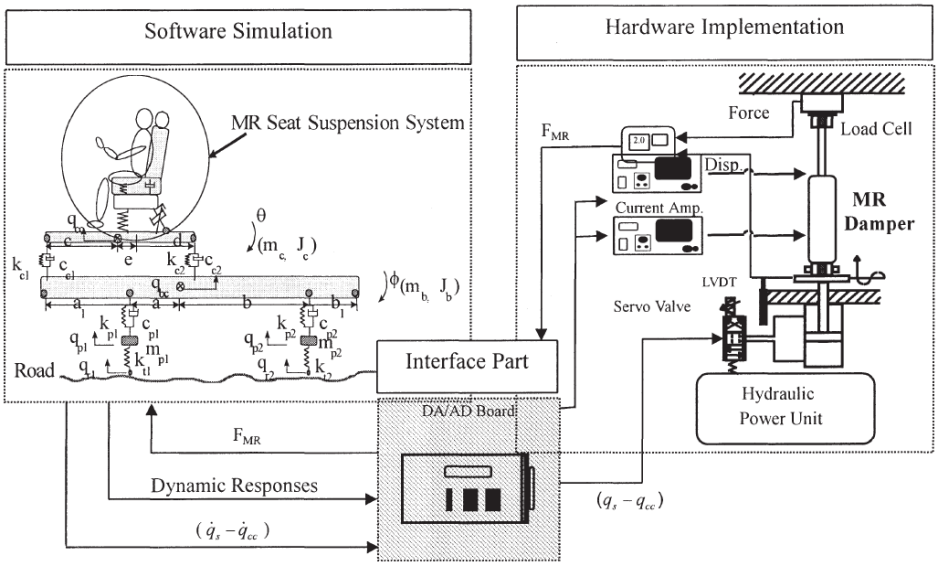

Fig. 2-20 Hardware-in-the-loop schema [41]

Test-bench experiment

A more advanced approach to simulation is an experiment on some test-bench representing railway vehicles. It is usually impossible to have a full-scale physical model, so the test-bench must be simplified and reduced in size. Compared to a purely virtual simulation, the real model is simpler, but it contains effects of the real environment that are difficult or impossible to model in the simulation.

Codeca et al. [7] used a test bench to reproduce the lateral dynamics of a railway vehicle (Fig. 2-21). It represents the lateral inertia of the carbody of the train. This mass can move horizontally with 1 degree of freedom. This mass is connected to a force actuator and a suspension system. The suspension consists of a gas spring and a semi-active damper. The stand was excited by a signal that reproduced real measurements on the track at high speed.

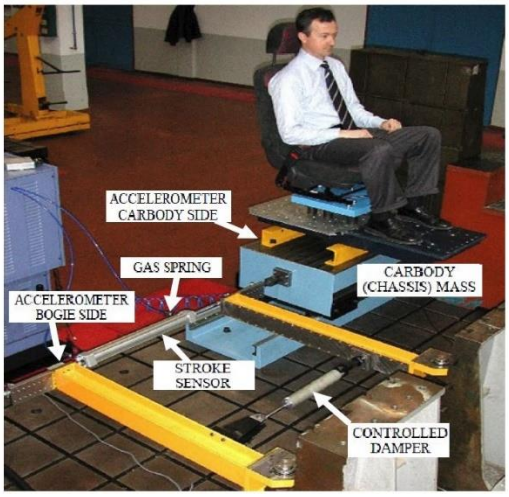

Fig. 2-21 Test-bench of carbody lateral movement [7]

Shin et al. [12] used a 1/5 scaled railway vehicle on a roller rig (Fig. 2-22). The vehicle consists of a wheelset, bogie, half of the body, suspension and centre pivot. The secondary suspension was implemented using ball rollers and coil springs to separate dynamic characteristics of lateral and vertical directions, and the MR damper was mounted between the bogie and the carbody. The model was used to simulate lateral movement of the carbody when S/A control is used.

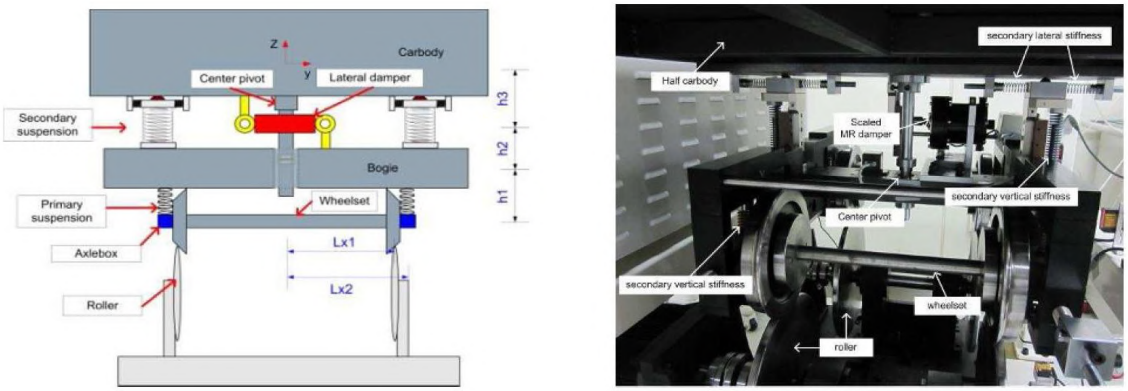

Fig. 2-22 Railway vehicle model in 1/5 scale [12]

Hudha et al. [13] have a small-scale 17 DoF railway vehicle test rig for experimental testing of the Skyhook controller. This rig simulates track irregularities using two linear motor units mounted on the front and rear bogies.

2.4 Approaches to improve MR valve behaviour

2.4.1 Examples of MR dampers

This chapter describes the parameters of the MR dampers used in the above and some other researches. Some researchers use commercially available MR dampers, such as those from Delphi Company (BWI Group) or any parts of them.

MR damper with piston group from Delphi MR damper [61] have a maximal force of 1 200 N (piston velocity of 0.6 ms^{-1}) and dynamic force range of approximately 9, see Fig. 2-23, and response time of 19-22 ms on standard voltage mode and 8-10 ms using current control mode.

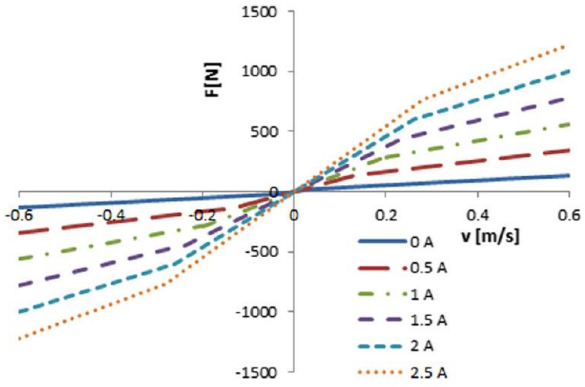

Fig. 2-23 F-v curves of Delphi MR damper

Lee et al. [72] used an MR damper with a maximal force of 2 200 N and a small dynamic range of 4 (piston velocity of 0.3 ms^{-1}). See Fig. 2-24 (left). This damper has a special design. It does not use a gap in the damper piston as is common with other dampers but has a special gap in the outer cylinder, see Fig. 2-24 (right).

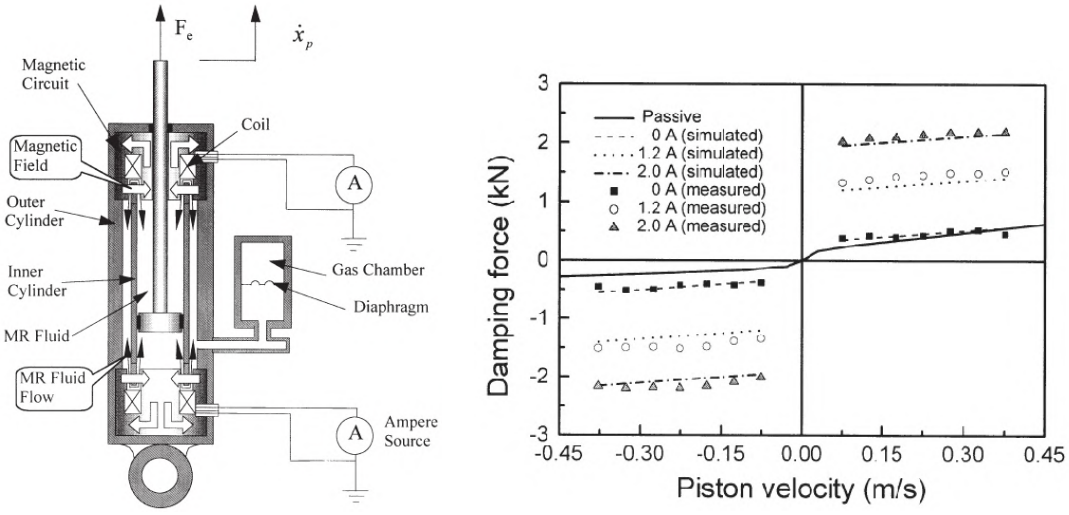

Fig. 2-24 Schema of MR damper with gap in the outer cylinder (left), and its F-v curves [72]

Choi et al. [41] used an MR damper with a maximal force of 530 N (piston velocity 0.15 ms^{-1}) and a small dynamic range of 2-3.3 in dependence on piston velocity. This MR damper was for a vehicle seat.

Shin et al. [12] developed a small damper with a maximal force of 150 N (0.04 ms^{-1}) but with a dynamic force range of 20 (Fig. 2-25). The value of damper force response time is not listed in the last three mentioned publications.

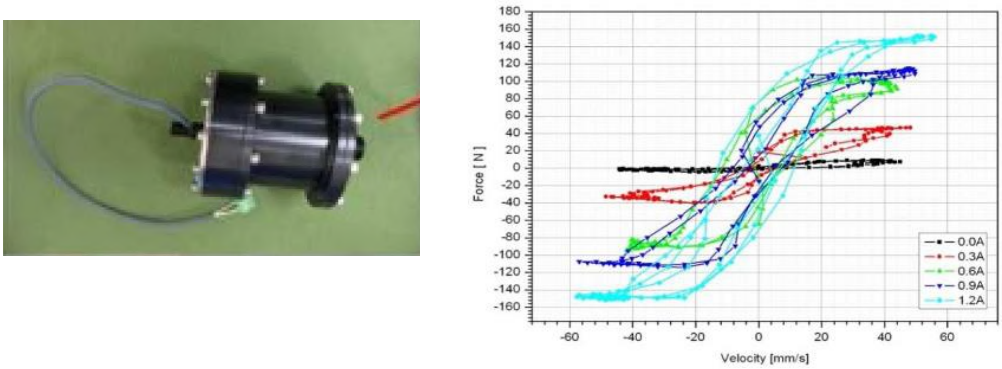

Fig. 2-25 Small damper with big dynamic range (left), and its F-v curves [12]

Yang et al. [47] designed a large-scale MR damper for civil engineering structures. This damper has a maximum force of 200 kN (piston velocity 0.06 ms-1) and a dynamic force range of about 20 (Fig. 2-26). This damper has a long force response time, minimally 100 ms.

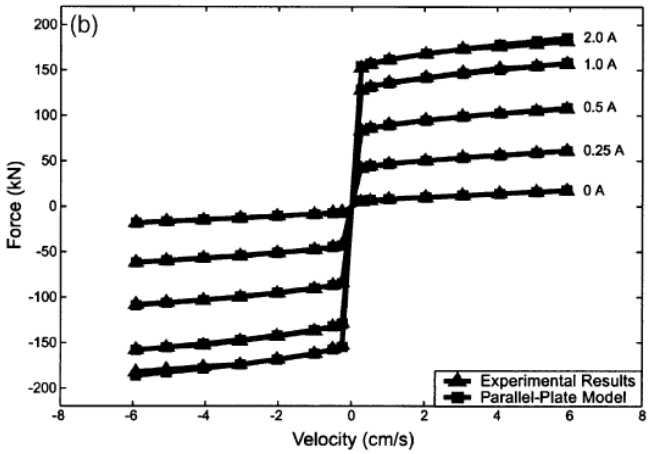

Fig. 2-26 F-v curves of large-scale MR damper [47]

2.4.2 Main sources of MR damper response time

Strecker et al. [76] defined three main sources that prolong the response time: (a) MRF, (b) electrical circuit (the coil inductance), and (c) magnetic circuit (eddy currents). For the electrical circuit problem, they designed a special current controller that minimizes the response time of the electrical circuit when switching on and off using the overvoltage method [54].

It is shown that a reduction in force response time can be achieved by modifying the valve design to limit the effect of eddy currents. Eddy currents are loops of electric current generated in a conductor by a changing magnetic field. They flow in a plane perpendicular to the direction of the magnetic field. Eddy currents have their own magnetic field, in the opposite direction to the magnetic field that causes the eddy currents (Fig. 2-27) [77]. Therefore, the eddy currents slow down the rise of the magnetic field when the control current changes. There are two different approaches to reducing eddy currents: the material and the shape approach.

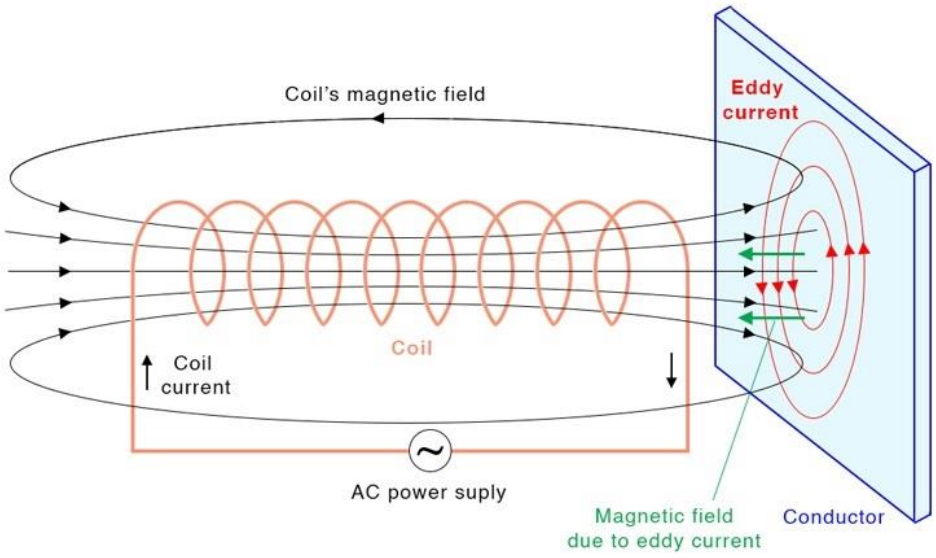

Fig. 2-27 Eddy currents generation scheme [77]

2.4.3 Material approach to reduce eddy currents

The first approach is the material approach. The material approach uses materials with high electrical resistivity, such as ferrites [57, 78], permalloys, or Soft Magnetic Composites (SMC). These materials are composed of ferromagnetic particles (Fe alloy powder, for example) with an insulating film between them, see Fig. 2-28 (left). The smaller the size of the loops, the smaller the effect of the eddy currents, resulting in a shorter time response of the MR damper.

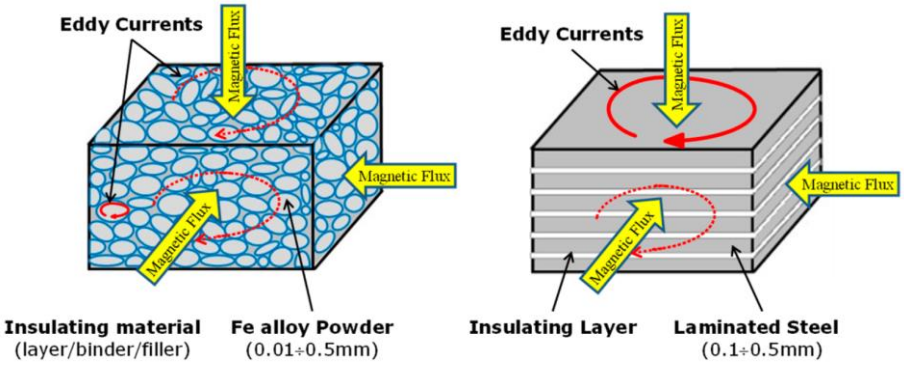

Fig. 2-28 Eddy currents in magnetic core composite (left) and laminated (right) [79]

These materials have lower permeability or a lower magnetic saturation limit than pure iron, but they have high electrical resistivity, which prevents the formation of eddy currents. Other problems with these materials are their low mechanical strength, low impact resistance, high cost, and, in most cases, poor machinability [80]. Nevertheless, the material approach is commonly used in electrical engineering for electromagnetic valves, high-frequency transformers and inductor cores in switching power supplies. [81, 82].

Kubík et al. [55] designed an external MR valve with a damper core from Epcos N95 ferrite (green parts – rod and ring, see Fig. 2-29). The valve reaches a force response time of about 4 ms and a dynamic force range of about 8.

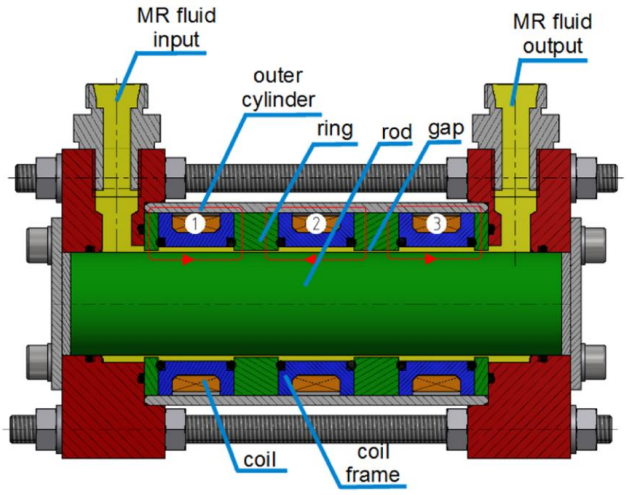

Fig. 2-29 External MR valve with core from ferrite (rod, ring) [83]

2.4.4 Shape approach to reduce eddy currents

The second approach is the shape approach [84–86]. The shape approach consists of placing electrically non-conductive obstacles in the path of the eddy currents, either by using insulated plates [87, 88], see Fig. 2-28 (right), as in low-frequency transformers, or by using complex-shaped grooves that intersect the path of the eddy currents [67, 89]. It lengthens the path of the eddy current. A longer path results in higher electrical resistance. Shaped grooves are more suitable for magnetic circuits with complicated shapes, such as MR damper.

Goldasz [88] proposed the concept of a piston for automotive MR damper, which uses a core made out of six SiFe laminated stacks with radially projecting arms away from the centre of the core (Fig. 2-30). The damper should have a dynamic range of 14 at a piston velocity of 0.2 m/s and a short response time. However, these are only assumed values since this is a concept.

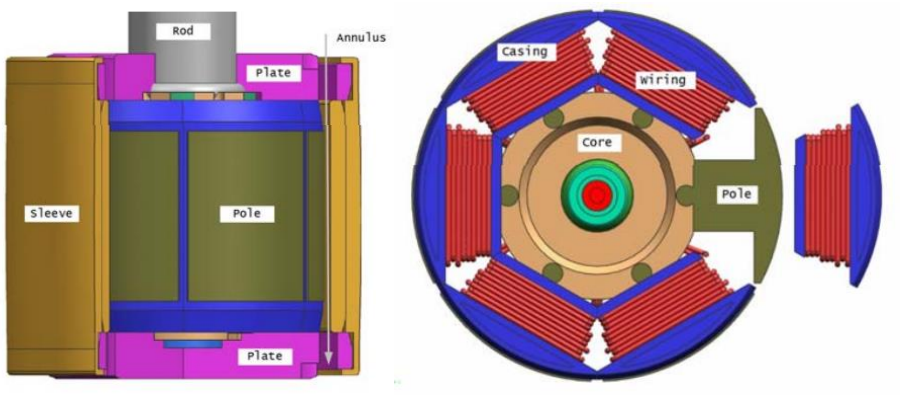

Fig. 2-30 MR valve with laminated stacks [88]

Yoon et al. [67] introduced an MR damper with a grooved valve core and outer cylinder (Fig. 2-31). The magnetic circuit is made from SMC. The damper force response time is about 2 ms, see Fig. 2-31 (right). The dynamic range read from the graph in Fig. 2-31 (right) is only 2.5.

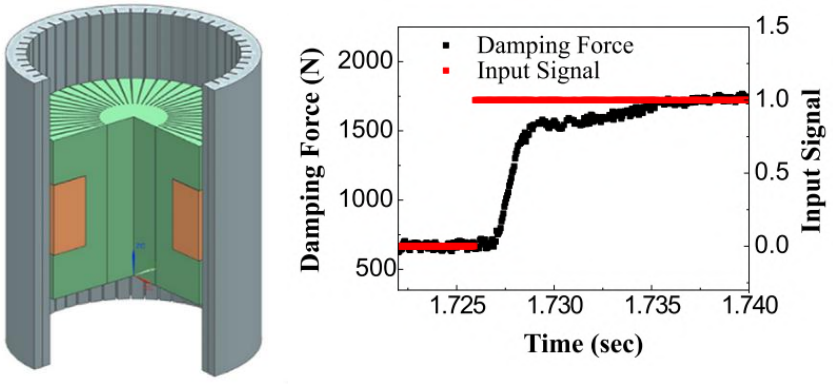

Fig. 2-31 Grooved core and outer cylinder valve of MR damper (left), damping force response (right) [67]

Omekanda et al. [89] patented the design of electromagnetic actuator for fuel injector. Structure with grooves (Fig. 2-32) eliminates eddy currents in the magnetic circuit of the electro-magnetic actuator. The force profile of the electromagnetic actuator with eddy currents and without eddy currents is shown in Fig. 2-33. This causes the armature force to respond more quickly to changes in current flow through the injector.

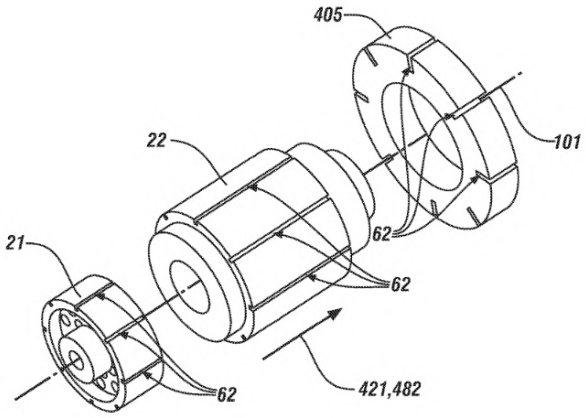

Fig. 2-32 Design of electromagnetic actuator for fuel injector [89]

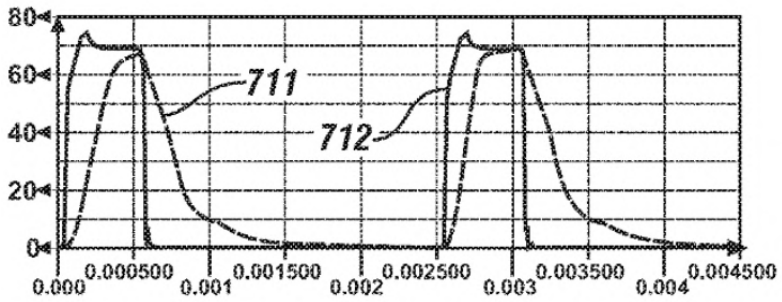

Fig. 2-33 Force profile of electromagnetic actuator with eddy currents (711) and without eddy currents (712) [89]

Strecker et al. [59] have developed a special MR damper valve manufactured from pure iron by selective laser melting (SLM). The valve includes a structured core and outer cylinder (Fig. 2-34), which reduce eddy currents in the magnetic circuit. The reduction in eddy currents leads to a huge reduction in damper force response time. The authors report a damper force response time of 1.32 ms. The dynamic force range of the damper is 5.1.

Fig. 2-34 Structured core and outer cylinder of MR damper valve made by SLM [59]

2.5 Approaches to fail-safe MR damper design

Research about fail-safe dampers shows that fail-safe behaviour can be achieved by placing a permanent magnet inside the MR damper valve. The permanent magnet creates magnetic field that prevents the damping force from dropping to a minimum during a power failure. The maximum damping force is achieved with a positive electric current through the coil, and the minimum damping force is achieved with an opposing electric current.

Boese et al. [90] designed an MR damper with two permanent magnets and a coil in the piston, see Fig. 2-35 – left. In the case of a power failure, the damping force is approximately 1/3 of the maximum damping force (Fig. 2-35 – right).

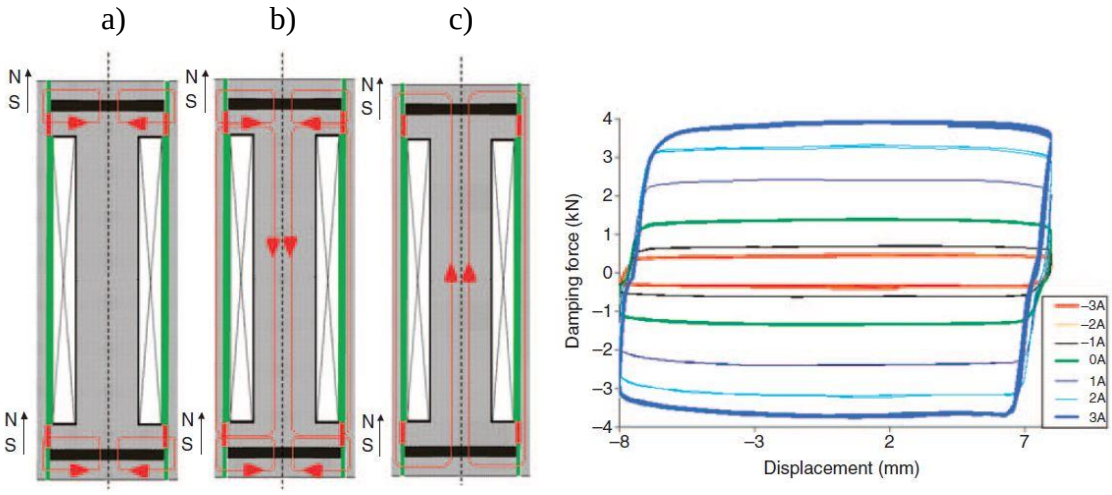

Fig. 2-35 Schema of the magnetic model of fail-safe MR damper a) without coil current, b) with positive coil current, c) with negative coil current. F-v curves of fail-safe MR damper (right) [90].

Zhang et al. [91] designed a fail-safe MR damper with a bypass (Fig. 2-36 - left). This valve has been designed to provide a wide dynamic force range and a low minimum damping force. The MR fluid flows through the area between the piston and the damper cylinder (yellow area), where it is not affected by the magnetic field, and through the gap in the piston (pink area), where the magnetic field can be varied using a coil. Two rings of neodymium magnets maintain the magnetic flux in the gap when the coil is not powered. The authors report the value of force dynamic range value of 8, and the damping force in the no-current mode is about one-third of the maximum damping force (Fig. 2-36 - right). Interestingly, when the opposite electric current is applied, the damping force decreases only up to about -1.5 A and remains almost the same until -4 A.

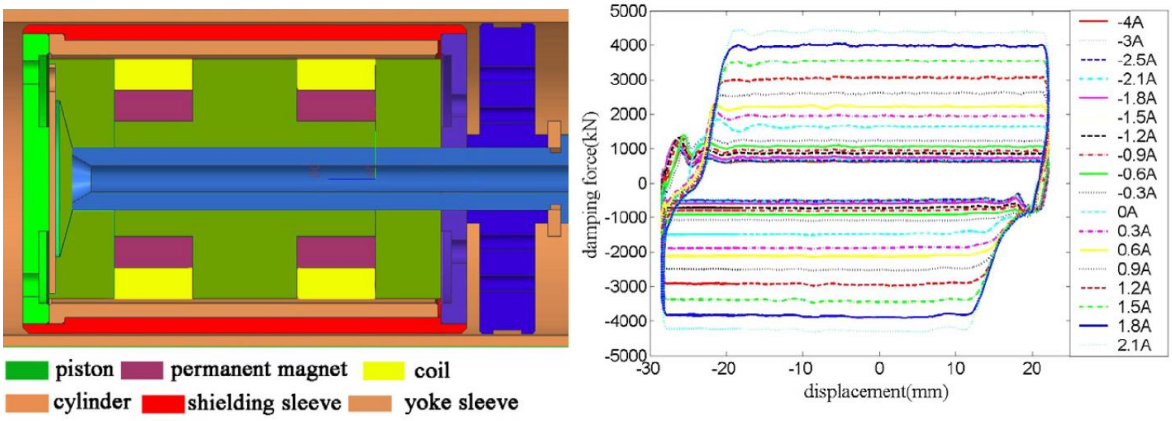

Fig. 2-36 Schema of the magnetic model of fail-safe MR damper with bypass (left), F-v curves of fail-safe MR damper (right) [91]

Xiao et al. [92] introduced the design of an MR damper with a permanent magnet and magnetic valve see Fig. 2-37. It contains the damp channel between the piston and the outer cylinder. A permanent magnet maintains a constant level of magnetic induction in this active zone. The damper also contains an internal channel that is closed by a magnetic valve to allow the damping force to change. When the damping force needs to be reduced, the valve opens. Therefore, in the case of a power failure, the damper remains at maximum power. The force dynamic range of this MR damper is approximately 10.

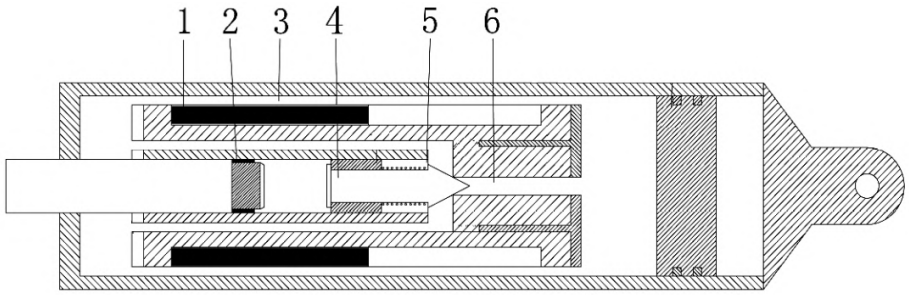

Fig. 2-37 Schema of fail-safe MR damper with permanent magnet and magnetic valve, (1) circular permanent magnet, (2) magnet coil, (3) damp channel, (4) valve plug, (5) back spring, (6) magnetic valve pipe, [92], picture edited.

Fail-safe MR dampers are also available for use in civil engineering applications [93, 94]. Wei-ming et al. [93] have designed an MR damper with an external valve. The valve contains a set of electrical coils in the outer part of the valve and permanent magnets in the inner part, see Fig. 2-38. By using coils, it is possible to completely eliminate the magnetic field of the permanent magnets in the gap (13 – damping channel,). The damping force of this MR damper in fail-safe mode is approximately 55 % of the maximum damping force. The maximum damping force is approximately 110 kN, fail-safe force is approximately 60 kN and minimum force is approximately 20 kN.

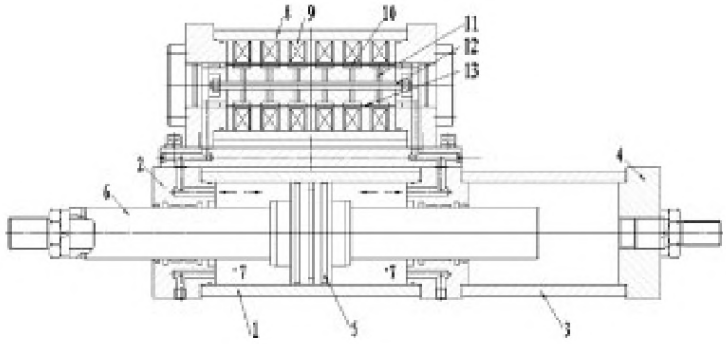

Fig. 2-38 Schema of fail-safe MR damper for civil engineering, (9) electric coil, (11) permanent magnet, (13) damping channel [93].

The permanent magnet in the damper can also be used for purposes other than ensuring the fail-safe mode, for example, to reduce energy consumption [95] or to eliminate the bypass of the MR fluid between the piston and cylinder [96].

2.6 Control strategies for semi-actively controlled MR dampers

This thesis deals with semi-active control of MR damper. Therefore, the basic algorithms for this control are briefly described here.

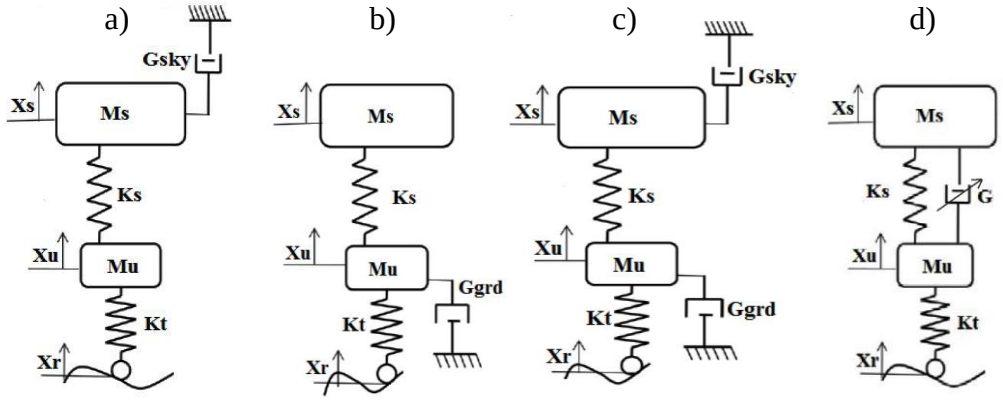

Fig. 2-39 Schema of ideal Skyhook (a), ideal Groundhook (b), ideal Hybrid control and real situation (d) [97]

Skyhook (ON/OFF)

The Skyhook is the most used semi-active algorithm for damper control [98]. It aims to keep the sprung mass velocity at 0 ms^{-1}. It can be imagined as a firmly fixed mass in the sky, see Fig. 2-39 a) – therefore, it is called Skyhook. In practice, the algorithm tries to prevent the sprung mass from oscillating. In other words, it tries to minimize the transmission of motion from the unsprung mass (Mu) to the sprung mass (Ms). If the unsprung mass velocity exceeds the sprung mass velocity, the damper is deactivated so that the unsprung mass does not excite the sprung mass. Otherwise, when the sprung mass velocity exceeds the unsprung mass velocity, the damper is activated to slow the sprung mass motion. Mathematically, this is described as follows:

$$F = \begin{cases} b(\dot{x}_2 - \dot{x}_1), & \dot{x}_2(\dot{x}_2 - \dot{x}_1) \geq 0 \\ 0, & \dot{x}_2(\dot{x}_2 - \dot{x}_1) < 0 \end{cases} \quad (4)$$

where:

F	[N]	damping force
b	[Nsm^{-1}]	damping coefficient
$\dot{x}_2$	[ms^{-1}]	sprung mass velocity
$\dot{x}_1$	[ms^{-1}]	unsprung mass velocity

This variant of Skyhook is called “two-state Skyhook” or “ON/OFF Skyhook” because it only switches between maximum and minimum force.

Skyhook linear

However, there is also an advanced version of the Skyhook – the "linear Skyhook"- which continuously switches between maximum and minimum damping force [99, 100]. The principle of the algorithm is similar. The difference is that with the linear Skyhook, the damping force depends on the velocity ratio $\dot{x}_2/(\dot{x}_2 - \dot{x}_1)$, i.e. at a high piston velocity or at a low velocity of the sprung mass, the algorithm reduces the damping force. This eliminates shocks when the damper state suddenly changes, further calming the system. Mathematically:

$$F(v) = \begin{cases} F_{min}(v), & \dot{x}_2(\dot{x}_2 - \dot{x}_1) \leq 0 \\ sat\left(\dfrac{\alpha \cdot F_{max}(v) \cdot (\dot{x}_2 - \dot{x}_1) + (1-\alpha) \cdot F_{max}(v) \cdot \dot{x}_2}{(\dot{x}_2 - \dot{x}_1)}\right), & \dot{x}_2(\dot{x}_2 - \dot{x}_1) > 0 \end{cases} \quad (5)$$

where:

$F(v)$	[N]	damping force
$F_{max}(v)$	[N]	damping force at a current of I_{max}
$F_{min}(v)$	[N]	damping force at a current of I_{min}
$\dot{x}_2$	[ms^{-1}]	sprung mass velocity
$\dot{x}_1$	[ms^{-1}]	unsprung mass velocity
α	[-]	$\alpha \in [0,1]$ is tuning between Shyhook linear and Skyhook ON/OFF

and **sat** denotes that $F \in [F_{min}(v),\ F_{max}(v)]$.

Groundhook

This algorithm aims to increase wheel grip by reducing the fluctuation of force between the wheel and a road (it tries to prevent their mutual movement, Fig. 2-39 b). There are also two variants of the algorithm: two-state and linear Groundhook [101]. Another variant of Groundhook is the Modified Groundhook, designed for easier use in practice [61]. This two-state variant assumes that a bump in the road will begin to exert a force on the sprung mass, causing it to accelerate. The accelerometer senses acceleration and the damper is deactivated to allow the unsprung mass to follow the bump trajectory without transferring motion to the sprung mass. The moment the bump disappears, it stops exerting a force on the unsprung mass, and it begins to decelerate. At that moment, the damper is activated to slow down the mass and allow it to continue to follow the trajectory of the bump. Mathematically:

$$F = \begin{cases} b(\dot{x}_2 - \dot{x}_1), & \ddot{x}_1(\dot{x}_2 - \dot{x}_1) \geq 0 \\ 0, & \ddot{x}_1(\dot{x}_2 - \dot{x}_1) < 0 \end{cases} \quad (6)$$

where:

F	[N]	damping force
b	[Nsm^{-1}]	damping coefficient
$\dot{x}_2$	[ms^{-1}]	sprung mass velocity
$\dot{x}_1$	[ms^{-1}]	unsprung mass velocity
$\ddot{x}_1$	[ms^{-2}]	unsprung mass acceleration

Hybrid control

The algorithm combines the advantages of the Skyhook and Groundhook algorithms (Fig. 2-39 c)). The coefficient α (0-1) is used to determine which algorithm will have a greater influence on damper control [102]. Mathematically:

$$\sigma_{sky} = \begin{cases} \dot{x_2}, & \dot{x_2}(\dot{x_2} - \dot{x_1}) \geq 0 \\ 0, & \dot{x_2}(\dot{x_2} - \dot{x_1}) < 0 \end{cases} \tag{7}$$

$$\sigma_{gnd} = \begin{cases} \dot{x_1}, & \dot{x_1}(\dot{x_2} - \dot{x_1}) < 0 \\ 0, & \dot{x_1}(\dot{x_2} - \dot{x_1}) \geq 0 \end{cases} \tag{8}$$

$$F = b \left[\alpha \, \sigma_{sky} + (1 - \alpha) \, \sigma_{gnd} \right] \tag{9}$$

where:

F	[N]	damping force
b	[-]	damping coefficient
α	[-]	tuning parameter switching between algorithms Skyhook and Groundhook
σ_{sky}	[ms^{-1}]	Skyhook part of damping force calculation
σ_{gnd}	[ms^{-1}]	Groundhook part of damping force calculation
$\dot{x}_2$	[ms^{-1}]	sprung mass velocity
$\dot{x}_1$	[ms^{-1}]	unsprung mass velocity

Acceleration driven damping

This algorithm is similar to the Skyhook algorithm. But instead of sprung mass velocity, it works with sprung mass acceleration. So, it is suitable for applications where it is desirable to increase vibration from an acceleration point of view [101, 103]. Mathematically:

$$F = \begin{cases} b(\dot{x_2} - \dot{x_1}), & \ddot{x}_2(\dot{x_2} - \dot{x_1}) \geq 0 \\ 0, & \ddot{x}_2(\dot{x_2} - \dot{x_1}) < 0 \end{cases} \tag{10}$$

where:

F	[N]	damping force
b	[-]	damping coefficient
$\dot{x}_2$	[ms^{-1}]	sprung mass velocity
$\dot{x}_1$	[ms^{-1}]	unsprung mass velocity
$\ddot{x}_2$	[ms^{-2}]	sprung mass acceleration

Power driven damping

A more complex algorithm that calculates the required damper force using the Hamiltonian technique, given the stiffness of the system [104]. Mathematically:

$$F = \begin{cases} F_{min}, & k(x_2 - x_1)(\dot{x}_2 - \dot{x}_1) + F_{min} \leq 0 \\ F_{max}, & k(x_2 - x_1)(\dot{x}_2 - \dot{x}_1) + F_{max} > 0 \\ \dfrac{F_{max} + F_{min}}{2}, & (x_2 - x_1) \neq 0 \; AND \; (\dot{x}_2 - \dot{x}_1) = 0 \\ -\dfrac{k(\dot{x}_2 - \dot{x}_1)}{(\dot{x}_2 - \dot{x}_1)}, & otherwise \end{cases} \tag{11}$$

where:

F	[N]	damping force
F_{max}	[N]	damping force at a current of I_{max}
F_{min}	[N]	damping force at a current of I_{min}
k	[Nm^{-1}]	spring stiffness
x_2	[m]	sprung mass displacement
x_1	[m]	unsprung mass displacement
$\dot{x}_2$	[ms^{-1}]	sprung mass velocity
$\dot{x}_1$	[ms^{-1}]	unsprung mass velocity

Mix-SH-ADD

This algorithm is a combination of the Acceleration Driven Damping and Skyhook algorithms. It should combine the advantages of both algorithms[101]. Mathematically:

$$F = \begin{cases} F_{max}, & \left[\left(\ddot{x}_2 - \alpha^2 {\dot{x}_2}^2\right) \leq 0 \; AND \; \dot{x}_2(\dot{x}_2 - \dot{x}_1) \geq 0\right] OR \\ & \left[\left(\ddot{x}_2 - \alpha^2 {\dot{x}_2}^2\right) > 0 \; AND \; \dot{x}_2(\dot{x}_2 - \dot{x}_1) \geq 0\right] \\ F_{min}, & otherwise \end{cases} \tag{12}$$

where:

F	[N]	damping force
F_{max}	[N]	damping force at a current of I_{max}
F_{min}	[N]	damping force at a current of I_{min}
$\dot{x}_2$	[ms^{-1}]	sprung mass velocity
$\dot{x}_1$	[ms^{-1}]	unsprung mass velocity
$\ddot{x}_2$	[ms^{-2}]	sprung mass acceleration
α	[-]	tuning parameter switching between algorithms SH and ADD

Other algorithms

In addition to the above, there are many other algorithms, such as Displacement Skyhook, Relative Displacement Skyhook, Continuous Skyhook, Two-States, and Continuous Balance Control.[105], Mixed Skyhook-Acceleration Driven Damping, Hybrid MPC control, LQR, LQG, LPV semi-active control [101].

3 ANALYSIS AND CONCLUSION OF LITERATURE REVIEW

3.1 About improvement of MR valve behaviour

As mentioned, the transient behaviour of the magnetorheological damper fundamentally affects the effectiveness of the S/A control [61, 76]. Key parameters are damper force response time and damper force dynamic range. Standard semi-actively controlled dampers have a force response time in the range of 15-100 ms [8, 58, 61]. It is not a good response time for fast S/A control. In virtual simulations, where the time response is often neglected, achieving a satisfactory efficiency of S/A control is possible, but in real use, the results would be significantly worse.

However, researchers are aware of this, and several studies have focused on designing an MR valve with a fast force response time. It has been found that an effective way to reduce response time is to reduce the eddy currents in the magnetic circuit [55, 67]. Eddy currents are generated when the magnetic field generated by the coil changes and creates a magnetic field of opposite orientation to the coil magnetic field, thus prolonging the formation of the magnetic field in the valve gap and prolonging the time response.

There are two approaches to eddy current reduction: the material [78] and the shape approach [86]. The material approach uses materials with high electrical resistance, and the shape approach uses the special shape of a magnetic circuit to prolong the path for eddy currents. A longer path results in higher electrical resistance. Publications show that reducing the force response time below 1.5 ms is possible using the shape approach [59, 67]. However, these designs achieve relatively low dynamic ranges of 5 and less. S/A controlled dampers typically can have a dynamic force range of 10-20 [8, 12]. The damper dynamic force range is also a key parameter that affects the effectiveness of the S/A control. It must to be large enough for effective control.

It seems that reducing the force response time by eliminating eddy currents may result in an undesirable reduction in dynamic range. However, the influence of different materials and different shapes of the magnetic circuit has not yet been sufficiently investigated. It would also be appropriate to evaluate the materials in terms of their applicability to the MR damper and its possible serial production. It means evaluating mechanical properties, price, impact resistance and machinability [80]. In the same way, it is necessary to evaluate the possible shapes of the cores. The complicated shape of the grooves is virtually impossible to produce using conventional methods, as the grooves must also be structured within the core material. Additive technologies can be used to produce such complex cores, particularly selective laser melting (SLM), which enables 3D printing from metal powder [59].

3.2 About failsafe magnetorheological damper

As mentioned in the introduction, one of the key requirements for a modern railway vehicle is the requirement for safety. From a safety point of view, the worst situation can occur is a derailment [14][15]. Therefore, it is necessary to ensure sufficient stability of the railway vehicle under all circumstances. The suspension system, i.e. the system of springs and dampers, is responsible for the stability of the vehicle. At the moment of loss of damping force, the vehicle's stability could be lost. This would significantly reduce comfort and, in extreme cases, could cause the vehicle to derail.

Under this assumption, there is a problem with the possible use of the MR damper in the suspension of the railway vehicle because the MR damper works in such a way that its damping force increases when the electric current is applied. The higher the electric current, the higher the damping force. The minimum damping force of a conventional MR damper is achieved with no power supply [61]. In the case of a power failure, the damping force of the MR damper would be lost, resulting in a significant reduction in comfort and a potentially dangerous situation.

Designers of MR dampers are aware of this problem. Several scientific teams have been working to develop a so-called fail-safe damper that would avoid this problem. In order for the damping force not to drop to a minimum in the case of a power failure, it is necessary to maintain a permanent magnetic field in the MR damper. A permanent magnet is best suited for this purpose [90, 91].

There are several designs of failsafe MR dampers with permanent magnets. The magnet can be located in the damper core under the coil [91], next to the coil [90] or in the outer cylinder on the other side of the gap [83]. But there are also variants without an electric coil with an electromagnetic valve [92]. Most designs have a valve inside the damper body, but there are also variants with an external valve [83].

The damping characteristics of fail-safe dampers are well described in the literature. In most cases, the damping force in fail-safe mode is approximately 1/3 of the maximum damping force.[90], [91], but it can also be higher [92]. One-third of the maximum damping force should be sufficient to maintain railway vehicle stability in case of power failure.

Unfortunately, no studies have described the transient behaviour of MR valves with permanent magnets. So, from this point of view, it is not possible to compare the studies. However, as already mentioned, the effectiveness of semi-active control depends strongly on the transient behaviour of the damper [61]. It is unknown whether a permanent magnet in the MR valve will make the transient behaviour of the damper worse, better or unchanged. For the efficient use of MR fail-safe dampers on railway vehicles, it is first necessary to study their transient behaviour.

3.3 About S/A controlled lateral dampers of railway vehicle

Most studies on semi-active control of railway vehicle motion deal with the control of lateral carbody movement. The goal is to reduce carbody vibration and increase passenger comfort. Simulation [9, 13] and experimental [7, 12] studies show that semi-active control of lateral secondary dampers can reduce carbody vibration by approximately 30-40 %. [7, 9]. However, passenger comfort can also be increased by a semi-actively controlled vertical secondary damper [71]. The most commonly used semi-active dampers are MR dampers based on the magnetorheological effect [12, 106]. Replacing the lateral or vertical secondary dampers with active actuators or semi-actively controlled dampers is relatively simple, so this technology can be easily applied to the current vehicles which want to improve their comfort. It can also be applied to the new generation of high-speed railway vehicles.

It is well known that damper force response time and dynamic range significantly affect the effectiveness of S/A control [61, 76], but the impact and the acceptable value of force response time and dynamic range for different algorithms and for railway vehicle is not known. For some MR dampers, the time response value is not even listed [12, 41, 72]. For a dynamic system with a natural frequency of 11 Hz, the ideal response time is 0 ms [83], but the natural frequency of the railway vehicle body is quite low. It is also known that the damper force response time when the electric current is changed is different for the force rise and the force drop [8, 59]. However, when simulating with the implemented response time of the damper, the response time is assumed to be the same for both force rise and force drop. It is not known if this simplification is allowed. In general, the S/A controlled dampers perform better at higher damping forces than the ideal a passive damper [61]. However, the ideal damping force for a S/A lateral secondary railway vehicle damper is unknown.

There are several algorithms for semi-active damper control, but only a small part of them have been verified in the application to the secondary suspension of a railway vehicle. The most commonly used control strategy on railway vehicles is the algorithm Shyhook [98]. It can be assumed that a similar Skyhook linear, which has not yet been verified on a railway vehicle, could achieve slightly better results [100]. A simple Acceleration Driven Damping algorithm should also give very good results [45]. The influence of the response time on the effectiveness of these and other algorithms should be appropriately investigated.

The S/A control of railway vehicle dampers has been verified by a virtual simulation [3, 69] or a scaled-down and simplified physical model [7, 12]. The advantages of virtual simulation are price, variability, and the possibility of a relatively complex vehicle model. The disadvantage is the need to create a complex model of the behaviour of the MR damper, including transient behaviour, magnetic and hydraulic hysteresis, temperature dependence, etc., which is quite complex and, among other things, can lead to considerable calculation time. The advantage of the physical model is that there is no need to create a complex virtual model of the MR damper. The disadvantage is the need to build a model of the vehicle that

must be simplified. Other disadvantages are price and low variability. The ideal way to test the effect of MR damper characteristics could be hardware-in-the-loop simulation (HILS) [41, 72]. It is a compromise between the two previous methods. In HIL simulation, the real damper is mounted in a pulsator that is controlled by a computer running a virtual vehicle model. The pulsator measures the damping force, which serves as input to the virtual model. In this way, HIL simulation combines the advantages of virtual and physical models.

3.4 Lack of knowledge – key points

The main unexplored areas are the influence of the material and shape of the damper magnetic circuit and the additional permanent magnet in the magnetic circuit on the damper dynamic behaviour. And the effect of the damper dynamic behaviour on the performance of the semi-actively controlled suspension of railway vehicles.

- It is known that the force response time of the MR damper can be reduced by eliminating eddy currents in the damper magnetic circuit using a material or shape approach. However, a significant lack of knowledge is the influence of different materials and shapes of the magnetic circuit of the MR damper on its dynamic behaviour (damper force response time and force dynamic range). A short force response time and a high dynamic force range are necessary for the effectiveness of S/A control. It is not known if it is true that a shorter response time is associated with a lower dynamic range, as reported in known publications.
- There are many materials from which the magnetic circuit of an MR damper can be made. Which material is the best in terms of response time is not known. It is not known which materials will cause a short force response time of the MR damper even without a special shape and which materials will require a special shape to achieve a low response. And how complex this shape needs to be for different materials. Furthermore, it is unknown what difference in time response can be achieved using the shape approach in an otherwise unsuitable material.
- In order for a damper to be used on a railway in operating, the safe behaviour of the railway vehicle in the case of a loss of power supply of the damper must be ensured. Fail-safe behaviour can be achieved by placing a permanent magnet into the damper piston. The magnet creates a permanent magnetic field that generates a non-zero damping force in the event of a power failure. Unfortunately, nothing is known about the dynamic behaviour of the MR damper with the permanent magnet in the damper piston. It is not known how the permanent magnet affect the dynamic behaviour of the MR damper compared to the MR damper without a magnet. It is not known if the force rise and the force drop response time will be different and what the effect of the magnetic hysteresis of the magnetic circuit will be.

- Another lack of knowledge is the influence of damper force response time on the effectiveness of semi-actively controlled suspension of railway vehicles. Many studies neglect the damper force response time. However, it is known that a large response time significantly degrades the results of the S/A control strategies. The effect of response time increases with the frequency of the damped motion. The railway carbody vibration frequency should be up to 2 Hz [107], which is a relatively low frequency. Theoretically, therefore, the long response time of the S/A controlled damper in a railway vehicle bogie would not necessarily be such a problem. Actual damper response times range from 1.28 ms [55] to 100 ms [7], which will certainly cause a difference in the effectiveness of semi-active control. However, the impact of this effect on various S/A algorithms has not been directly investigated. An acceptable response time value for a semi-actively controlled secondary lateral MR damper is unknown.
- It is known that the damper force response time is different for the force rise and the force drop. However, in the case of simulation with the implemented response time of the damper, the response time is assumed to be the same for both force rise and force drop. It is not known if this simplification is allowed.
- The dynamic range of the damper has a similar effect as the damper response time. The dynamic range is the ratio of damping forces in the activated and deactivated state. The greater the dynamic range, the more effective the semi-active control. The real dynamic range is from 2 to 25 [47, 108]. The influence of the MR damper dynamic range on S/A damping of a railway vehicle suspension is unknown.
- The S/A control efficiency depends on the F-v curves of the damper used. From experience [61], the damping force of an ideal S/A damper is about 1.5 times the damping force of an ideal passive damper. However, the ideal F-v curves for secondary lateral MR dampers of railway vehicles are unknown.
- Most of the studies deal with the model of the railway vehicle and the model of the MR damper. This is understandable because experiments on real vehicles in operation are very demanding and expensive. However, the MR dampers exhibit highly nonlinear behaviour that is difficult to model correctly. The MR damper models used in simulations are always simplified and often do not correspond to the force generated by the real MR damper, which degrades the results of semi-active suspension simulations. Verification of the S/A control of the railway vehicle MR damper and the influence of the secondary lateral damper behaviour by on-road testing or at least by Hardware-in-the-loop simulation is unknown.

These are the lacks of knowledge that need to be filled before designing an MR damping system for a railway vehicle. Scientific questions and hypotheses were formulated based on some assumptions to fill the lack of knowledge. The sub-aims of the thesis were defined to test the hypotheses, which together form the overall aim.

4 AIM OF THE THESIS

The main aim of the dissertation thesis is to investigate the possibilities of improving the damper dynamic behaviour and the effect of damper dynamic behaviour on the performance of the semi-actively controlled suspension of railway vehicle, where the performance parameter is **the comfort of the passengers**. The research has been divided into three sub-aims.

The first sub-aim is to investigate **the possibilities of improving the damper dynamic behaviour using the material and the shape approaches** to reduce eddy currents. Based on the results of this sub-aim, the MR damper design for the third sub-aim will be selected. The following steps need to be taken to achieve this aim of the thesis:

- Selection of materials to be used for the core and outer cylinder of the damper piston for material approach study.
- Designing a special shape of the core and outer cylinder to reduce the eddy currents.
- Simulation of the value of magnetic flux density in the gap of the damper piston and its response time for both material and also shape approach.
- Manufacture of cores and outer cylinders based on material and shape approach design.
- Measurement of the magnetic flux density in the gap and its response time on damper piston assemblies.
- Measurement of damper force response time for all manufactured variants.

The second of the sub-aims is to investigate **the effect of the permanent magnet in the damper piston on the dynamic behaviour of the damper**. The following steps must be taken to achieve this aim of the thesis:

- Selection of the type of permanent magnet type and its location in the damper piston.
- Simulation of the magnetic behaviour of the selected type of piston. It means the B-I curve, the course and the response time of the magnetic flux density when the electric current changes.
- Manufacture of damper piston with permanent magnet.
- Measurement of the magnetic behaviour of manufactured pistons and comparison with simulations.
- Fail-safe MR damper assembly and measuring of damper behaviour. Includes the damper F-v curve and damper force response time.

The third of the sub-aims is to investigate **the influence of the behaviour of a semi-actively controlled secondary lateral MR damper on the comfort of railway vehicle,** i.e. the influence of the damper dynamic range and the damper response time for the force rise and the force drop. The following steps have to be taken to achieve this goal of the thesis:

- Design and identification of a suitable railway vehicle dynamic model.
- Selection or design of an MR damper S/A control strategy for railway vehicle lateral secondary dampers that will increase vehicle comfort.
- Selection of the MR damper design based on the results of the first sub-aim.
- Design of the hardware-in-the-loop simulation assembly.
- Select or design the excitation of the virtual model in hardware-in-the-loop simulation.
- Design a method to control the dynamic range and response time in the case of a real damper.
- Investigate the effect of the damper response time and dynamic range on S/A control efficiency for different control algorithms in the hardware-in-the-loop simulation.

4.1 Scientific questions

Based on the conclusions of the critical literature review and the defined aims of the dissertation thesis, the following scientific questions and relevant working hypotheses are formulated:

Q1:

How does the material and geometry of the MR damper magnetic circuit affect force response time and dynamic range? Is a shorter damper force response time always associated with a smaller force dynamic range?

Q2:

Will the permanent magnet in the MR valve affect the response time of the MR damper? Will the response time of the force rise and force drop be different?

Q3:

How does damper force rise response time, force drop response time, and dynamic range affect the effectiveness of S/A control of railway vehicle lateral secondary MR dampers? Is there a difference between the effect of the force rise response time and the effect of the force drop response time on the efficiency of S/A control? What is the acceptable value of damper force response time and dynamic range for this control?

4.2 Hypothesis

H1:

Based on several publications, it may appear that the shorter damper force response time is associated with a smaller force dynamic range. The hypothesis is that this occurs only in the case of the material approach when materials with high electrical resistivity but with a low saturation limit of magnetic flux density (ferrite, for example) are used [67]. It can be assumed that if only a material approach is used, the shortest response time will be achieved by using the material with the highest electrical resistivity, and the highest dynamic force range will be achieved when using the material with the highest magnetic saturation. It can be assumed that the shape approach shortens the response time by at least five times, as in the case of a structured core [59]. It can be assumed that it will be possible to achieve a short force response time in combination with a high dynamic force range by using a combination of the material and the shape approaches.

H2:

It can be assumed that the response time of the force rise will be slower than the response time of the force drop, as in the case of the MR damper without a magnet [55, 59]. The difference in response time for force rise and drop is due to the compressibility of the MR fluid and the entire damper system [58, 109]. When the electric current is applied and the force rises, the MR fluid and the entire damper system must first be compressed slightly, which slows the force rise. On the other hand, when the current is turned off and the force is released, the preloaded system quickly returns to its original state, and the force drops quickly. If a permanent magnet is used, only the B-I curve in the gap will shift, but the stationary magnetic field of the permanent magnet should have no effect on the generation and decay of the magnetic field in the magnetic circuit.

H3:

Since, in principle, the algorithms switch once at zero piston velocity and once at non-zero velocity (see equations 4-12), it is expected that the response time for force rise will have a different effect on the effectiveness of S/A control than the response time for force drop. The importance of the response time for force rise and drop is likely to vary depending on the S/A strategy used. An acceptable force dynamic range is assumed to be about 10 as for the general suspension system here [110]. Due to the low vibration frequency of the railway vehicle body up to 2 Hz [107], it can be assumed that the ideal force response time will be relatively long in this case. If the response must be at least 10 times faster than the highest vibration frequency for at least functional control [76], we assume that the ideal response time could be 50 times faster than the highest vibration frequency. Thus, a maximum vibration frequency of 2 Hz would imply an ideal time response of about 10 ms.

4.3 Thesis layout

The main part of the dissertation thesis consists of three scientific papers published in peer-reviewed journals with an impact factor.

The first paper [I.] answers the first scientific question about reducing the damper force response time using the material and the shape approaches. The paper presents a novel approach to the design of an ultra-fast MR valve based on materials with high electrical resistivity (material approach) or materials with low electrical resistivity (shape approach). This paper is a follow-up to earlier research by the author's team, which tested an ultra-fast MR damper with a ferrite magnetic circuit [55, 76, 83]. The low-impact resistance and poor machinability of ferrite prompted further investigation into materials suitable for use in an ultra-fast MR valve. This paper includes an evaluation of individual approaches based on the length of response time and dynamic force range. A transient simulation of the magnetic circuit was the main tool for material selection or groove design. The output of the model is the time dependence of the magnetic flux density when the electric current is switched on (step signal). The response time of the magnetic flux density can be determined from this curve. The simulation was performed for six materials of the magnetic circuit with different electrical conductivity (material approach) and two grooved variants (shape approach) to achieve the shortest response time and high dynamic range. The simulated variants were verified by magnetic field measurements. Since the MR valve was specifically designed for use in an MR damper, the response time of the damping force was also measured.

The second paper [II.] focuses on answering the second scientific question about the force response time of the fail-safe MR valve with a permanent magnet. The main aim of this paper is to present the dynamic behaviour of a fail-safe MR valve with a permanent magnet and to compare it with the dynamic behaviour of an MR valve without a magnet. A damper of similar design as in the previous cases is used. The core and outer cylinder of the damper piston are made of 11SMn30 cutting steel. The core design was modified to accommodate a permanent magnet. Two ring neodymium magnets are used to provide a fail-safe magnetic field. The response time of the magnetic field and the force to the control signal step are determined experimentally and by virtual simulation using the magnetic models.

The third paper [III.] focuses on answering the third scientific question concerning the effect of the MR damper behaviour on the S/A control efficiency in the lateral movement of the railway vehicle body. The main aim of the paper is to investigate in detail the effect of selected parameters of the MR damper on the suspension performance of railway vehicles. The response time of the damping force rise, the damping force drop, and the dynamic force range are studied separately. Hardware-in-the-loop simulation with a real MR damper

is used to account for several non-linearity in the damper dynamics. A damper of a similar design as in the previous cases is used. The magnetic circuit of the damper is made of SMC. A simple virtual model of a railway vehicle with 2 DOF is used. The simulations are evaluated for several known S/A damper control algorithms and one newly designed algorithm (Acceleration Driven Damper Linear).

I. STRECKER, Z.; JENIŠ, F.; KUBÍK, M.; MACHÁČEK, O.; CHOI, S. Novel Approaches to the Design of an Ultra-Fast Magnetorheological Valve for Semi-Active Control. *Materials, 2021*, roč. 14, č. 10, s. 1-20. ISSN: 1996-1944. *Journal impact factor = 3.4 (2022, WOS) Autor's contribution: 40%*

II. JENIŠ, F.; KUBÍK, M.; MACHÁČEK, O.; ŠEBESTA, K.; STRECKER, Z. Insight into the response time of fail-safe magnetorheological damper. *Smart Materials and Structures*, 2020, roč. 1, č. 30, s. 1-13. ISSN: 1361-665X. *Journal impact factor = 4.1 (2022, WOS) Autor's contribution: 55%*

III. JENIŠ, F; KUBÍK, M; MICHÁLEK, T; STRECKER, Z; ŽÁČEK, J; MAZŮREK, I. Effect of the magneto-rheological damper dynamic behaviour on the rail vehicle comfort: hardware-in-the-loop simulation. *Actuators*, 2023, roč. 12, č. 2, s. 1-14. ISSN: 2076-0825. *Journal impact factor = 2.6 (2022, WOS) Autor's contribution: 80%*

5 MATERIALS AND METHODS

This chapter briefly describes the methods used in the thesis. It is divided into three parts. The first part discusses materials and methods for investigating the material and the shape approach to improving MR damper behaviour. The second part discusses the investigation of fail-safe MR damper behaviour. And the third part discusses methods for studying the effect of MR damper behaviour on S/A control of railway vehicle suspension. The workflow of the thesis is shown in Fig. 5-1. The methods are described in more detail in published papers.

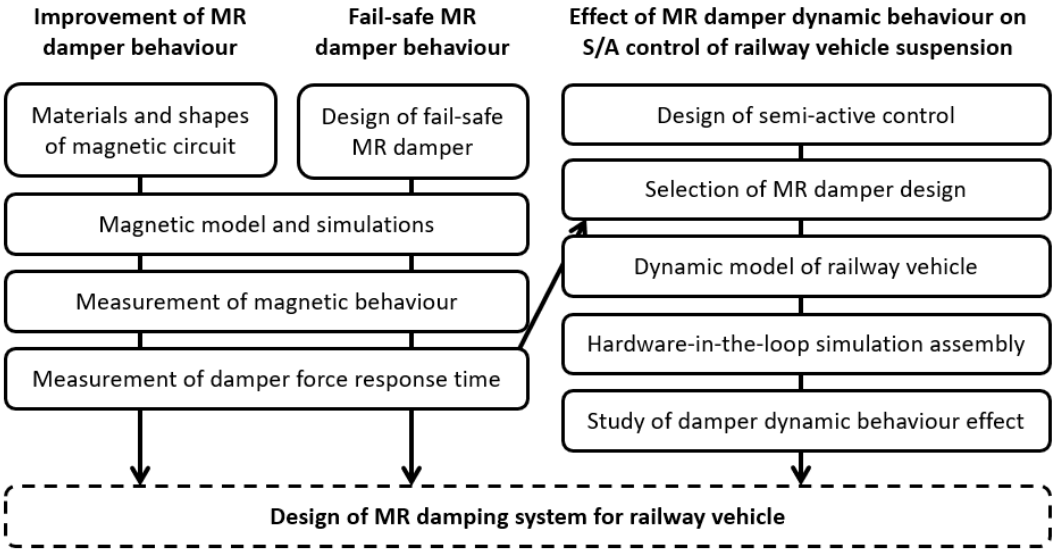

Fig. 5-1 Scheme of thesis workflow.

5.1 Improvement of Damper dynamic behaviour

5.1.1 Geometry of MR valve

The geometry of a simulated and tested MR valve is identical for all variants, see Fig. 5-2. The coil has 120 turns.

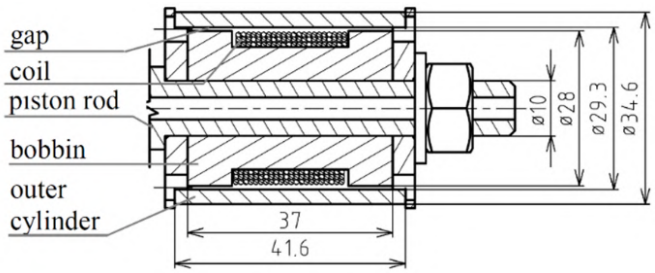

Fig. 5-2 Geometry of the MR valve used for simulation and testing [111].

5.1.2 Model for transient magnetic simulations

A simulation model was created in Ansys Electronics Desktop 2016.1—Electromagnetic Suite 17.1. The output of the simulation is a response of the magnetic flux density to the electric current (step signal) in the gap. The 3D model had to be used to simulate grooved variants (shape approach) that could not be simulated by 2D symmetry. Fig. 5-3 shows the constituent components of the model. All simulations for response time determination were performed with MRF in the gap.

The boundary conditions were set as follows:

a) electrical insulation between the coil and core and between the coil and piston rod;
b) normal magnetic flux passing through the plane of symmetry (plane x–z);
c) coil as "stranded" with 60 turns (1/2 of the total number of turns). The excitation was an electric current step with a rising edge duration of 0.3 ms.

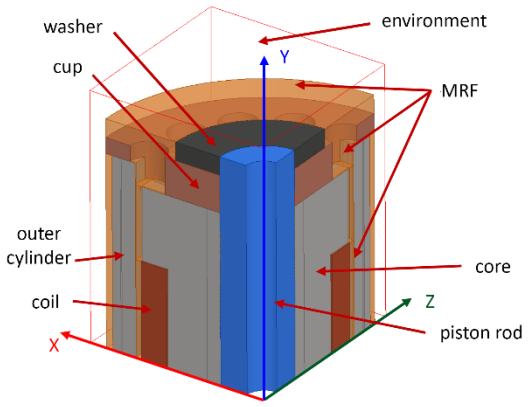

Fig. 5-3 Axis and plane symmetry of the model [111].

5.1.3 Materials for the magnetic circuit

The following materials have been selected for testing:

- Cutting steel 11SMn30
- N87 ferrite
- Sintex SMC prototyping
- Stainless steel AISI 420A
- Pure iron – SLM
- Vacoflux 50

5.1.4 Shape Approach

The shape approach is only used for low electrical resistivity materials, with a long response time without the grooves. The groove intersects the eddy current flow in Fig. 5-4b and prevents the generation of eddy currents in such an extension. The number and shape of the grooves were proposed based on transient analysis to obtain a resulting response time. In a grooved variant, the main contribution to achieving the shorter response time can be attributed to an increase in the total electrical resistance caused by the electric current flowing along the longer path and through places with a much smaller cross-section (Fig. 5-4).

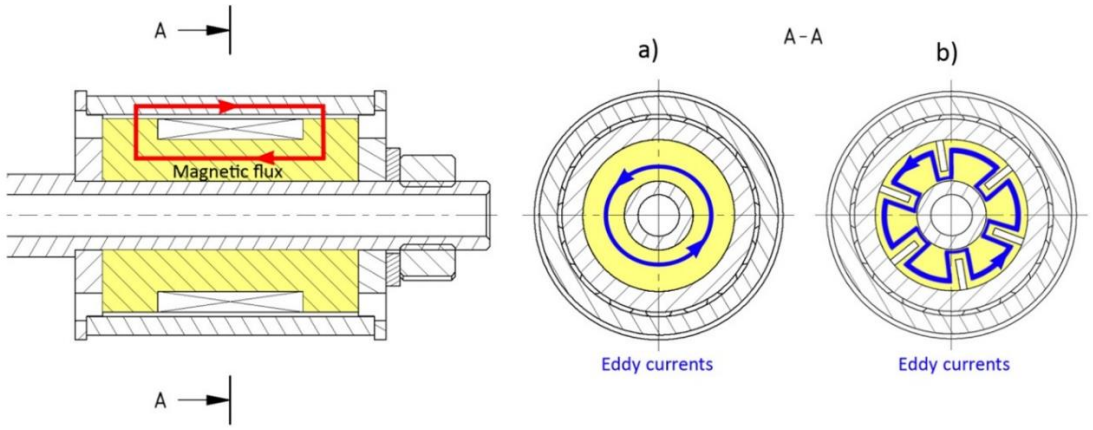

Fig. 5-4 The comparison of eddy current paths in the core (**a**) without grooves and (**b**) with grooves [111].

The final variant was selected from a number of combinations of groove shape and quantity, including groove thicknesses ranging from 0.1 to 0.7 mm, groove depths from 1 to 8 mm, and groove numbers from 4 to 76. The final design has 48 grooves with a thickness of 0.35 mm and a depth of 7.5 mm.

5.1.5 Measurement of the magnetic flux density

This measurement was carried out to verify the simulation model. The output of the model was a time history of the magnetic flux density as the magnetic field was switched on and off. The simulations were calculated with the MRF in the gap. However, in order to compare the model and the measurement, the air in the gap was used instead of the MRF, as the measurement with the MRF cannot give accurate results. Two types of measurements were carried out with almost identical configurations:

a) static properties of the magnetic circuit (dependence of the magnetic flux density on input current to the coil;
b) the response of the magnetic flux density to the current step.

For response measurements, a patented current controller developed by our team was used instead of the usual power supply [54, 61, 76]. The magnetic flux density was measured

using a teslameter (F.W. Bell 5180) with an ultra-thin transverse probe (STB1X-0201, F.W. Bell). The magnitude of the electric current in the coil is obtained by measuring it with a Fluke i30 current clamp. These two signals and the voltage across the coil contacts are recorded and processed at a sampling frequency of 200 kHz by a Dewetron USB-50-USB2-8 front-end connected to a laptop.

5.1.6 Measurement of F-v curves and damper force response time

The tested MR valve was purposely designed to work in a hydraulic tube and can generate a damping force for the evaluation of the overall response time of an MR device, including the response of the electric circuit, magnetic field, and MR fluid (Fig. 5-5).

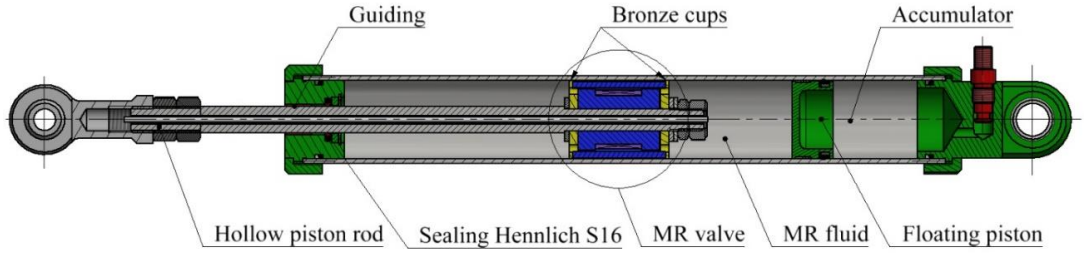

Fig. 5-5 Testing device for measuring an overall damper force response time [111].

A hydraulic damper tester from Inova was used for the measurements. The damping force was measured by an HBM U2AD1/2 load gauge, the position of the piston rod by a VLP15$A150 resistance sensor, and the current was calculated from a voltage drop across a 0.1 Ω power shunt. These three signals were recorded and processed at a sampling frequency of 50 kHz using a Dewetron Dewe-800 analyser. The piston velocity was calculated by derivation of the piston position. First, the *F-v–I* map (dependence of damping force on piston velocity for different electric currents) was measured. From this dependency, the dynamic range of the valve can be determined. For the transient measurement, the same current controller and hydraulic piston controller were used to generate the step signal for a magnetic flux density measurement.

The damper was excited by a triangular position signal, ensuring that the velocity remained constant throughout the stroke. The current was alternately switched on and off after two strokes. The exact moment of switching on and off was in the middle of the stroke.

5.2 Response time of fail-safe MR damper with permanent magnet

5.2.1 Design of MR damper with permanent magnet

The MR damper is similar in design to the previous case (Fig. 5-5). The design differs in that the internal diameter of the cylinder is expanded to 40 mm. The MR damper also differs in the design of the MR valve, which is adapted to accommodate a permanent magnet, see Fig. 5-6. The piston unit consists of a core (1, 2), outer cylinder (3), plates (4), piston rod (5), permanent magnets (6), and an electromagnetic coil (7). The damper was filled with 200 ml of MRF Lord MRF 132-DG and pressurised to 30 bar.

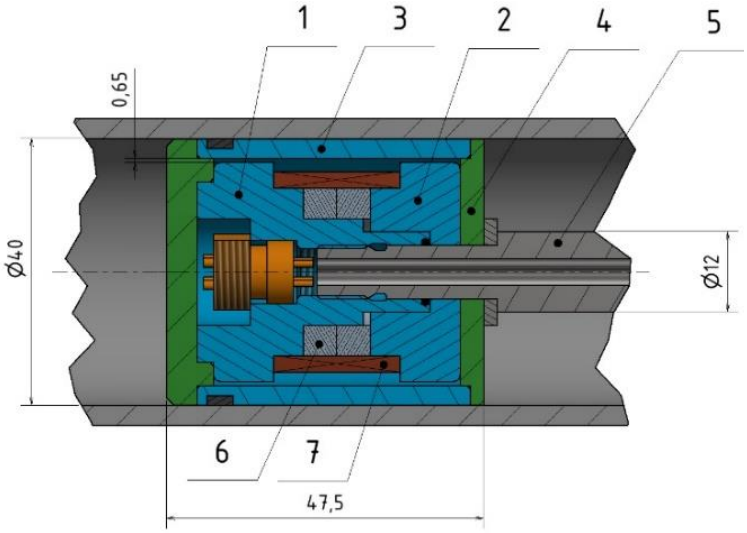

Fig. 5-6 The detail of the MR valve with permanent magnet [112].

The wire of the electromagnetic coil was connected to the connector integrated into the piston rod. The magnetic circuit (parts 1, 2, 3) was made of cutting steel (11SMn30 with a carbon content of less than 1%). This steel was chosen mainly because of the acceptable price. It would be advisable to use this steel for the cores in series production (provided, of course, that the transient behaviour of the valve is acceptable). Two neodymium permanent magnets in the form of a ring 25x16x5 mm class N42 were used. An electromagnetic coil was wound by 190 turns of copper wire with a diameter of 0.5 mm.

Fig. 5-7 shows the main idea of the working principle of the damper with the magnet. In the case of the positive polarity of the electric current $+I$, the magnetic flux density in the gap is $B_{max} = B_{mag} + B_{coil}$. In the case of the negative polarity of the electric current $-I$, the magnetic flux density in the gap is $B_{min} = B_{mag} - B_{coil}$. In the case of no electric current, the magnetic flux density in the gap is $B_{fail} = B_{mag}$.

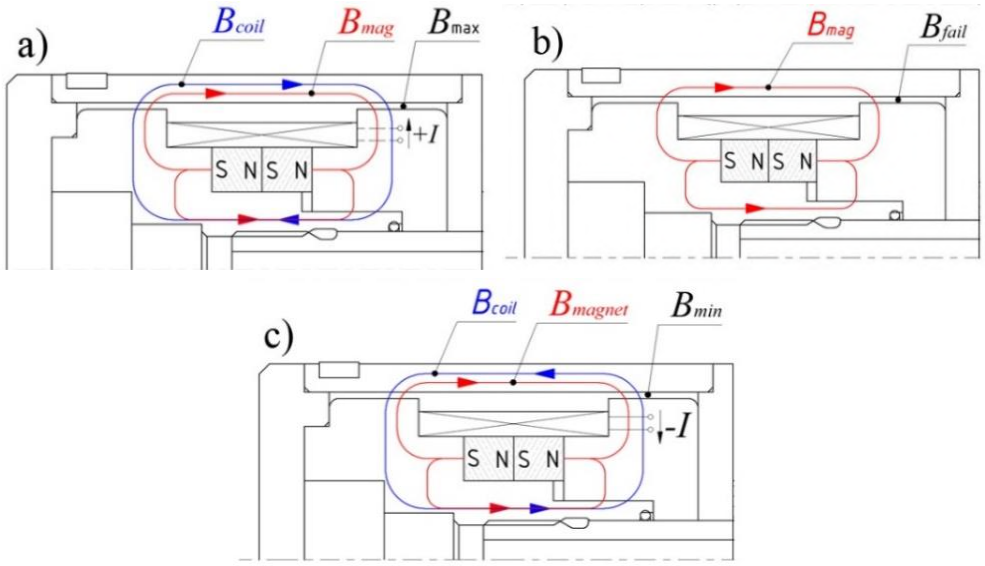

Fig. 5-7 The main principle of MR valve function with permanent magnet;
a) current +I, b) no current, c) –I current [112].

5.2.2 Magnetic model

The FE magnetic model is necessary to calculate the magnetic circuit properties, including significant non-linearities (magnetisation curve, magnetic hysteresis, etc.). The analytical approach is significantly inaccurate due to the complexity of the model. The Ansys Electronics Desktop 2018 with a co-simulation of Ansys Twin Builder 2018 was used for the presented models. The magnetorheological valve in the damper was assumed to be asymmetric about the centre line Z in a cylindrical coordinate system. The simplified geometry of the MR valve for magnetic simulation is shown in Fig. 5-8.

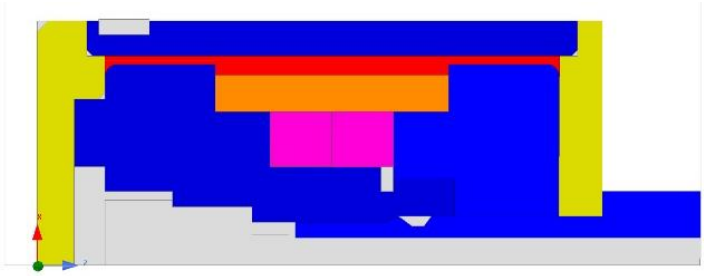

Fig. 5-8 Simplified geometry of MR valve for the magnetic model; steel 11SMn30 (blue), MR fluid or Air (red), bronze (yellow), NdFe42 magnet (pink), copper (orange) and air surrounding (white) [112].

The virgin and hysteresis magnetization curves were experimentally determined for the sample of this steel using the Remagraph C-500 system. The measured hysteresis loop determined the coercivity and remanence: H_c = 427 A/m and B_r = 1.05 T.

The electrical bulk conductivity used was σ = 5.8 MS/m. The lids were made of bronze with relative permeability $\mu_r = 1$ and electrical bulk conductivity σ =10 MS/m. The MRF 132-DG

was used for the models. The magnetic hysteresis of the MR fluid was neglected. The vector hysteresis modelling feature available in the Ansys system was applied to the electromagnetic model of the MR valve. A more detailed description of this model can be found in the publication [53]. The curve fit to the experimental hysteresis data for the steel 11SMn30 was created by the Ansys software. The agreement is good except at low magnetic field strengths. The NdFe42 permanent magnet was used in the model. The exact geometry and type of magnet were chosen according to market availability.

The proposed magnetic model was used in two cases with different time scales to determine the quasi-static and transient behaviour of the magnetic circuit.

Quasi-static magnetic model

This model was used to determine the hysteresis behaviour of a magnetic circuit in two configurations: with air in the gap and with MRF in the gap. The effect of eddy currents was neglected due to the slow changes in electric current. The setting of this model was used in these configurations:

a) magnetic circuit with the electromagnetic coil (air in the gap),
b) magnetic circuit with electromagnetic coil and magnet (air and MRF in the gap).

This model allows us to design a proper geometry of the magnetic circuit to maximise fail-safe magnetic flux and minimize the effect of the magnet in the gap in the off-state.

Transient magnetic model

This model calculates the magnetic induction (flux density) course in the gap on step current input. The response times are determined from this data. The final value of the electric current (T_c) was reached at T_c = 0.2 ms. It is therefore assumed to be the step control signal in the simulation. This value was chosen based on previous experimental experience. The electric current waveforms were different for different settings of this simulation. The constant simulation time step was set to 0.2 ms. The mesh was generated with refinement at the edges of the magnetic circuit due to the rapid generation of eddy currents in these areas. The setup of this model was used in these configurations:

a) magnetic circuit with electromagnetic coil and MRF in the gap,
b) magnetic circuit with an electromagnetic coil, permanent magnet, and air in the gap,
c) magnetic circuit with an electromagnetic coil, permanent magnet, and MRF in the gap.

5.2.3 Measurement setups of magnetic behaviour, F-v-I map and force response time

To measure the behaviour of the manufactured MR valve and the entire MR damper, the same measurement setups will be used as in the previous research, see chapters 5.1.5 and 5.1.6.

Four types of magnetic flux density measurements will be carried out with almost identical configurations of measuring setup:

a) quasi-static properties of the magnetic circuit with permanent magnet and electromagnetic coil;
b) quasi-static properties of the magnetic circuit with electromagnetic coil;
c) response time of the magnetic flux density on the electric current step in configuration with permanent magnet and electromagnetic coil;
d) response time of the magnetic flux density on the electric current step in configuration with an electromagnetic coil.

The F-v-I map will be measured for constant electric currents 1A, 2A, 0A(+) and with opposite polarity -1A, -2A, 0A(-). Piston velocity was calculated from piston position. The F-v-I map was calculated from the measured data by selecting the zero acceleration points (mid-stroke).

The transient response was measured for piston velocity 0.2 m/s and electric currents 0.5A, 1A, 1.5A, 2A, and the same values with opposite polarity. The rise and drop of the force was measured 5 times, and the response time was determined as the average of these values for each electric current.

5.3 Effect of MR damper behaviour on railway vehicle lateral damping

5.3.1 Semi-active control

To evaluate the effect of the force response time on different control strategies on railway vehicle lateral damping, this research used passive mode and three well-known semi-active algorithms: two-state Skyhook (SH-2) [98], Skyhook linear (SH-L) [99], two-state Acceleration Driven Damper (ADD-2) [103] and a newly designed: Acceleration Driven Damper Linear (ADD-L).

This variant of the Acceleration Driven Damper algorithm has not yet been described in the literature. The ADD-2 algorithm has been modified to a linear form according to the Skyhook linear pattern:

$$I = \begin{cases} sat\left(\frac{I_{max} \cdot \dot{y}_2}{(\dot{y}_2 - \dot{y}_1)}\right), & \ddot{y}_2(\dot{y}_2 - \dot{y}_1) \geq 0 \\ I_{min}, & \ddot{y}_2(\dot{y}_2 - \dot{y}_1) < 0 \end{cases} \quad (13)$$

where:

I	[A]	required electric current,
I_{max}	[A]	maximal electric current
I_{min}	[A]	minimal electric current
$\ddot{y}_2$	[ms^{-2}]	carbody lateral acceleration
$\dot{y}_2$	[ms^{-1}]	carbody lateral velocity
$\dot{y}_1$	[ms^{-1}]	bogie frame lateral velocity

sat denotes that $I \in [I_{min}(v),\ I_{max}(v)]$.

Semi-active algorithms Mix-SH-ADD [101] and Power Driven Damper [104] were also used in the initial phase of the research. However, their results were unsatisfactory, so they are not listed below.

5.3.2 Magnetorheological damper

In this study, a real MR damper of the similar design as in the previous studies is used instead of the secondary lateral passive damper. The magnetic circuit is made of SMC. Thanks to the design modification and the expansion of the internal diameter of the cylinder to 40 mm, the damper has a higher dynamic range than the MR damper used in Research paper I [111]. This design change slightly increase the damper force response time.

The maximum damping force of this damper is 1 900 N (0.2 m/s), and the dynamic force range at a piston velocity of 0.1 ms^{-1} is dr = 7.6. The response times for damper force rise τ_{63}, and for damper force drop τ_{63} at unit-step electric current rise and drop are determined from the measured data in this paper. The damper force response time was measured at τ_{63} = 1.8 ms for force rise and τ_{36} = 1.1 ms for force drop.

5.3.3 Lateral vehicle model with 2 degrees of freedom

A lateral motion model of a railway vehicle with 2 degrees of freedom has been developed. The model represents one wheelset, half of the bogie frame and a quarter of carbody. The model layout is shown in Fig. 5-9. The model parameters are derived from a four-axle locomotive weighing 90 tonnes. The lateral damper used is reduced in scale. Therefore, the parameters of the vehicle model are also reduced by a ratio of 1:5 (Tab. 5-1).

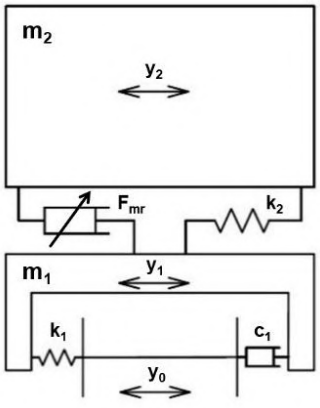

Fig. 5-9 Railway vehicle simplified model schema [113]

Tab. 5-1 Model parameters

Parameter	Symbol	Original	1:5 scale
half bogie frame weight	m1	5000 kg	1000 kg
quarter carbody weight	m2	13,750 kg	2750 kg
wheelset-bogie frame bond stiffness	k1	10 kN/mm	2 kN/mm
bogie frame-carbody bond stiffness	k2	1 kN/mm	0.2 kN/mm
wheelset-bogie frame bond damping	c1	10 kNs/m	2 kNs/m

5.3.4 Hardware-in-the-loop simulation

HIL simulation is used to bring simulation closer to reality. This simulation allows to study the effect of the damper response time and the dynamic range on the S/A control on a real MR damper without the need for a real vehicle or physical model.

The damper is mounted in a hydraulic pulsator, controlled by a control system (dSpace RTI1104 in this case). A virtual railway vehicle model was created in Matlab/Simulink and transferred to the Control Desk program that controls the dSpace system. Based on the measured damping force, the simulation calculates the virtual position of the sprung and unsprung masses (y_2 and y_1) in real time. The calculated Control signal 1 with the damper stroke $y_2 - y_1$ is sent to the hydraulic pulsator, which excites the MR damper. The Control signal 2 with the desired current is also sent in real time to the Current controller, which excites the MR damper.

The Current controller is a self-made device operating in analogue voltage input - analogue current output mode [54]. The damping force data is entered for the virtual model.

5.3.5 Test cases and evaluation methods

Four case studies will be reported:

1) the influence of the force rise response time,
2) the influence of the force drop response time,
3) the influence of the force rise and drop response time together in real proportions,
4) the influence of the dynamic force range.

The influence of the response time was monitored from the shortest possible response time determined by the damper design (τ_{63} = 1.8 ms and τ_{36} = 1.1 ms, see section 5.4.2), to response times of 56 ms. The longer force response times, then 1.8 ms and 1.1 ms, were created using the Current controller. The required dynamic force range (DR) will be set by I_{min}. It was found that S/A algorithms have the best performance when the maximum electrical current is I_{max} = 2 A, and the passive damping performed best when the current is I = 0.5 A. These currents were, therefore, used in HILS.

Above all, the lateral acceleration of the carbody is the main measure of ride comfort. The overall RMS of lateral acceleration in relevant track sections will be used to evaluate the comfort of the railway vehicle in on-track tests. This evaluation is also used by the EN 14363 standard [114].

6 RESULTS AND DISCUSSIONS

6.1 Research paper I

The first paper deals with approaches to improve the behaviour of the MR damper. Based on the material and the shape approach, several valve variants of the MR damper were designed and manufactured. Their transient behaviour was investigated by virtual simulation on a magnetic model and verified by measurements.

The findings of this study about magnetic flux density in MR damper valves, based on measurements, are as follows:

MR valves made from ferrite materials have the fastest magnetic flux density response time of the variants studied (0.31 ms). Ferrite material also has the lowest remanence of 3 mT. However, only a low magnetic flux density can be achieved (134 mT). Another disadvantage of ferrite is its price and poor machinability.

Valves made from Sintex (SMC) are as fast as those made from ferrite (magnetic flux density response time of 0.35 ms) despite having a lower electrical resistivity than ferrite. The magnetic flux is 152 mT, which is significantly higher than that of ferrite. This results in a higher dynamic force range.

The SLM sample (with and without the grooves) shows the highest magnetic flux density (221 mT with grooves and 230 mT without grooves) due to the high magnetic saturation limit of the pure iron powder. The response time of the valve without grooves is 2.21 ms, which is the longest of all the samples measured. This was expected due to the lowest resistivity of pure iron. **On the contrary, the magnetic flux response time of the grooved version was about 5 times shorter** (0.49 ms)**.**

Vacoflux variants have a high magnetic flux density of 206 mT, higher than steels, and a magnetic flux density response time of 1 ms. Six grooves in the damper core reduce the response time by 23%.

The AISI 420A stainless steel valve without grooves has a response time of 0.93 ms and a high magnetic flux density of 180 mT. Unfortunately, it has the highest remanence of the variants tested – 33 mT. High remanence reduces the dynamic force range of the valve, which is disadvantageous for fast current control.

For the 11SMn30 cutting steel sample, 48 grooves must be fabricated to achieve the same magnetic flux response time as the Sintex (SMC) valve (0.35 ms). The magnetic flux density is 187 mT, which is higher than that of the Sintex valve but slightly lower than that of the pure iron valve produced by SLM.

There is some difference between the simulated and measured values. This is probably due to the fact that the input B-H curves and electrical resistivity of the materials were taken from datasheets. Previous research has shown that the exact composition of alloys and, thus, *B-H* curves can differ for a smelting batch. In addition, heat treatment and mechanical loading can change the magnetic and electrical properties. B-H curves and the resistivity of the materials used in the circuit must be measured individually to obtain more accurate results from the model. However, the model presented is an effective tool for determining the transient behaviour of a magnetic circuit.

The findings of this study about damper force response time and dynamic range, based on measurements, are as follows:

The force response times of MR valves made of solid parts correspond with their electrical resistivity. A higher electrical resistivity results in a shorter force response time.

Grooves rapidly reduce the response time of low carbon steel MR valves. For steel 11SMn30, the response time of damper force using a grooved piston has been reduced 6 times to 1.74 ms, while the dynamic force range has been reduced by only 12 % to 5.

The force response course is similar to that of first-order dynamic systems only for pistons made of solid steel. In this case, the secondary response time is approximately 3 times longer than the primary response time. The secondary response time for pistons made of materials with high electrical resistivity is much shorter. The response of the force follows the course of the electric current with some delay.

The simulations for grooved pistons or pistons made of materials with high electrical resistivity predicted a significantly shorter magnetic field response time (basically the same as the current response time). The difference between the measured and simulated values can be explained by the response time of the MR fluid itself. There is always a time delay of approximately 0.6 ms between the beginning of the electric current rise (or drop) and the force rise (or drop). This phenomenon is practically independent of piston material and velocity.

The best dynamic range is achieved with the piston made of Hiperco/Vacoflux - dynamic range of 6.4. This reflects the fact that Hiperco/Vacoflux has a much higher magnetic saturation limit than other materials. Unfortunately, the Hiperco/Vacoflux valve has a long force response time of 3.57 ms due to the low electrical resistivity of the material. A significant reduction in force response time can be expected using the Hiperco/Vacoflux valve with grooves.

In the case of pistons with a force secondary response time of up to 3 ms, the course of force exhibits quite heavy oscillations. This is probably due to the compliance of the MR fluid and other parts of the MR damper. This problem was explained by Kubík et al. [53].

6.2 Research paper II

The second paper deals with the transient behaviour of a fail-safe MR damper with a permanent magnet. A fail-safe valve for the MR damper was designed, manufactured and assembled. Its transient behaviour was investigated by virtual simulation on a magnetic model and verified by measurements. The findings of this study are as follows:

The magnetic flux density in the gap at zero electric current produces approximately 1/4 – 1/3 of the maximum magnetic flux density and is dependent on magnetisation history due to the hysteresis behaviour of the magnetic circuit material. The magnetic flux density at zero current is in the range of 127-178 mT, while the maximum magnetic flux density is 483 mT (measured with MRF in the gap).

The magnetic flux density in the gap decreases to the off-state much faster than it increases to the on-state. This is probably due to the effect of the permanent magnet.

The fail-safe damping force at zero electric current also depends on the magnetisation history and is approximately 1/3 of the maximum damping force. The difference in the fail-safe forces is due to the hysteresis behaviour of the magnetic circuit. The damping force at zero current is in the range of 505-592 N, while the maximum magnetic flux density is 1850 N at a piston velocity of 0.1 ms^{-1}. So, the force range in fail-safe mode is approximately 90 N, which is approximately 5 % of the maximum damping force, which is acceptable.

The dynamic force range of the fail-safe MR damper achieved a value of 8.5, which is similar to the common MR damper design [61]. The dynamic range is relatively large compared to previous research due to the use of cutting steel and a more advanced valve core shape. Such a dynamic range should be sufficient for effective S/A control. The maximum damping forces are also comparable.

The increase of the damping force from the fail-safe state to the on-state (positive polarity of the electric current) is faster than the decrease from the on-state back to the fail-safe state. The primary response time of the damping force is 7 ms for the electric current step from 0 A to 2 A (on-state) and 12 ms for the electric current step from 2 A to 0 A. **The response time of the force rise from the fail-safe state to the on-state is strongly dependent on the magnitude of the electric current.** The primary response time of the damping force is 7 ms for the electric current step from 0 A to 2 A but 17 ms for the electric current step from 0 A to 0.5 A

The increase of the damping force from the off-state (negative polarity of the electric current) to the fail-safe state is faster than the decrease from the fail-safe state back to the off-state. The primary response time of the damping force is 1.5 ms for the electric current step from -2 A (off-state) to 0 A and 2 ms for the electric current step from 0 A to -2 A. The same response time applies to the current step from -1 A to 0 A and back from 0 A

to -1 A, so the damper behaviour in these cases is independent of the magnitude of the electrical current.

It is also clear that the changes between off-state and failsafe forces are significantly faster than changes between on-state and failsafe forces.

Force response time is 1.5 ms for the force rise from off-state to fail-safe force and 12-14 ms for the force drop from on-state to fail-safe force. So, with the exception of the current of 0.5 A, the rise from the fail-safe force to the maximum force is faster than the drop back from the maximum force to the fail-safe force, which is unexpected. The effect of the permanent magnet is probably responsible for this unusual damper behaviour.

The initial time delay of 0.5 - 0.8 ms between the course of the force and an electric current was observed. This delay wasn't observed when measuring the magnetic flux density. Therefore, this delay is probably caused by the compliance of the hydraulic system or the response time of the MR fluid.

Virtual simulations show that the magnetic flux density response time is very similar for the MR valve without magnet and the MR valve with magnet (from the fail-safe state to the on-state). **So, it can be stated that the permanent magnet does not worsen the transient behaviour of the MR damper.**

The response time determined from the magnetic model fitted well with the experimental force data of the MR damper. Therefore, transient magnetic simulation is an effective tool for determining the dynamic behaviour of the MR damper.

6.3 Research paper III

The third paper deals with the MR damper dynamic behaviour and its influence on the efficiency of four algorithms for semi-active control of railway vehicle body. A simple 2-degree-of-freedom model of the lateral motion of a railway vehicle body was used for the study. The natural frequency of the sprung mass in this model was 1.35 Hz, and the excitation signal contained frequencies up to about 2 Hz. The hardware-in-the-loop simulation was used for a more realistic simulation. It has been confirmed that S/A control of MR dampers can significantly reduce carbody vibrations and improve passenger comfort. For the selected dynamic system, the selected excitation method and four selected control strategies, the findings of this study are as follows:

The force drop response time is more important than the force rise response time for S/A control performance. The two-state Skyhook algorithm is most affected by this. The efficiency of the algorithm decreases rapidly as the force drop response time increases.

The ideal response time for both the drop and the rise is around τ = 8 ms. And it makes no sense to reduce the response time to less than this value. In this research, an MR damper with a response time of τ_{63} = 1.8 ms was used, but this damper was scaled 1:5. The original scaled damper would have a longer response time. However, the response time of τ_{63} = 8 ms is also achievable with a large MR damper for railway vehicles [108].

The newly developed Acceleration Driven Damper Linear algorithm is best suited to damping the lateral movement of railway vehicle body. Under ideal conditions, vibrations were reduced by 34 %. Interestingly, the ADD-2 and ADD-L algorithms work best with a force-drop response time of around τ_{36} = 45 ms. This is probably because at this response time the function of the ADD algorithms is similar to the function of the SH-L algorithm. However, a real MR damper does not have such a long response time. Therefore, it is necessary to slow down the force drop by software.

Acceleration Driven Damper (two states) achieves the same effectiveness as Skyhook Linear. However, ADD is easier to implement in real vehicles. Skyhook works based on the velocity of the sprung mass. It can be obtained by integrating the acceleration of the sprung mass, but integration causes many problems. In contrast, the Acceleration Driven Damper works directly on the acceleration of the sprung mass, so there is no problem with integration, and the control can work better.

The semi-active algorithms work well with a damper dynamic range of 7.6, which is the dynamic range of the damper used. However, increasing the dynamic range for better results would be advisable. **The dependency of the efficiency of the algorithm on the dynamic range suggests that the ideal dynamic range can be around 10**, and after that, efficiency will rise only slowly.

In this research, the damper was mounted in the pulsator without silentblocks, which is probably impossible in practice. However, the soft mounting of the damper will worsen the hysteretic behaviour of the system and reduce the effectiveness of the S/A control. Silentblocks of different stiffness are manufactured in the industry. It would be appropriate to investigate the dependence of the S/A control effectiveness on the stiffness of the damper mounting and to determine what stiffness of the silentblock is acceptable for the S/A control. This will be part of the follow-up research.

materials

MDPI

Article

Novel Approaches to the Design of an Ultra-Fast Magnetorheological Valve for Semi-Active Control

Zbyněk Strecker [1,*], Filip Jeniš [1], Michal Kubík [1], Ondřej Macháček [1] and Seung-Bok Choi [2,*]

[1] Institute of Machine and Industrial Design, Faculty of Mechanical Engineering, Brno University of Technology, Technicka 2, 616 69 Brno, Czech Republic; Filip.Jenis@vutbr.cz (F.J.); Michal.Kubik@vutbr.cz (M.K.); Ondrej.Machacek@vutbr.cz (O.M.)

[2] Department of Mechanical Engineering, The State University of New York at Korea (SUNY Korea), Incheon 21985, Korea

* Correspondence: Zbynek.Strecker@vutbr.cz (Z.S.); seungbok.choi@sunykorea.ac.kr (S.-B.C.); Tel.: +420-541-143-216 (Z.S.); +82-10-3109-7329 (S.-B.C.)

Abstract: This article presents a list of suitable techniques and materials leading to the design of an ultra-fast magnetorheological (MR) valve. Two approaches for achieving the short response time are proposed: (a) by means of material, and (b) by means of the shape. Within the shape approach, the revolutionary technique of 3D metal printing using a selective laser melting (SLM) method was tested. The suitability of the materials and techniques is addressed based on the length of the response time, which is determined by the FEM. The simulation results determine the response time of the magnetic flux density on the step signal of the current. Subsequently, the response time is verified by the measurement of the simple magnetorheological valve. The following materials were tested: martensitic stainless steel AISI 420A (X20Cr13), cutting steel 11SMn30, pure iron for SLM, Sintex SMC STX prototyping material, ferrite N87, and Vacoflux 50. A special technique involving grooves was used for preventing eddy currents on materials with a high electrical conductivity. The simulation and experimental results indicate that a response time shorter than 2.5 ms can be achieved using materials such as Sintex SMC prototyping, ferrite N87, and grooved variants of metal pistons.

Keywords: magnetorheological valve; response time; eddy currents; magnetic simulations; SMC material

Citation: Strecker, Z.; Jeniš, F.; Kubík, M.; Macháček, O.; Choi, S.-B. Novel Approaches to the Design of an Ultra-Fast Magnetorheological Valve for Semi-Active Control. *Materials* **2021**, *14*, 2500. https://doi.org/10.3390/ma14102500

Academic Editor: Tomáš Plachý

Received: 12 March 2021
Accepted: 6 May 2021
Published: 12 May 2021

1. Introduction

In 1948, Jacob Rabinow discovered a new class of smart materials, currently known as magnetorheological fluids (MRFs) [1]. MRFs are generally made of three basic compounds: micron-sized iron particles, carrier oil, and additives. Immediately upon the application of an external magnetic field, the state of the MRF changes from a fluid to semi-solid or plastic. With the new state, the MRF exhibits a viscoplastic behavior, characterized by the initial stress (yield stress) that varies based on the magnitude of the applied magnetic field [2–7].

MRF is most commonly used in dampers, especially in (a) the primary suspension systems of vehicles [8–13], (b) the secondary suspension of driver seats in trucks [14–18], (c) the damping of vibration for seismic activity protection [19–22], or (d) the damping of cable bridge vibrations caused by wind and rain [23,24]. Semi-active control can be easily applied to magnetorheological (MR) dampers. Many research teams simulated semi-active algorithms only on the virtual quarter models or full models of the cars [25–27]. These simulations are working with different phenomenological models of MR dampers. One of the most complex models including the hysteretic behavior of an MR damper is described in paper [28]. The performance of semi-active algorithms depends on a dynamic force range, which should be as large as possible. There are papers [29–31] dealing with the optimal design of an MR valve using finite element analysis (FEA), but they are focused only on maximizing the static magnetic field range in the gap of the damper, and the

dynamic behavior (response time) of the MR damper is not taken into consideration. Lee et al. [32] proposed methods for optimizing the magnetic field range of the MR damper and, also, the dynamic behavior. However, the proposed MR valve exhibited a response time between 28–125 ms, which is too long for use in semi-active car suspension. To secure effective control of the system, the response time of the MR damper should be smaller than approximately 1/10 of the highest controlled frequency of the system. If the response time is longer, the system is not able to react on the change of the damper state and the efficiency is lower [33,34]. Koo et al. [35] measured the transient response of the LORD Motion Master automotive damper. The overall response time of the damper was identified in the range of 15–55 ms. Based on the previous study, Strecker et al. [36] defined three main sources which prolong the response time: (i) MRF, (ii) electrical circuit—especially the coil inductance, and (iii) magnetic circuit. Subsequently, they designed a special current controller, minimizing the response time of the electrical circuit when switching on and also switching off [37] with the overvoltage method. The maximum measured response time caused by the electrical circuit was around 0.5 ms. Goncalves et al. [38] defined the response time of the MRF between 0.45 and 0.6 ms under varying magnetic field strengths at high shear rates. Jolly et al. [39] presented that the chain dynamics response time (rheological response time) of MRF depends on the viscosity of the currier fluid, particle concentration, and magnitude of the applied magnetic field. However, the main source of the overall delay of the damper is caused by the magnetic circuit (around 20 ms for the fastest valve), specifically by occurring eddy currents as a reaction on the extremely fast change in the magnetic field size. The eddy currents are generated in the magnetic circuit, which create the magnetic field acting in the opposite direction to that desired magnetic field [37]. The resulting field is therefore significantly lower. The size of the eddy currents is proportional to the rate of change in the generated magnetic field [40]. The higher the control speed, the more pronounced is the effect of the eddy currents, which greatly extend the final response time [41]. The influence of the eddy currents on the overall magnetic field in the MR device was published in the paper by Maas and Güth [42]. They used a ferrite as a material for the magnetic circuit in their experimental MR clutch and measured the response time between 4.1 and 5.3 ms.

The problem of eddy currents can be solved by two approaches: (a) by means of material, and (b) by means of shape. The material solution is easier but is a compromise between the static and transient efficiency of the magnetic circuit. Materials like ferrites, permalloys, or soft material composites (SMC) generally have lower permeability or a lower magnetic saturation limit compared to pure iron [43,44]. However, they have high electrical resistivity, thus preventing the formation of the eddy currents. Other problems with these materials are their low mechanical strength, low impact resistance, high cost, and in the most cases poor machinability [45]. On the other hand, the material approach is commonly used in electrical engineering for electromagnetic valves or high frequency transformer and inductor cores in switching power supplies [46,47].

The second approach for prevention of eddy current formation is the shape approach [41,44]. For instance, this approach is applied at low frequency transformers using isolated sheets. A MR valve with a magnetic circuit composed of isolated sheets was also published in [48,49]. However, this solution allows the elimination of eddy currents only to a certain extent. For more significant elimination of the eddy currents as well as circuits of complicated shapes, the application of simple sheets is not suitable and it requires the use of complex shaped grooves intersecting the path of the eddy currents [50,51]. This way, the same response time as in the case of the material approach can be achieved. However, the complicated shape of the grooves is practically unmanufacturable by conventional methods because the grooves must also be structured within the core material. For the fabrication of such complex cores, additive technologies can be used, particularly the selective laser melting (SLM) method that allows 3D printing from metal powder [52].

This paper introduces a novel approach to the design of an ultra-fast MR valve based on materials with high electrical resistivity (material approach) or materials with low

electrical resistivity (shape approach). This paper is a follow-up to earlier research made by the author's team, where an ultra-fast MR damper with a magnetic circuit from ferrite was tested [37,53,54]. The low-impact resistance and bad machinability of ferrite prompted more study in the field of materials suitable for use in an ultra-fast MR valve. This paper includes an evaluation of individual approaches on the basis of the length of response time and dynamic force range. A transient simulation of the magnetic circuit was the main tool for material selection or groove designing. The output from the model is the time flow of the magnetic flux density when the electric current is switched on (step signal). From this course, the response time of the magnetic flux density can be determined. The simulation was carried out for six materials of the magnetic circuit with different electric conductivity (material approach) and for two grooved variants (shape approach) for achieving the shortest response time and high dynamic range. The simulated variants were verified by magnetic field measurement. Since the MR valve was purposely designed for use in an MR damper, the response time of the damping force was also measured. The knowledge from this study aims to contribute to the development of the new generation of ultra-fast magnetorheological elements, particularly semi-active controlled MR dampers.

2. Materials and Methods

The geometry of a simulated and tested MR valve is identical for all variants and is shown in the drawing in Figure 1. The coil has 120 turns.

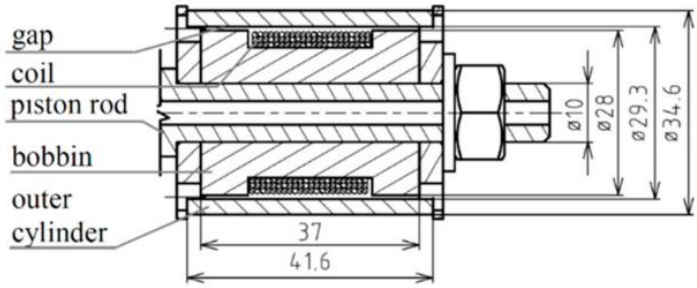

Figure 1. Geometry of the MR valve used for simulation and testing.

2.1. Definition of Response Time

The simplest dynamic system which can serve as an approximation of dynamic behavior of an MR valve is a first-order system. The response of such a system on a step control signal is shown in Figure 2. The response is expressed by time constant τ (primary response time), which determines the time when 63.2% of maximal controlled value is achieved (see Figure 2).

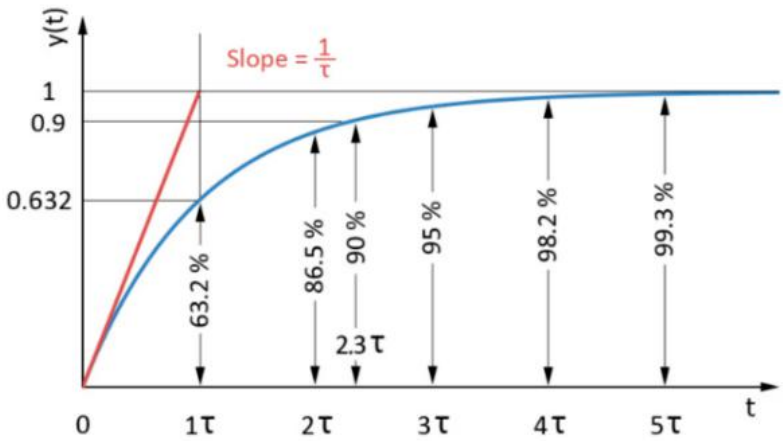

Figure 2. Time response description of the first-order dynamic system to a unit step.

Because the behavior of the MR valve does not always correspond to the first-order dynamic system, the criterion of 90%—secondary response time T_s of maximal controlled value—was also defined. This value is frequently used to determine the transient response of actuators in the industry.

The rate between the secondary and primary response times indicates the level of correspondence between the measured system and its approximation by the first-order dynamic system. The rate between the secondary response time and primary response time for the ideal first-order dynamic system is 2.3 (see Figure 2).

Figure 3 shows the details of the force response time of the MR valve with the primary response time T_p and secondary response time T_s. Figure 3 is used simply for illustration. The data for this figure were obtained without fast current controller.

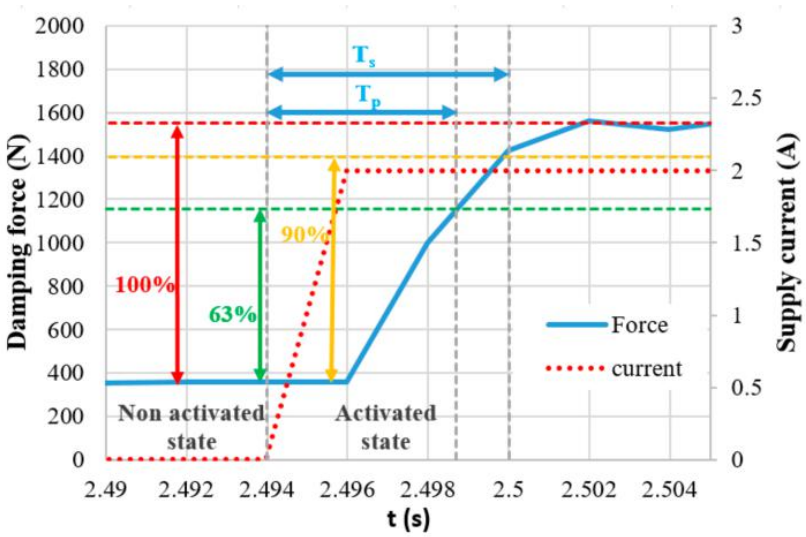

Figure 3. Detail of the damper's force response in electric current step 0–2 A with determination of the primary response time T_p and secondary response time T_s.

2.2. Transient Magnetic Simulation

A simulation model was created in Ansys Electronics Desktop 2016.1—Electromagnetic Suite 17.1. The output from the simulation is a response of the magnetic flux density on electric current (step signal) in the gap.

The 3D model had to be used for simulation of grooved variants (shape approach), which could not be simulated by 2D symmetry. The axis (y-axis) and plane (x–z) symmetry were used within the model creation for reducing the calculation time (see Figure 4). Figure 4 also shows the constituent components of the model. All details such as groove for line of the coil power supply, fillets, or rounds of the corners or chamfer of edges were neglected for simplification of the mesh. All simulations for response time determination were carried out with MRF in the gap; however, for model verification by measurement of magnetic flux density, the air in the gap was prescribed because this measurement could not be realized with MRF. The eddy currents were switched off for faster calculation on electric non-conducting materials or materials with conductivity lower than 1 MS·m^{-1}. This condition is met by MRF (0.01 MS·m^{-1}), environment (vacuum), and the coil which, in the model, is represented by solid conducting material but, in fact, is combined from individual isolated wires. The details of the parts used in the model are listed in Table 1. The outer cylinder and core are fabricated from tested materials, and their properties are mentioned below in a separate table as well as *B-H* curves (Figure 5) for inputs to the model.

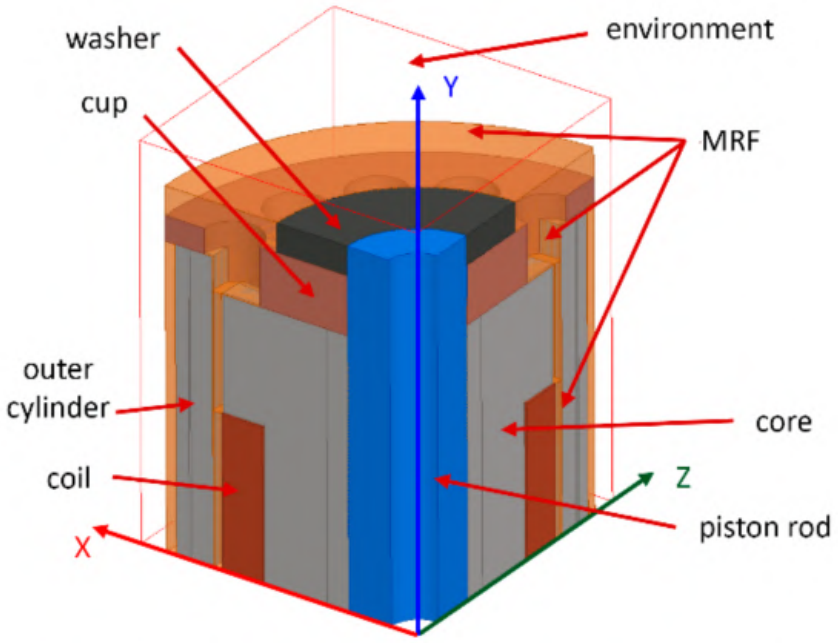

Figure 4. Axis and plane symmetry of the model.

Table 1. Description of materials used in the model.

Part	Material	Electrical Conductivity (MSm^{-1})	Electrical Resistivity(10^{-6} Ω·m)	Eddy Currents	Relative Permeability
Piston rod	S235JRG	6.3	0.16	Yes	*B-H* curve
Washer	S235JRG	6.3	0.16	Yes	*B-H* curve
Coil	copper	58.0	0.02	No	1
Cup	bronze	10.0	0.10	Yes	1
Environment	vacuum	0	-	No	1
MRF	MRF-132DG	0.01	100	No	*B-H* curve

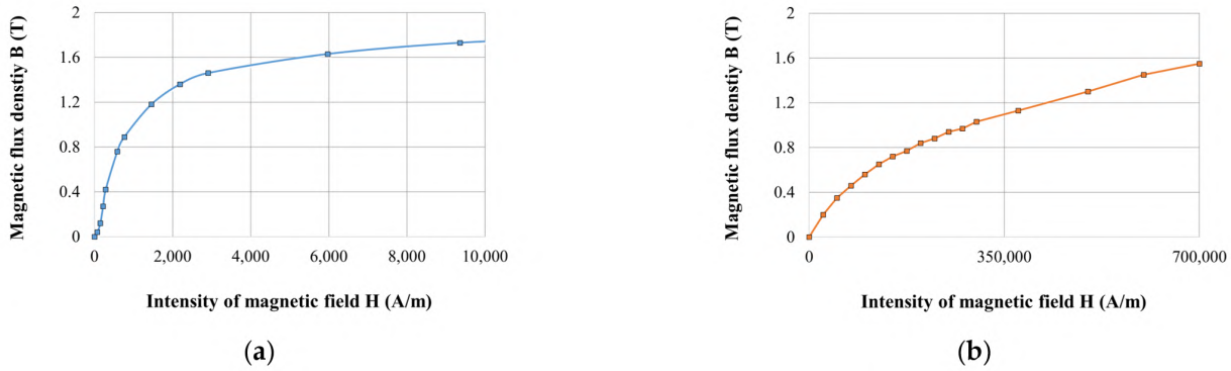

Figure 5. (**a**) *B-H* curve of steel used for piston rod (own measurement); (**b**) magnetorheological fluid LORD MRF-132DG (datasheet).

Boundary conditions were set as follows: (a) electrical insulation between the coil and core and between the coil and piston rod; (b) normal magnetic flux passes through the plane of symmetry (plane x–z); (c) coil as "stranded" with 60 turns (1/2 of total turns). The excitation was an electric current step with a rising edge duration of 0.3 ms. The resulting achieved magnetic flux density B was determined as an average value from the whole volume of the active zone (gap). This is especially important for results of grooved variants

because the magnetic flux density is slightly different for the area in front of the groove and jag.

The finite element mesh was set differently for both the material and the shape approach. The mesh for the material approach was generated as a default mesh with subsequent fining leading to the resulting size, as shown in Table 2. Further fining of the mesh had negligible impact on the result. The final mesh setting of the shape approach is also stated there and described in detail below.

Table 2. The RMS edge length of mesh elements.

Size of Element (mm)	Piston Rod	Coil	Cup	Environment	MRF	Outer Cylinder	Core
Material approach	0.9–1.8	1.6	1.4–1.8	2.2–2.7	0.8–1.1	0.9–1.3	1.5
Shape approach	0.9	1.2	1.3	1.0	0.7	0.9	max 1.35 and 0.8

For the shape approach, the setting of the mesh was more complicated because the thin grooves intersecting the lines of eddy currents have to be modeled. The problem was identified in the model with a high number of thin grooves (0.1 and 0.3 mm thick). On the boundary of the grooves and solid body, the observed elements were too large. This boundary is the most important for the propagation of eddy currents and, therefore, the right set of mesh has a significant influence on the results. This problem was only related to the outer cylinder and core. Finally, the mesh was optimized so that the grooves had elements with a length of only 0.8 mm, and the rest of the part had a length of 1.35 mm. The smaller size of the elements was tested but without any significant change in results. The timestep of the solver was set to 0.1 ms.

2.3. Materials for the Magnetic Circuit

The materials listed in Table 3 were selected for testing, and their corresponding *B-H* curves are plotted in Figure 6. For pure iron, the *B-H* curve of Behanit (ČSN 19 991) was applied because this steel has only 0.01% carbon. Instead of the stainless steel AISI 420A *B-H* curve, the available curve of AISI 430, which has a little lower content of carbon, was used. *B-H* curve of Vacoflux 50 corresponds to the *B-H* curve of HiperCo 50, which should be the identical material offered under another trade name. The *B-H* curve is obtained from the website [55].

Table 3. List of selected materials.

Material	Ultimate Strength (MPa)	Electrical Resistivity (10^{-6} Ω·m)	Magnetic Saturation (T)	Relative Permeability	Machinability	Price
Cutting steel 11SMn30	470	0.17	1.9	1200	very bad	Low
N87 ferrite	30	10,000,000	0.5	6400	very bad	Medium
Sintex SMC prototyping	75	2800	1.45	430	good	High
Stainless steel AISI 420A	760	0.60	1.6	950	good	Low
SLM (pure iron)	460	0.13	1.7	1900	good	High
Vacoflux 50	350	0.42	2.35	3850	good	High

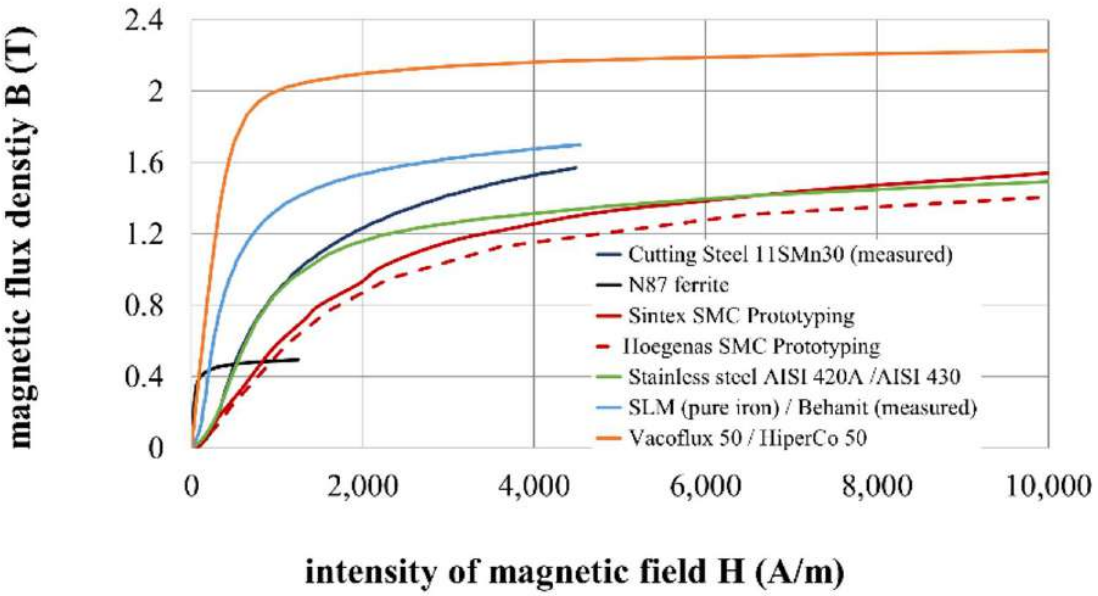

Figure 6. *B-H* curves of materials used in the simulation model.

Cutting steel 11SMn30 was selected as the default material representing common magnetic circuits. This steel has a low carbon content, which leads to low remanence and high magnetic saturation. The steel composition ensures very good machinability and sufficient strength.

Ferrite is mentioned in this paper because it was the first material that was tested as a material for an ultra-fast MR valve. Ferrite has high electrical resistivity but low magnetic saturation, which is limiting and causes low dynamic force range because the coil cannot generate a higher magnetic field in this material. However, ferrite has other and much worse properties—low resistance against impacts or shock loading, significant decrease of magnetic saturation with increasing temperature (25% decrease for a temperature rise from 25 to 100 °C), and bad machinability because of overly high hardness. Grinding with diamond tools is the only suitable process. Therefore, other materials were considered as a replacement for the ferrite.

Sintex SMC prototyping shows relatively high electrical resistivity and very good machinability, which ensures manufacturing by lathe-turning, milling, or drilling. On the other hand, the low permeability leads to high energy consumption when the magnetic field is generated.

Vacoflux was selected as a high-tech alloy with a high magnetic saturation level and, also, relatively high resistivity resulting in low eddy-current generation. The disadvantage of this alloy for real applications is its very high price.

Pure iron was selected as the material for the fabrication of the magnetic circuit by SLM as a second representative of the shape approach. The SLM method enables 3D printing from metal powder. Pure iron has only trace concentrations of carbon and, therefore, it has low remanence, high permeability, and high saturation. After the tuning of the process parameters of the print, the ultimate strength was measured at around 460 MPa, which is an almost identical value to the cutting steel 11SMn30 [56].

Figure 7 compares the electrical current density 0.4 ms after turning the electric current on for core and outer cylinder made of cutting steel material with high electrical conductivity (b) with the core and outer cylinder made of Sintex material with low electrical conductivity (c). The electrical current density in the coil is the same for both cases, but it can be seen that the electrical current density (eddy currents) is not present in the core and outer cylinder made of Sintex material.

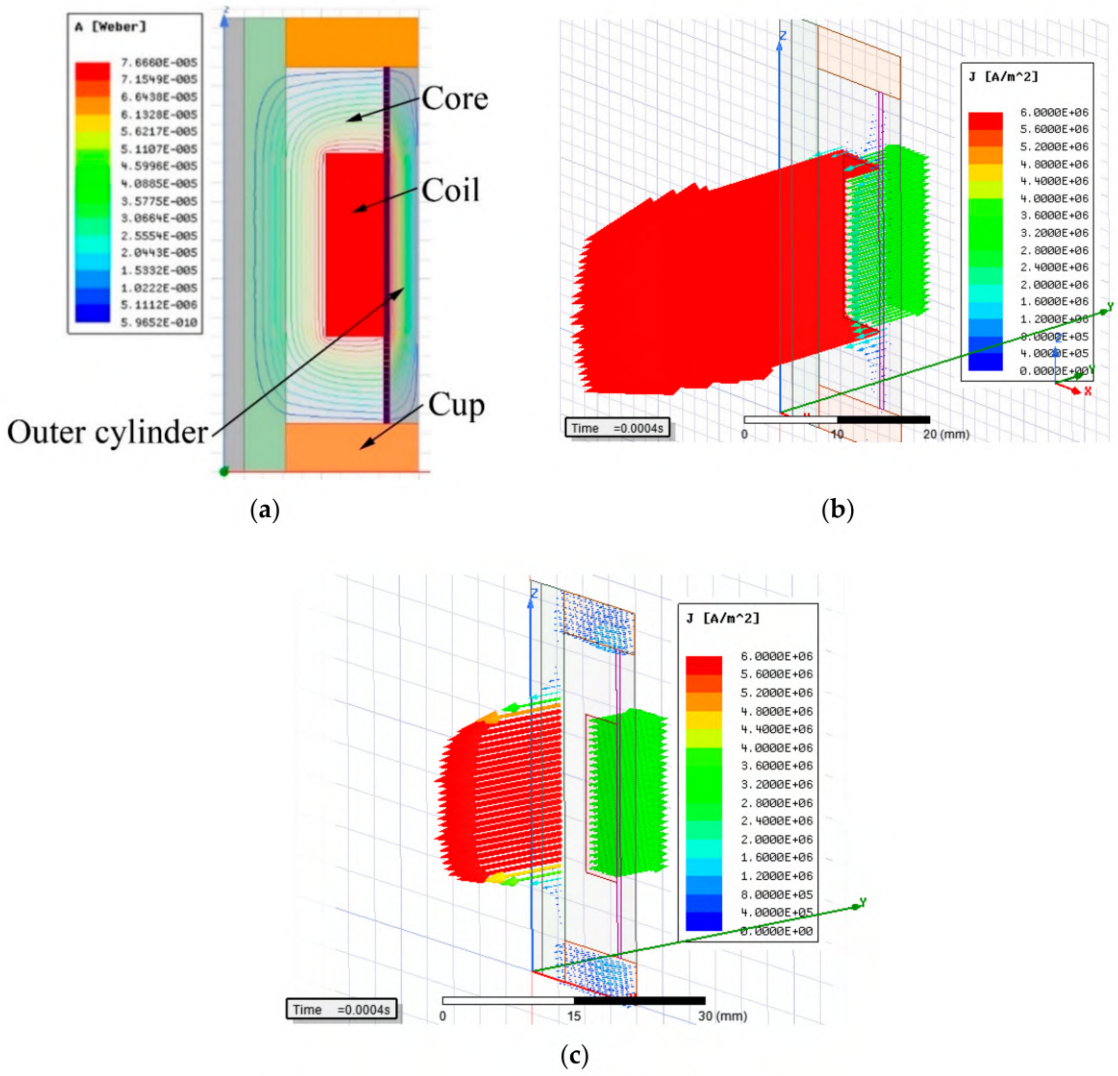

Figure 7. Explanatory example of eddy current generation (**a**) magnetic flux lines in a variant with solid steel core and outer cylinder; (**b**) eddy currents in the variant with solid steel core and outer cylinder; (**c**) eddy currents in a variant with Sintex core and outer cylinder (for comparison) at the identical time and exciting current—eddy currents are generated only in a piston rod which is made from structural steel; however, the rate of eddy currents is much lower because of the much lower magnetic field in this location.

2.4. Shape Approach—Preventing the Eddy Currents by Shaping the Grooves

The shape approach is applied only to materials which have low electrical resistivity and where a response time would be long without the grooves. The orientation of the plane, which includes the dominant dimensions of groove (length and width), should be identical to the plane in which the closed loop of the magnetic line lies (see Figure 7a). Furthermore, the grooves should be placed over the areas with maximal magnetic flux density so that the contribution of the grooves should also be maximal. For simple geometry of the magnetic circuit, the course of magnetic flux lines can be determined using Ampere's law (rule of the right hand); for complex geometry, it is better to use magnetostatic analysis of the solid steel variant (not grooved) of the magnetic circuit (Figure 8a). The groove oriented according to the displayed plane in Figure 7a intersects the flow of the eddy currents in Figure 8b, which prevents the generation of eddy currents in such an extension. However, the number and shape of grooves was proposed based on transient analysis to obtain a resulting response time because its accurate expression by analytical equations is impossible due to the result being influenced by several simultaneously acting phenomena: (i) the electrical resistance

of the overall eddy current path in the magnetic circuit increases with the number and size of grooves—the path is longer (see Figure 8b); (ii) the length and direction of the path for eddy currents is influenced by the local change in conductivity of the magnetic circuit and by direction of the magnetic flux; (iii) direction of the magnetic flux is influenced by a local change in magnetic resistivity caused by the presence of the grooves; (iv) the magnitude of the magnetic flux is influenced by local magnetic saturation of the material around the grooves. However, in a grooved variant, the main contribution for achieving the shorter response time can be attributed to an increase in the total electric resistance caused by the flow of the electric current along the longer path and through places with a much smaller cross-section (see Figure 8).

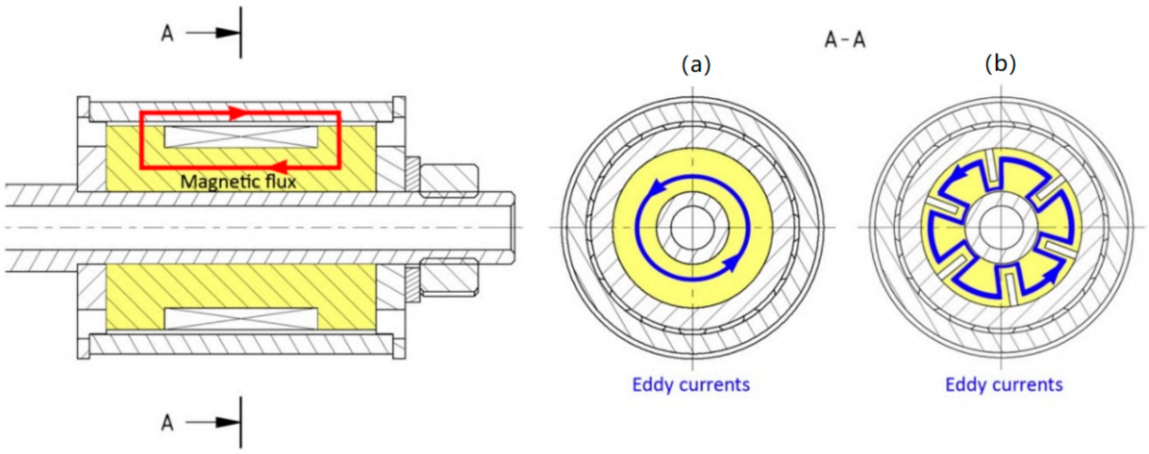

Figure 8. The comparison of eddy current paths in the core (**a**) without grooves; and (**b**) with grooves.

Since induced electric voltage based on Faraday's law remains the same at grooved and full variants due to identical supply to the coil, the eddy currents must be reduced due to the increasing resistance. It is important to note that the grooves will almost not decrease magnetic conductivity because they do not intersect the magnetic flux lines and almost do not decrease the effective cross-section of the circuit in the direction of the magnetic flux lines. Only some local changes around the grooves will occur. The exact quantification of the number and shape of grooves on the response time of the magnetic flux density in the gap cannot be calculated by any analytical equations. Therefore, the magnetic 3D FEM model must be used.

In simulation, the influence of a grooved core and outer cylinder was discovered separately, due to the reduction in calculation time. If any groove shape leads to a decrease in response time with a grooved core or outer cylinder, the same trend of response time reduction can be observed when this shape is applied on both grooved parts. The final variant was selected from combinations of groove shape and number, including groove thickness in the range from 0.1 to 0.7 mm, groove depth from 1 to 8 mm, and groove number from 4 to 76. The fabrication limitations of the SLM method and electro-erosive manufacturing were also taken into consideration. The final design of the grooves is shown in Figures 9 and 10. Both parts have 48 grooves. The groove thickness is limited by the wire thickness of electro-erosive manufacturing (0.35 mm) and by the process of vacuum casting of plastic into the grooves in order to inhibit the MRF flow through these grooves, which would lead to an increase in the cross-section of the gap and, consequently, a decrease in damping force. Grooved parts fabricated by 3D printing from iron powder had worse machinability due to the total absence of carbon, and the grooves were filled with removed material when lathe-turning. Therefore, the grooves on these parts were not cast by the plastic.

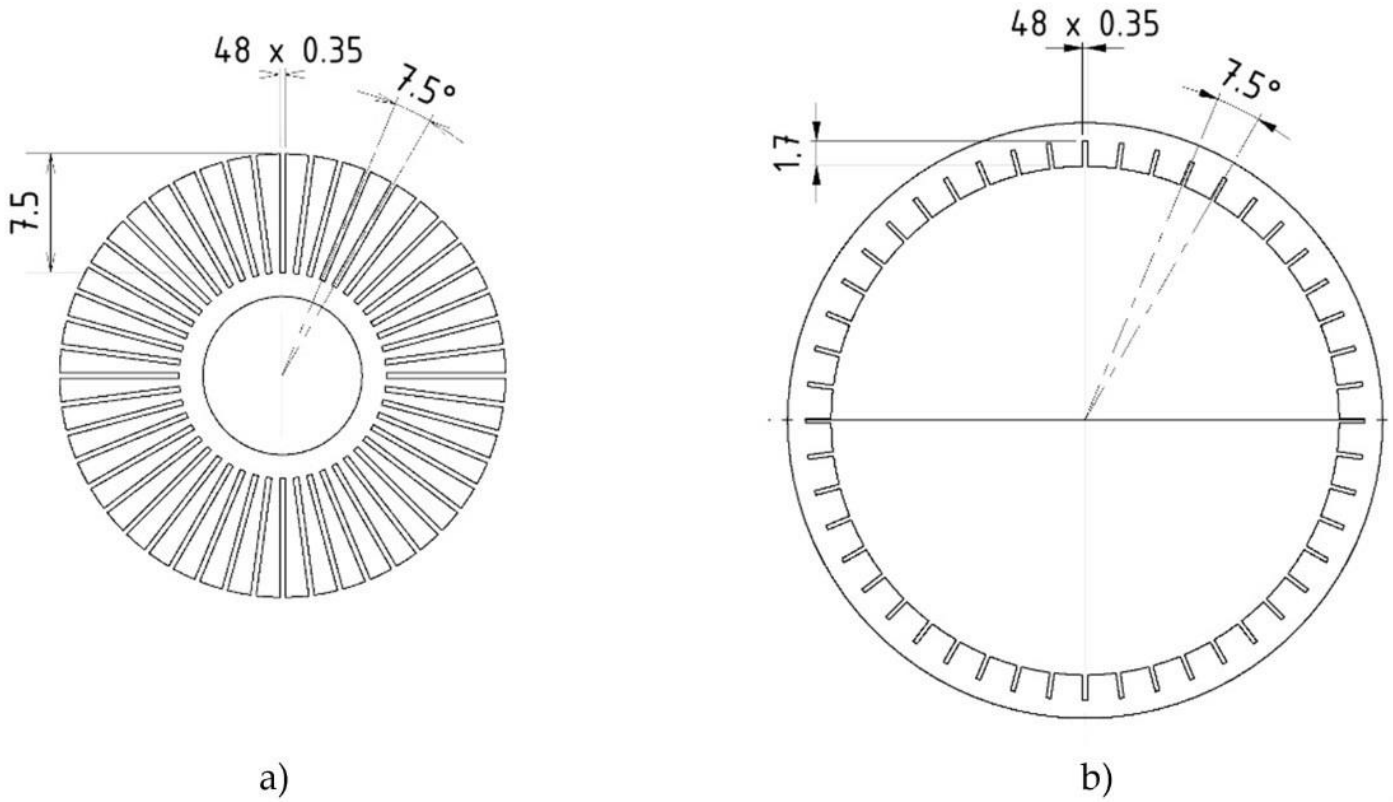

Figure 9. Drawing of grooved (**a**) core; and (**b**) outer cylinder.

Figure 10. Outer cylinder and parts of core fabricated by (**a**) electro-erosive manufacturing; (**b**) SLM—3D printing.

2.5. Measurement of the Magnetic Flux Density—Transient and Static Measurement

This measurement was carried out for verification of the simulation model. The output from the model was a time flow of magnetic flux density when the magnetic field is switched on or switched off. The simulations were calculated with the MRF in the gap. However, for comparison of the model and the measurement, the air instead of the MRF in the gap was set up because the measurement with MRF cannot provide accurate results. The thickness of the Hall probe is 0.55 mm, and the thickness of the gap is 0.65 mm. Therefore, the Hall probe takes almost all of the place between the magnetic poles in the gap, and since the relative permeability of the probe is 1, the acquired data would be drawn significantly by the presence of the probe (the permeability of MRF is from 4 to 6). However, if the model is valid for the air in the gap, the simulation with MRF should

also be valid. Two types of measurement with almost identical configuration were carried out: (a) measurement of static properties of the magnetic circuit (dependence of magnetic flux density on input current to the coil); and (b) response of the magnetic flux density on the current step (see Figure 11). For response measurement, a patented current controller developed by our team was used instead of the common power supply. The controller drives the rise and drop of the current using the overvoltage technique described in [36,37]. The controller is supplied by a voltage of 30 V and the input signal is generated from a control computer. The current rise from 0 A to 2 A took between 0.2–0.6 ms depending on the variant of the piston, drop from 2 A to 0 A took up to 0.2 ms for all the variants. The magnetic flux density was measured using a teslameter (F.W. Bell 5180) with an ultra-thin transverse probe (STB1X-0201, F.W. Bell, Portland, OR, USA). The magnitude of electric current in the coil is obtained by measuring with a Fluke i30 current clamp. These two signals together with the voltage on the coil contacts are recorded and conditioned with a sampling frequency of 200 kHz by a front-end Dewetron USB-50-USB2-8 connected to a laptop.

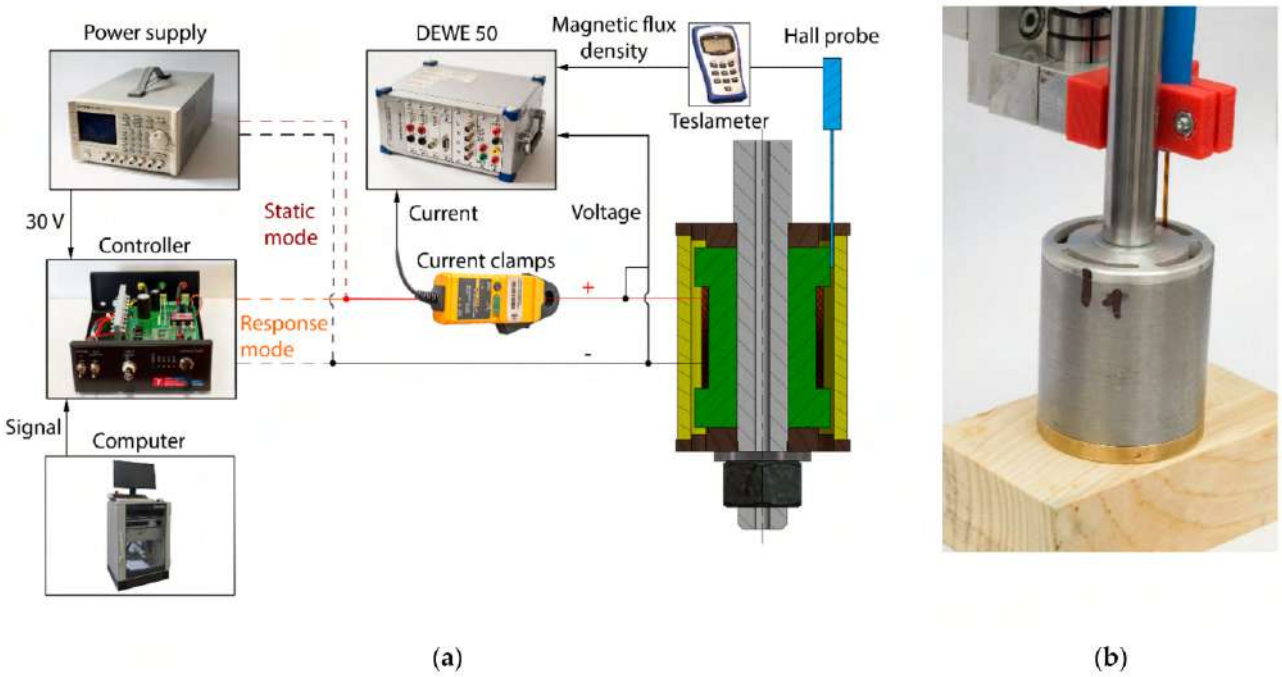

Figure 11. (**a**) Scheme of measurement configuration; (**b**) detail from measurement of MR valve with Hall probe.

2.6. Measurement of the Damping Force—Transient and F-v Curves Measurement

The tested MR valve was purposely designed to work in a hydraulic tube and can generate a damping force for the evaluation of the overall response time of an MR device, including the response of the electric circuit, magnetic field, and MR fluid. There are some simplifications (see Figure 12), such as low friction sealing and guiding (small leakage can occur), steep F-v curve (without bypass of the MR valve for modeling of the F-v curve), statically overdetermined system of piston guiding (sliding bearing and two bronze piston cups), or no sealing of the coil against MRF (only short-term testing considered).

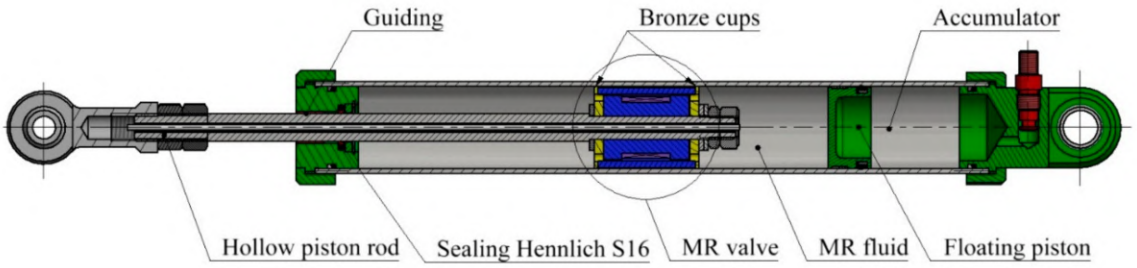

Figure 12. Testing device for measurement of overall response time of damping force.

For the measurements, a hydraulic damper tester by Inova was used (see Figure 13b). The damping force was measured by load gauge HBM U2AD1/2, the position of the piston rod by resistance sensor VLP15$A150, and the current was calculated from a voltage drop on a 0.1 Ω power shunt. These three signals were recorded and conditioned with a sampling frequency of 50 kHz by analyzer Dewe-800 by Dewetron (see Figure 13a). The piston velocity was calculated by derivation of the piston position. The temperature was monitored in order to not exceed 40 °C. If it did so, the test was temporarily interrupted.

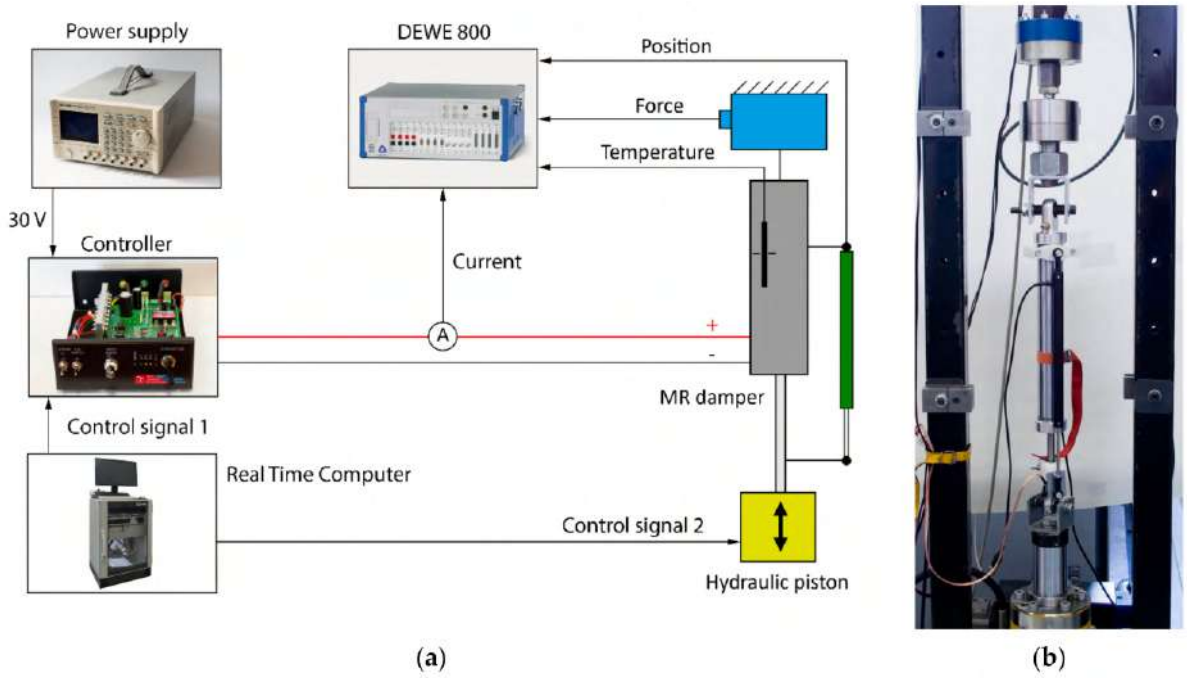

Figure 13. Measurement of damping force on tester Inova: (**a**) scheme; (**b**) tester with MR device.

Firstly, the *F-v–I* curves (dependence of damping force on piston velocity for different electric currents) were measured. The dynamic range of the valve can be determined from this dependency. The start-up test was applied with a frequency from 0.05 to 3 Hz, corresponding to a piston velocity of 0.01 to 0.45 m·s^{-1} with an amplitude of 24 mm. The *F-v–I* curves were measured for supplying currents of 0.0, 0.1, 0.2, 0.4, 0.5, 1.0, 2.0, and 2.5 A. The tester piston performed a harmonic motion. In post-processing analysis, only the damping force at the center of the stroke was selected. In this position, the velocity reaches maximum, and the acceleration is zero.

For the transient measurement, the same current controller and hydraulic piston controller were used for the generation of the step signal as a measurement of magnetic flux density (see Figure 13). The piston movement was excited by a triangle signal of position, ensuring the unchanging velocity during the whole stroke. The measurement of the transient response was carried out for piston velocities 0.1, 0.2, and 0.3 m·s^{-1} and for the current in the range from 0 to 2.5 A, with an increments of 0.5 A. The current was switched on and switched off alternately always after two strokes. The exact moment of switching on or off was in the center of the stroke (see Figures 3 and 14).

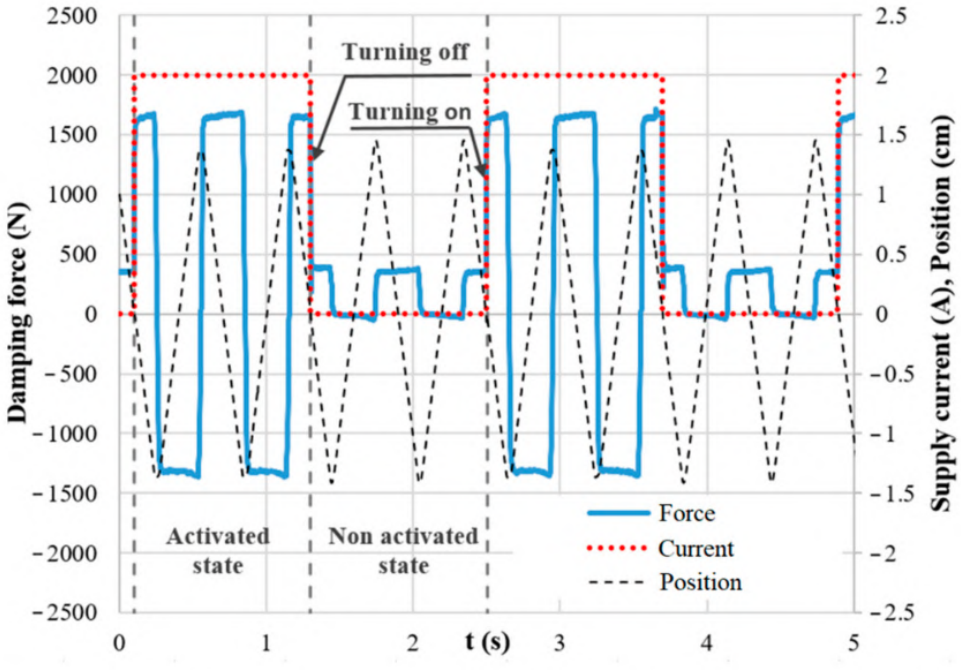

Figure 14. The force courses, input control, and position signal during response time measurement.

3. Results and Discussion

3.1. Transient Responses of Magnetic Flux Density in the Gap with Air

The material approach was primarily considered as a basis for the reduction of the response time. Figure 15 indicates the achieved response time dependent on representative electrical resistivity. The results are obtained as an output from the transient simulation and are valid only for the specific geometry of the MR valve shown in Figure 1, and the current rise and drop in the coil within 0.3 ms, which corresponds to the used current controller. Although the absolute value of the response time is valid only for this specific case, the trend is valid generally. This analysis can be useful particularly for designers of semi-active MR devices. For instance, if a response time shorter than 2 ms is needed (marked in blue in Figure 15), the materials lying under the line must be used. However, if a shape approach on materials above the line is applied, the required response time can also be achieved. The higher the material above the line, the more complex the solution of the shape approach (grooves). For instance, it means that only several grooves for stainless steel AISI 420A are needed, contrary to pure iron. On the other hand, the application of a material with higher electrical resistivity than 10^{-4} Ω·m seems superfluous.

For the verification of transient simulation, six materials were selected (see Table 3). When the response time was longer than required, the shape approach was applied. All simulated and tested variants with the achieved results of magnetic flux density measurement are mentioned below in Table 4. The number of grooves for Vacoflux 50, pure iron from SLM, and 11SMn30 was proposed on the basis of transient simulation to achieve the required response time of 2 ms or better in a model with MRF. It has to be noted that the following results are measured and simulated with air in the gap. Hence, the resulting response time is lower with air than with MRF. This is caused by the approximately four times lower relative permeability of the air. Since the gap displays the major magnetic resistance of the circuit (typically more than 90%), the MRF presence leads to a much higher magnetic flux and corresponding magnetic field intensity, which causes a more significant influence of the occurring eddy currents and a longer rise of magnetic field at the identical speed, because a much higher value has to be achieved. For material AISI 420A, more grooved variants were suggested in order that the contribution of a higher number of grooves was illustrated.

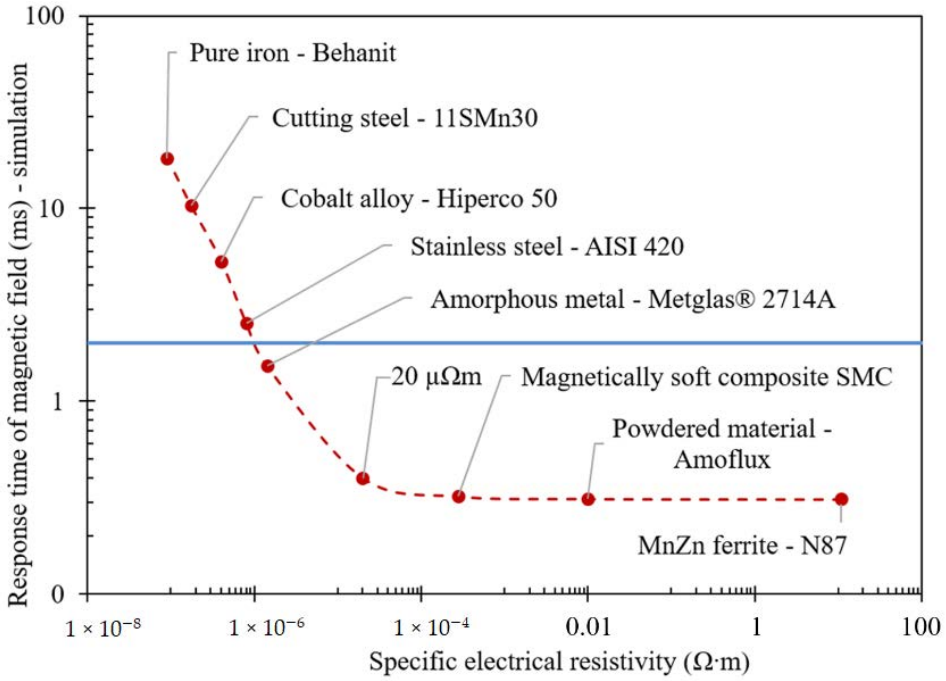

Figure 15. Material approach—response time of magnetic flux on step signal of 2 A for materials with various electrical resistivities (valid for specific geometry of MR valve with MRF).

Table 4. Overview of tested variants using material and shape approach and results of measurement of the magnetic flux density (with air in the gap).

Material	Measurement					Model	
	Grooves No. in Core/Outer Cylinder (-)	Max. Magnetic Flux Density at 2 A (mT)	Remanence at 0 A (mT)	Response Time Signal Rise (ms)	Response Time Signal Drop (ms)	Response Time Signal Drop (ms)	Max. Magnetic Flux at 2 A (mT)
11SMn30	0	173	14	1.43	1.61	2.1	202
11SMn 30	48/48	187	15	0.35	0.35	0.52	200
Hiperco/ Vacoflux 50	0	208	8	1	0.92	0.68	223
Hiperco/ Vacoflux 50	3/0	207	8.2	0.72	0.69	0.40	223
Hiperco/ Vacoflux 50	6/0	206	6.6	0.67	0.61	0.32	223
stainless steel AISI 420A	0	180	33	0.93	0.68	0.67	211
SLM (pure iron)	0	230	16	2.21	2.41	3.62	215
SLM (pure iron)	48/48	221	16	0.49	0.45	0.35	217
Ferrite N87	0	134	3	0.31	0.35	0.23	156
Sintex SMC	0	152	11	0.35	0.29	0.27	184
Sintex (core) 11SMn30 (cylinder)	0/48	190	14	0.64	0.61	0.57	197

The measurement and simulation resulted in following conclusions:

- MR valves made of ferrite materials exhibit the fastest response time. Ferrite material also exhibits the lowest remanence; however, only a small magnetic flux density can be achieved.
- Valves made of Sintex (SMC) are as fast as those of ferrite, despite a lower electrical resistivity than the ferrite. A magnetic circuit made of Sintex material achieves just as

short a response time without grooves. The magnetic flux is significantly higher than in the case of ferrite.

- Vacoflux variants exhibit very high magnetic flux density and lower response time of magnetic flux density than any metal material. Six grooves reduced the response time almost to the level of the Sintex valve.
- The SLM sample (with and w/o the grooves) shows a high magnetic flux density because of the high permeability/magnetic saturation limit of the pure iron powder. The response time of the valve without grooves is the longest of all measured samples. This result was expected due to the lowest resistivity of pure iron. On the contrary, the version with grooves showed a more than 10 times shorter response time.
- The AISI 420A valve without grooves shows quite a low response time and high magnetic density, but also the highest remanence. High remanence is reducing the dynamic force range of the valve and it is also not advantageous for a fast current controller.
- In the 11SMn30 sample, an identical number of grooves as for the SLM must be fabricated in order to achieve a similar response time as the Sintex valve. The magnetic flux density is higher than in case of the Sintex valve, but slightly lower than the valve made of pure iron by SLM. During e fabrication, the parts of the magnetic circuit were cooled and the cutting speed was low in order to prevent overheating. Thanks to this, the valve exhibits low remanence and high permeability.
- There is some difference between the simulated and measured values. This is probably caused by input *B-H* curves and electrical resistivity of materials being taken from datasheets. Previous research has shown that the exact composition of alloys and, thus, *B-H* curves can differ for a smelting batch. In addition, the heat treatment and mechanical loading can change the magnetic and electrical properties. For more precise results, *B-H* curves and the resistivity of materials used for the circuit must be measured individually. However, the presented model is an effective tool for determining the transient behavior of a magnetic circuit.

3.2. Transient Responses of MR Damper Force

Figures 16–22 show the detail of rises and drops of force in a response in the electric current step. The orange dashed line shows the force level corresponding to primary response τ_{63}, τ_{36} time and the green dashed line shows the level corresponding to secondary response time τ_{90}, τ_{10}. The overall results based on the average from three measurements are summed up in Table 5. The table also compares the overall time response of the MR valve with the response time of the simulated magnetic field as a most important source of the overall MR valve response time. The influence of MR fluid and compliance of the hydraulic system is not incorporated in the simulation results.

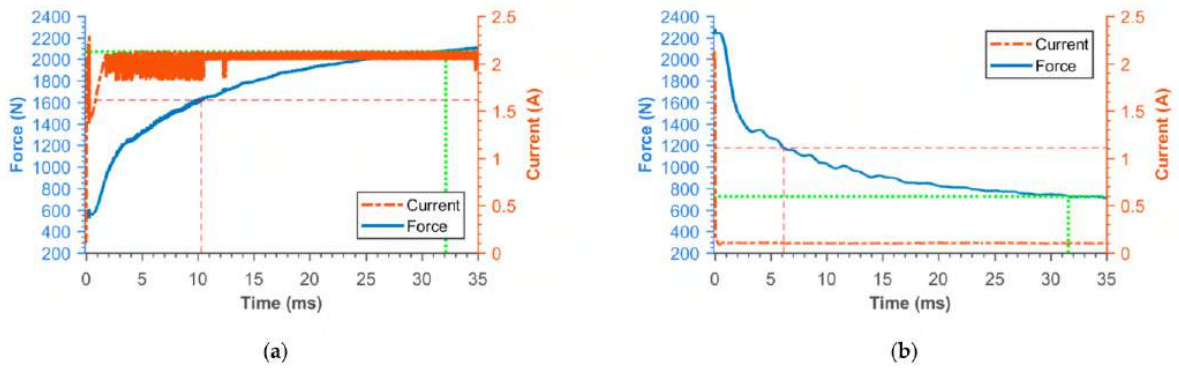

Figure 16. Detail of force rise (**a**) and drop (**b**) of 11SMn30 solid piston.

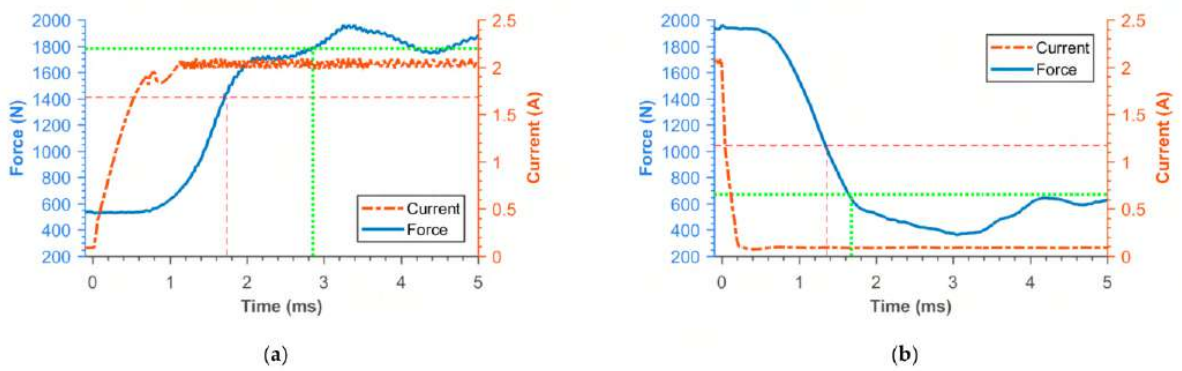

Figure 17. Detail of force rise (**a**) and drop (**b**) of 11SMn30 grooved piston.

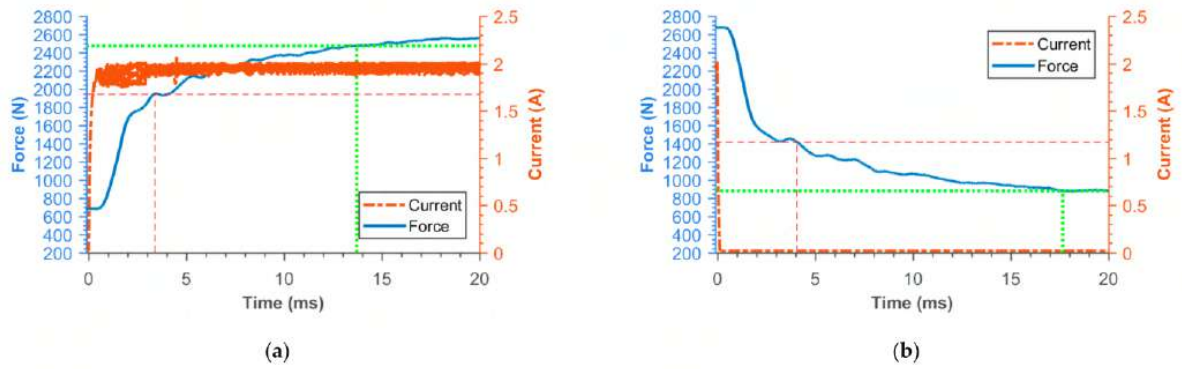

Figure 18. Detail of force rise (**a**) and drop (**b**) of 11SMn30 Hiperco/Vacoflux piston.

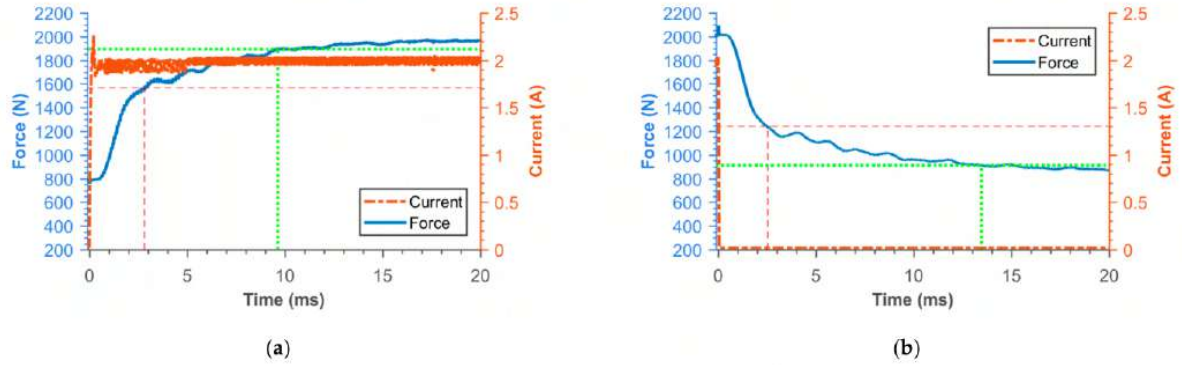

Figure 19. Detail of force rise (**a**) and drop (**b**) of AISI420 piston.

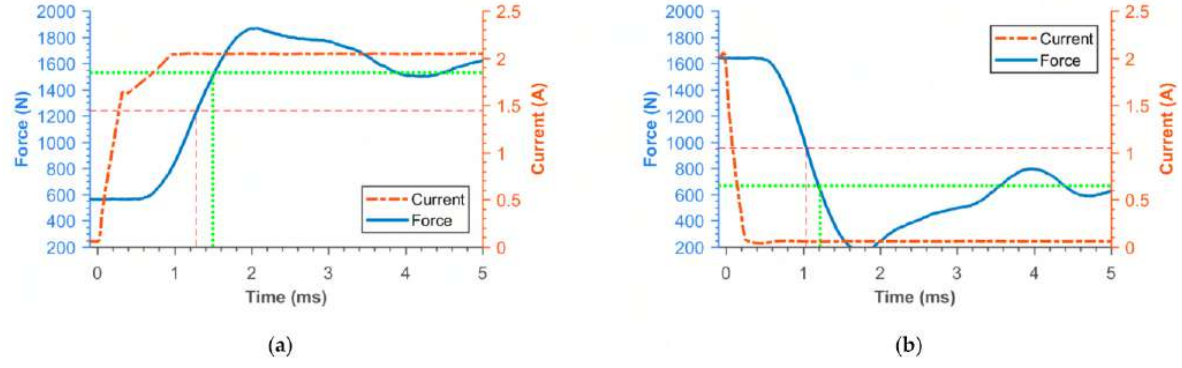

Figure 20. Detail of force rise (**a**) and drop (**b**) of SMC piston.

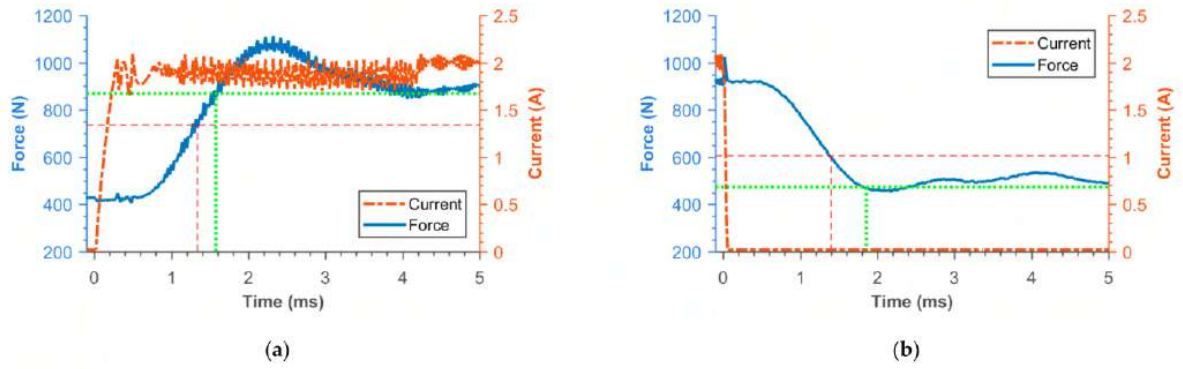

Figure 21. Detail of force rise (**a**) and drop (**b**) of piston consisting from Ferrite N87 bobbin and 11SMn30 outer cylinder.

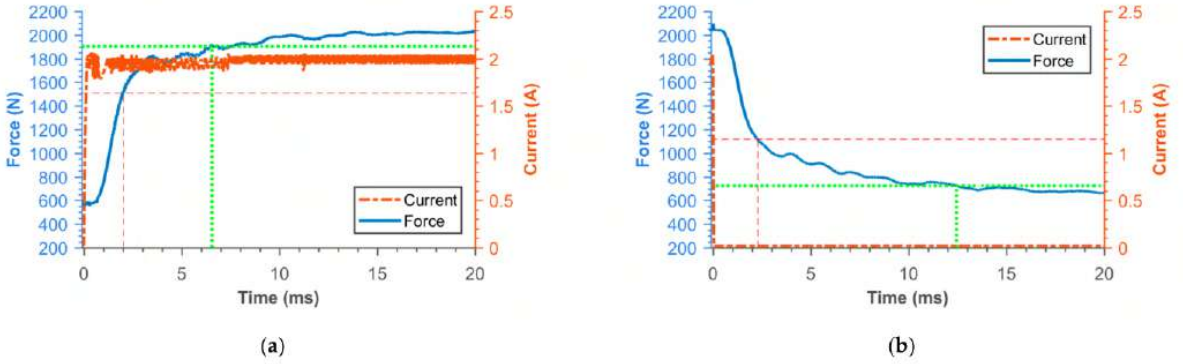

Figure 22. Detail of force rise (**a**) and drop (**b**) of SLM (pure iron) grooved piston.

Table 5. Performance comparison of pistons.

Type of Piston	Measurement			Model		
	Primary Force Response Time τ_{63} (ms)	Secondary Force Response Time τ_{63} (ms)	Dynamic Force Range (-)	Primary Response Time of Magnetic Field (ms)	Secondary Response Time of Magnetic Field (ms)	Flux Density at 2 A (mT)
Solid piston (11SMn30)	10.3	32.7	5.73	7.6	21.9	505
Groved piston (11SMn 30)	1.74	2.86	5.05	0.61	3	481
Hiperco/Vacoflux 50 piston	3.57	14.14	6.4	4.45	13.5	689
AISI 420A piston	2.82	9.69	3.17	2.38	6.2	452
SLM (pure iron) 48/48	2.03	6.78	5.25	0.78	4.3	516
Ferrite N87 bobbin + 11SMn30 outer cylinder	1.34	1.54	3.5	0.39	3.05	361
SMC piston	1.28	1.49	4.03	0.23	0.38	467

The measurements showed the following conclusions:

- The response times of MR valves made of solid parts corresponds with their electrical resistivity.
- Grooves rapidly speed up the response time of MR valves made of metals.

- The force response course is similar to first-order dynamic systems only for pistons made of solid steel. In this case, the secondary response time is approximately 3 times longer than the primary response time.
- The secondary response time for pistons made of materials with high electrical resistivity is much shorter. The response of the force is copying the course of electric current with some delay. Approximation by a first-order dynamic system is therefore not very suitable.
- The simulations for grooved pistons or pistons made of materials with high electrical resistivity predicted significantly shorter response time of the magnetic field (basically the same as the response time of the current). The difference between the measured and simulated values can be explained by the response time of the MR fluid itself. There is always a time delay of approximately 0.6 ms between the beginning of the electric current rise (or drop) and the force rise (or drop). This phenomenon is practically not dependent on piston material, or velocity.
- The best dynamic range can be achieved with the piston made of Hiperco/Vacoflux.
- The course of force in the case of pistons with a force secondary response time up to 3 ms exhibits quite heavy oscillations. This is probably caused by the compliance of MR fluid and other parts of the MR damper. This problem was explained in [57].

4. Conclusions

The response time of a MR damper can be reduced by the reduction of eddy currents during fast changes of the magnetic field in an electrical current. The eddy currents can almost be eliminated by the use of special materials with very high electrical resistivity such as ferrite or soft magnetic composites. The use of these materials, however, significantly reduces the dynamic range due to the lower permeability or lower magnetic saturation level. In addition, the mechanical properties are poor. However, total eddy current elimination is not necessary because of the response time of the magnetorheological fluid itself. Efforts to reduce the response time of the magnetic flux density in the gap to shorter values than the response time of the MR fluid cannot bring a significant reduction of the damper's force response time. From this point of view, the shape attitude can bring advantages. If the eddy currents in steel are reduced by grooves so that the response time of the magnetic flux density will be in the same range as the response time of the MR fluid, an overall response time comparable to that of the ferrite or SMC magnetic circuit can be achieved in the MR damper. In addition, the dynamic range and mechanical properties can be significantly better due to the better magnetic and mechanical properties of steel. The measurements also showed some phenomena which are, in most of cases, not reflected in simulations employing MR devices. The waveform of the force in a response in the control signal step differs for different constructions of MR valve. Whereas the response time of the MR valves made of iron, steel, or Hiperco/Vacoflux without grooves can be considered as first-order dynamic systems, the secondary response time of MR valves made of materials with high resistance or grooved variants is much shorter. In other words, the force response in the control signal step does not correspond to the exponential function. In addition, there is always a delay between 0.6 and 0.8 ms between the control signal and the start of the force change, which is not significant for MR valves with a long response time; however, neglecting it in fast semi-active system simulations can cause low fidelity of model behavior.

Author Contributions: Conceptualization, Z.S., F.J., M.K.; methodology, F.J., O.M.; software, Z.S., M.K.; validation, Z.S., M.K.; formal analysis, F.J., O.M.; investigation, F.J., M.K., O.M.; data curation, F.J., M.K.; writing—original draft preparation, Z.S., F.J.; writing—review and editing, Z.S., F.J., M.K., O.M., S.-B.C.; visualization, Z.S., F.J.; supervision, Z.S., S.-B.C.; project administration, Z.S., M.K; funding acquisition, Z.S., M.K. All authors have read and agreed to the published version of the manuscript.

Funding: The research project which led to the specific results reported in this article received funding from GAČR 20-23261Y and FSI-S-20-6247.

Institutional Review Board Statement: Not applicable.

Informed Consent Statement: Not applicable.

Data Availability Statement: The data presented in this study are available on request from the corresponding author.

Conflicts of Interest: The authors declare no conflict of interest.

References

1. Rabinow, J. The Magnetic Fluid Clutch. *Trans. Am. Inst. Electr. Eng.* **1948**, *67*, 1308–1315. [CrossRef]
2. Klingenberg, D.J. Magnetorheology: Applications and challenges. *Am. Inst. Chem. Eng.* **2001**, *47*, 246–249. [CrossRef]
3. Bossis, G.; Lacis, S.; Meunier, A.; Volkova, O. Magnetorheological fluids. *J. Magn. Magn. Mater.* **2002**, *252*, 224–228. [CrossRef]
4. Simon, T.M.; Reitich, F.; Jolly, M.R.; Ito, K.; Banks, H.T. The effective magnetic properties of magnetorheological fluids. *Math. Comput. Model.* **2001**, *33*, 273–284. [CrossRef]
5. Carlson, J.D.; Jolly, M.R. MR fluid, foam and elastomer devices. *Mechatronics* **2000**, *10*, 555–569. [CrossRef]
6. De Vicente, J.; Klingenberg, D.J.; Hidalgo-Alvarez, R. Magnetorheological fluids: A review. *Soft Matter* **2011**, *7*, 3701. [CrossRef]
7. Plachy, T.; Cvek, M.; Kozakova, Z.; Sedlacik, M.; Moucka, R. The enhanced MR performance of dimorphic MR suspensions containing either magnetic rods or their non-magnetic analogs. *Smart Mater. Struct.* **2017**, *26*, 025026. [CrossRef]
8. Karnopp, D. Active Damping in Road Vehicle Suspension Systems. *Veh. Syst. Dyn.* **1983**, *12*, 291–311. [CrossRef]
9. Crews, J.H.; Mattson, M.G.; Buckner, G.D. Multi-objective control optimization for semi-active vehicle suspensions. *J. Sound Vib.* **2011**, *330*, 5502–5516. [CrossRef]
10. Song, X.; Ahmadian, M.; Southward, S.; Miller, L.R. An Adaptive Semiactive Control Algorithm for Magnetorheological Suspension Systems. *J. Vib. Acoust.* **2005**, *127*, 493. [CrossRef]
11. Seong, M.S.; Choi, S.B.; Sung, K.G. Control Strategies for Vehicle Suspension System Featuring Magnetorheological (MR) Damper. In *Vibration Analysis and Control: New Trends and Developments*; InTech: London, UK, 2011; pp. 97–114.
12. Goldasz, J. Study of a modular magnetorheological valve 2017. In Proceedings of the 18th International Carpathian Control Conference (ICCC), Sinaia, Romania, 28–31 May 2017; Volume 63, pp. 306–309.
13. Gołdasz, J.; Dzierżek, S. Parametric study on the performance of automotive MR shock absorbers. *IOP Conf. Ser. Mater. Sci. Eng.* **2016**, *148*, 012004. [CrossRef]
14. Carlson, J.D.; Catanzarite, D.M.; St. Clair, K.A. Commercial magneto-rheological fluid devices. *Int. J. Mod. Phys. B* **1996**, *10*, 2857–2865. [CrossRef]
15. Wu, X.; Griffin, M.J. A semi-active control policy to reduce the occurrence and severity of end-stop impacts in a suspension seat with an electrorheological fluid damper. *J. Sound Vib.* **1997**, *203*, 781–793. [CrossRef]
16. Choi, S.B.; Nam, M.H.; Lee, B.K. Vibration Control of a MR Seat Damper for Commercial Vehicles. *J. Intell. Mater. Syst. Struct.* **2000**, *11*, 936–944. [CrossRef]
17. McManus, S.J.; St. Clair, K.A.; Boileau, P.É.; Boutin, J.; Rakheja, S. Evaluation of vibration and shock attenuation performance of a suspension seat with a semi-active magnetorheological fluid damper. *J. Sound Vib.* **2002**, *253*, 313–327. [CrossRef]
18. Choi, Y.T.; Wereley, N.M. Mitigation of biodynamic response to vibratory and blast-induced shock loads using magnetorheological seat suspensions. *Proc. Inst. Mech. Eng. Part D J. Automob. Eng.* **2005**, *219*, 741–753. [CrossRef]
19. Dyke, S.J.; Spencer, B.F.; Sain, M.K.; Carlson, J.D. An experimental study of MR dampers for seismic protection. *Smart Mater. Struct.* **1998**, *7*, 693–703. [CrossRef]
20. Li, H.; Wang, J. Experimental investigation of the seismic control of a nonlinear soil-structure system using MR dampers. *Smart Mater. Struct.* **2011**, *20*, 085026. [CrossRef]
21. Dyke, S.J.; Spencer, B.F.; Sain, M.K.; Carlson, J.D. Modeling and control of magnetorheological dampers for seismic response reduction. *Smart Mater. Struct.* **1999**, *5*, 565–575. [CrossRef]
22. Yang, G.; Spencer, B.F.; Carlson, J.D.; Sain, M.K. Large-scale MR fluid dampers: Modeling and dynamic performance considerations. *Eng. Struct.* **2002**, *24*, 309–323. [CrossRef]
23. Ok, S.Y.; Kim, D.S.; Park, K.S.; Koh, H.M. Semi-active fuzzy control of cable-stayed bridges using magneto-rheological dampers. *Eng. Struct.* **2007**, *29*, 776–788. [CrossRef]
24. Kim, I.H.; Jung, H.J.; Koo, J.H. Experimental evaluation of a self-powered smart damping system in reducing vibrations of a full-scale stay cable. *IOP Sci. Smart Mater. Struct.* **2010**, *19*, 115027. [CrossRef]
25. BenLahcene, Z.; Faris, W.F.; Khan, M.R. Analysis of Semi-Active and Passive Suspensions System for Off-Road Vehicles. In Proceedings of the Conference on Intelligent Systems and Automation: 2nd Mediterranean Conference (CISA 2009), Zarzis, Tunisia, 23–25 March 2009; pp. 318–323.
26. Rae-Kwan, K.; Keum-Shik, H. Skyhook control using a full-vehicle model and four relative displacement sensors. In Proceedings of the International Conference on Control, Automation and Systems 2007, Seoul, Korea, 17–20 October 2007; pp. 268–272.
27. Rao, T.R.M.; Rao, G.V.; Rao, K.S.; Purushottam, A. Analysis of passive and semiactive controlled suspension for ride comfort in an omnibus passing over a speed bump. *Int. J. Res. Rev. Appl. Sci.* **2010**, *5*, 7–14.
28. Choi, S.B.; Seong, M.S.; Ha, S.H. Vibration control of an MR vehicle suspension system considering both hysteretic behavior and parameter variation. *Smart Mater. Struct.* **2009**, *18*, 125010. [CrossRef]

29. Yang, B.; Luo, J.; Dong, L. Magnetic circuit FEM analysis and optimum design for MR damper. *Int. J. Appl. Electromagn. Mech.* **2010**, *33*, 207–216. [CrossRef]
30. Zhu, X.; Lai, C. Design and performance analysis of a magnetorheological fluid damper for drillstring. *Int. J. Appl. Electromagn. Mech.* **2012**, *40*, 67–83. [CrossRef]
31. Nguyen, Q.H.; Choi, S.B. Optimal design of MR shock absorber and application to vehicle suspension. *Smart Mater. Struct.* **2009**, *18*, 035012. [CrossRef]
32. Lee, H.; Nam, Y.; Park, M. Electromagnetic design for performance improvement of an MR valve. *Int. J. Appl. Electromagn. Mech.* **2012**, *39*, 575–581. [CrossRef]
33. Strecker, Z.; Mazůrek, I.; Roupec, J.; Klapka, M. Influence of MR damper response time on semiactive suspension control efficiency. *Meccanica* **2015**, *50*, 1949–1959. [CrossRef]
34. Cha, Y.J.; Agrawal, A.K.; Dyke, S.J. Time delay effects on large-scale MR damper based semi-active control strategies. *Smart Mater. Struct.* **2013**, *22*, 015011. [CrossRef]
35. Koo, J.H.; Goncalves, F.D.; Ahmadian, M. A comprehensive analysis of the response time of MR dampers. *Smart Mater. Struct.* **2006**, *15*, 351–358. [CrossRef]
36. Strecker, Z.; Roupec, J.; Mazůrek, I. Limiting factors of the response time of the magnetorheological damper. *Int. J. Appl. Electromagn. Mech.* **2014**, *47*, 541–550. [CrossRef]
37. Strecker, Z.; Roupec, J.; Mazurek, I.; Machacek, O.; Kubik, M.; Klapka, M. Design of magnetorheological damper with short time response. *J. Intell. Mater. Syst. Struct.* **2015**, *26*, 1951–1958. [CrossRef]
38. Goncalves, F.D.; Ahmadian, M.; Carlson, J.D. Investigating the magnetorheological effect at high flow velocities. *Smart Mater. Struct.* **2005**, *15*, 75–85. [CrossRef]
39. Jolly, M.R.; Bender, J.W.; Mathers, R.T. Indirect Measurements of Microstructure Development in Magnetorheological Fluids. *Int. J. Mod. Phys. B* **1999**, *13*, 2036–2043. [CrossRef]
40. Jiang, Z.; Christenson, R.E. A fully dynamic magneto-rheological fluid damper model. *Smart Mater. Struct.* **2012**, *21*, 065002. [CrossRef]
41. Feeley, J.J. A simple dynamic model for eddy currents in a magnetic actuator. *IEEE Trans. Magn.* **1996**, *32*, 453–458. [CrossRef]
42. Maas, J.; Güth, D. Experimental investigation of the transient behaviour of MR fluids. In Proceedings of the ASME 2011 Conference on Smart Materials, Adaptive Structures and Intelligent Systems, Scottsdale, AZ, USA, 18–21 September 2011; pp. 229–238.
43. EPCOS. Data Book 2013: Ferrites and Accessories. 2013, p. 625. Available online: www.tdk-electronics.tdk.com/download/519704/069c210d0363d7b4682d9ff22c2ba503/ferrites-and-accessories-db-130501.pdf (accessed on 1 March 2021).
44. Heck, C. *Magnetic Materials and their Applications*; Butterworth: London, UK, 1974; p. 11.
45. Bhalla, D.; Singh, D.; Singh, S.; Seth, D. Material Processing Technology for Soft Ferrites Manufacturing. *Am. J. Mater. Sci.* **2013**, *2*, 165–170. [CrossRef]
46. Shokrollahi, H. The magnetic and structural properties of the most important alloys of iron produced by mechanical alloying. *Mater. Des.* **2009**, *30*, 3374–3387. [CrossRef]
47. Shokrollahi, H.; Janghorban, K. Soft magnetic composite materials (SMCs). *J. Mater. Process. Technol.* **2007**, *189*, 1–12. [CrossRef]
48. Gołdasz, J. Electro-mechanical analysis of a magnetorheological damper with electrical steel laminations | Koncepcja tłoka amortyzatora samochodowego z cieczą magnetoreologiczną. *Prz. Elektrotechniczny* **2013**, *89*, 8–12.
49. Kostamo, E.; Kostamo, J.; Kajaste, J.; Pietola, M. Magnetorheological valve in servo applications. *J. Intell. Mater. Syst. Struct.* **2012**, *23*, 1001–1010. [CrossRef]
50. Omekanda, A.M.; Nehl, T.W.; Namuduri, C.S.; Gopalakrishnan, S. Electromagnetic Actuator Structure. U.S. Patent 10480674B2, 19 November 2015.
51. Yoon, D.S.; Park, Y.J.; Choi, S.B. An eddy current effect on the response time of a magnetorheological damper: Analysis and experimental validation. *Mech. Syst. Signal Process.* **2019**, *127*, 136–158. [CrossRef]
52. Strecker, Z.; Kubík, M.; Vítek, P.; Roupec, J.; Paloušek, D.; Šreibr, V. Structured magnetic circuit for magnetorheological damper made by selective laser melting technology. *Smart Mater. Struct.* **2019**, *28*, 5. [CrossRef]
53. Kubík, M.; Macháček, O.; Strecker, Z.; Roupec, J.; Mazůrek, I. Design and testing of magnetorheological valve with fast force response time and great dynamic force range. *Smart Mater. Struct.* **2017**, *26*, 4. [CrossRef]
54. Strecker, Z.; Roupec, J.; Mazůrek, I.; Macháček, O.; Kubík, M. Influence of response time of magnetorheological valve in Skyhook controlled three-parameter damping system. *Adv. Mech. Eng.* **2018**, *10*, 168781401881119. [CrossRef]
55. Free B(H) & Core Loss Curves. Available online: magweb.us/free-bh-curves (accessed on 1 March 2021).
56. Roupec, J.; Mazurek, I.; Strecker, Z.; Kubik, M.; Macháček, O. Tensile strength of pure iron samples manufactured by Selective Laser Melting Method. *Eng. Mech.* **2017**, 830–833.
57. Kubík, M.; Goldasz, J. Multiphysics Model of an MR Damper including Magnetic Hysteresis. *Shock Vib.* **2019**, *2019*, 3246915. [CrossRef]

IOP Publishing Smart Materials and Structures
Smart Mater. Struct. **30** (2021) 017004 (12pp) https://doi.org/10.1088/1361-665X/abc26f

Technical Note

Insight into the response time of fail-safe magnetorheological damper

F Jeniš, M Kubík, O Macháček, K Šebesta and Z Strecker

Brno University of Technology, Brno, Czech Republic

E-mail: filip.jenis@vutbr.cz

Received 30 June 2020, revised 23 September 2020
Accepted for publication 19 October 2020
Published 9 December 2020

Abstract

The significant problem of magnetorheological (MR) dampers is their poor fail-safe ability. In the case of power supply failure, the damper remains in a low damping state which is dangerous for several technical applications. This can be solved by accommodating a permanent magnet to the magnetic circuit of the damper. Currently, the MR dampers are used in progressive semiactive (S/A) control of suspension systems. The dynamics (force response time) of the damper is an important parameter that affects the performance of S/A control. The main goal of this paper is to introduce the dynamic behavior of MR damper with a permanent magnet. The damper design with the permanent magnet in the magnetic circuit, transient magnetic simulation including magnetic hysteresis and eddy currents, and experiments are presented. The magnetic field response time and MR damper force response time are measured and also determined from magnetic simulation. The permanent magnet significantly influences the MR damper dynamics. The decrease of the damping force from a fail-safe state–medium damping to off-state–low damping is significantly faster (2 ms, −1 A) than the increase to on-state–high damping (12 ms, 1 A). The exact value is depending on the electric current magnitude and piston velocity. The damper achieved fail-safe damping force approximately 1/3 of the maximum damping force. The exact value of the fail-safe force is magnetization history-dependent. The maximum dynamic force range is 8.5 which is comparable with the common design of MR damper.

Keywords: magnetorheological valve, MR damper, response time, permanent magnet, fail-safe, transient response, damper dynamics

(Some figures may appear in colour only in the online journal)

1. Introduction

The main aim of the car suspension system is to provide maximum ride comfort and handling stability. Three types of suspension systems, namely, passive, semiactive (S/A), and active are commonly used. The passive suspension system can't effectively mitigate vehicle vibration on passengers because the damping cannot be changed according to the actual situation. In the case of the active suspension system, linear electric motor or electric pump [1], are used to control vehicle body motion over a wide frequency range. The main disadvantages of the active system are their high energy consumption, high cost, or stability problem. The S/A suspension systems offer a compromise between suspension system performance and cost. The S/A system requires low energy source and provide significantly higher ride comfort and handling stability than passive systems. Since the 1970s [2], the control strategy and suitable dampers have been widely studied for different technical applications.

The performance of S/A control of the suspension system is significantly influenced by the dynamic behavior of the damper. The response time of the damper on the control signal is a key factor [3]. A rapid increase or decrease of damping level (short response time) on the control signal is desired for all real-time S/A control applications [4]. Giua *et al* [5] simulated influence of damper response time on to S/A control

performance. The damper with response time 7 ms exhibits better results in terms of performance S/A suspension system than damping element with response time 30 ms. Similar conclusions can be found in publications [3, 6]. Suitable dampers for real-time S/A control are the hydraulic solenoid valve damper and the magnetorheological (MR) damper.

A solenoid valve damper varies the size of an orifice by an electromagnetic coil, which can give continuously variable damping characteristics. This technology offers several companies (Sachs ZF, Tenneco, etc) under various trade names such as CDC, DCC, etc. This damper can be designed with fail-safe behaviour, i.e. the maximum damping force is generated in a damper with no electric current. Qin *et al* [7] measured the dynamic behaviour of the CDC solenoid damper. The response time for the force rise (soft $\rightarrow$ hard) was in the range 16 ms to 24 ms; the response time for the force drop (hard $\rightarrow$ soft) was in the range 7 ms to 15 ms. The dynamic behavior of the solenoid valve damper has also been addressed in [8].

The MR damper utilizing MR fluid which, when subjected to magnetic stimuli generates yield stress thus increasing the apparent viscosity of the fluid [9]. MR fluid is a suspension of microsized ferromagnetic particles which are dispersed in the carrier fluid. These particles are chained in the direction of the magnetic field and cause a significant increase in the apparent viscosity and damping forces. The sedimentation stability of MR fluid (particles) is intensively addressed in [10–13]. In papers can be found several MR damper designs that differ in the number of coils [14–16], the arrangement of the magnetic circuit [17], the number of gaps [18, 19], etc. If the power supply of the coil is interrupted, the damper will stay at the minimum damping level. This is a significant problem for a wide range of MR damper applications (aerospace, rail, automotive, etc.). A suitable solution is to use a permanent magnet into the MR damper magnetic circuit. The permanent magnet creates a magnetic flux in the magnetic circuit, which ensures damping during a power supply failure—fail-safe state. In some designs, the permanent magnet is placed under the inner edge of the electromagnetic coil [20–23] or next to the electromagnetic coil on the edge of the piston gap [24, 25]. The damping level with no electric current and with permanent magnet usually achieved one-third of the maximum force. Also, a low-coercivity magnet accommodated in the magnetic circuit (e.g. Alnico, made of Aluminium–Nickel–Cobalt) can provide the MR damper with non-minimal damping forces without external power supply as mentioned in [24]. However, using a so-called switchable magnet does not ensure a full fail-safe ability of MR damper due to the possibility of magnet demagnetization.

The dynamic behavior of MR dampers dealt with only a handful of authors. Koo *et al* [4] experimentally determined the response time of a commercially available Lord Corporation's Motion Master® Ride Management System at approximately 17 ms (lowest measured value). However, the response time of damper is strongly dependent on the magnitude of the applied electric current and the piston velocity. Takesue *et al* [26] presented the design of the MR clutch where they improved the dynamic behavior of this actuator by reduction of eddy current in the magnetic circuit. The same aim had Strecker [27] and Kubík [16] who published the design of MR damper with a short response time where the ferrite material of the magnetic circuit was used. Strecker [17] published MR damper with a magnetic circuit manufactured by 3D metal printing, which allowed the MR damper design with a response time of 1.68 ms and a high dynamic range. This method is based on the design of the special shape of the magnetic circuit contributing to the reduction of eddy current. The effect of eddy currents on MR damper dynamics can be also reduced using a magnetic circuit made by laminated sheets [15, 28]. Sahin *et al* [29] compared two MR valves with similar material and different geometry. Sahin *et al* showed that the response time of the MR damper is also dependent on the geometry of the MR valve. The dynamic behavior of MR damper with a permanent magnet was examined only by Lee *et al* [30]. The damping force of this damper is realized by the variation of the magnetization area (position-dependent damper), not by the electromagnetic coil.

The *main aim* of this paper is to introduce the *dynamic behavior of fail-safe MR damper with a permanent magnet.* The response time of the magnetic field and force on the step the control signal are determined experimentally and using the magnetic models.

2. Materials and methods

2.1. MR damper response time

The dynamic behavior of MR damper is usually assumed as a first-order system, where the response time is determined at 63.2% of steady-state force value [9, 16, 27]. However, in many publications, the response time of MR damper is described as 90% [31, 32] or 95% [4, 17] of the steady-state force value. The criterion of 90% is frequently used for the description of the dynamic behavior of actuators in industrial applications [30]. Response time (τ) of the system indirectly implies cut-off frequency ($f = \frac{1}{2\pi\tau}$) which is connected with the controllable frequency range of the damper [33]. The primary response time $\tau_{63,}$ τ_{36} (63.2% for the rise and 36.8% for a drop of steady-state value) and secondary response time $\tau_{90,}$ τ_{10} (90% for the rise and 10% for a drop of steady-state value) on step electric current drop and rise will be determined from measured and simulated data in this paper, see figure 1. The measured and simulated data were normalized by the non-dimensional function N_o. A detailed description of this method in paper [30].

2.2. Design of MR damper with permanent magnet

The presented MR damper is a monotube design, where the high-pressure gas (6) is separated from the MR fluid (5) by a floating piston (2), see figure 2.

The piston rod was sealed by a piston rod seal from H-PU material and guided by bearing (4). The most important part of the damper is a piston unit (1). The damper was filled by 200 ml of MRF Lord MRF 132-DG and pressurized by 30 bar. The piston unit consists of a core (1, 2), sleeve (3), plates (4),

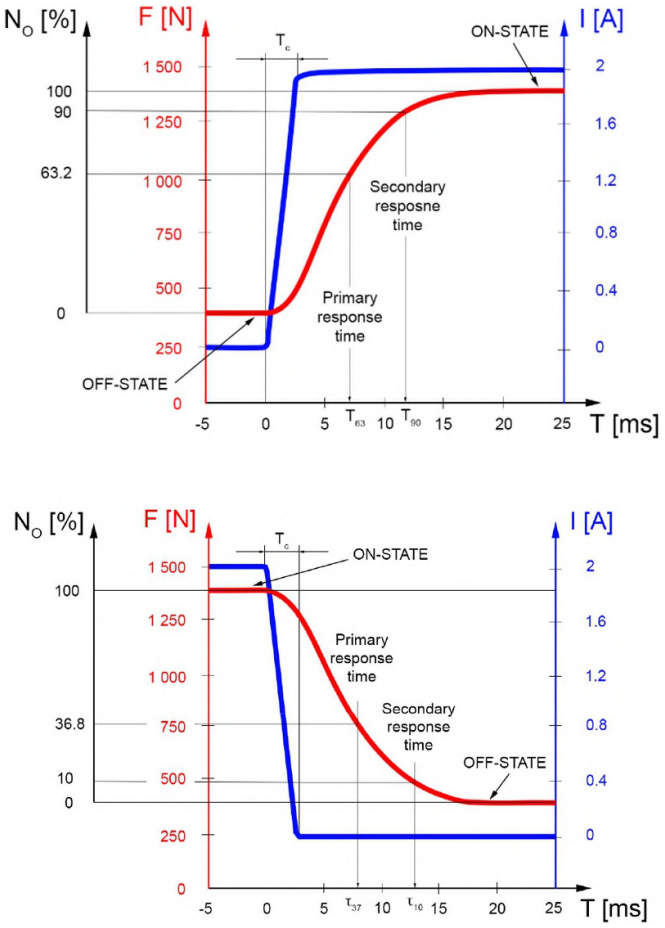

Figure 1. Definition of the response time of MR damper.

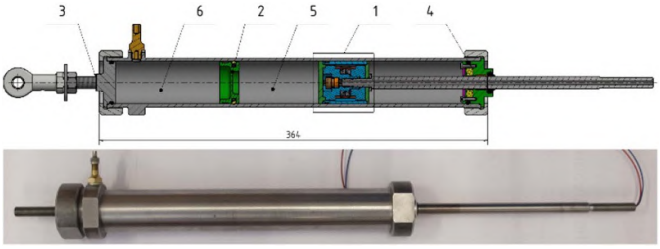

Figure 2. Design of MR damper with permanent magnet.

piston rod (5), permanent magnet (6), and an electromagnetic coil (7). The important dimensions are shown in figure 3.

The wire of the electromagnetic coil was connected to the connector integrated into the piston rod. The magnetic circuit (1, 2, 3) was made of cutting steel (11SMn30 with a carbon content of less than 1%). Two neodymium permanent magnets in the form of a ring 25 × 16 × 5 mm, class N42 was used. These magnets have been selected because they were up for sale. The maximum operating temperature is 80 °C.

An electromagnetic coil was winded by 190 turns of copper wire with a diameter of 0.5 mm. Figure 4 shows the main principle function idea of the damper with the magnet. In the case of the positive polarity of electric current $+I$, the magnetic flux density in the gap is $B_{max} = B_{mag} + B_{coil}$. In the case

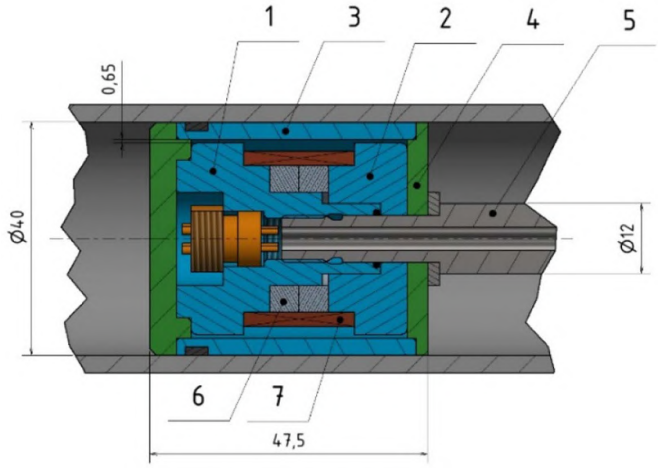

Figure 3. The detail of MR valve with permanent magnet.

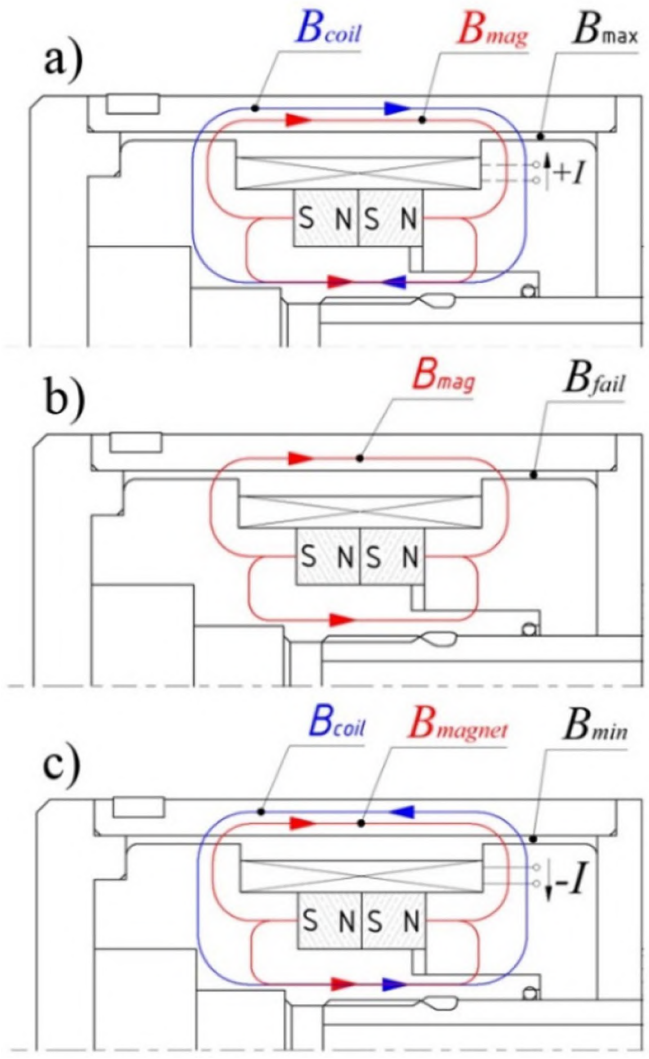

Figure 4. The main principle of MR valve function with permanent magnet; (a) current $+I$, (b) no current, (c) $-I$ current.

of the negative polarity of electric current $-I$, the magnetic flux density in the gap is $B_{min} = B_{mag} - B_{coil}$.

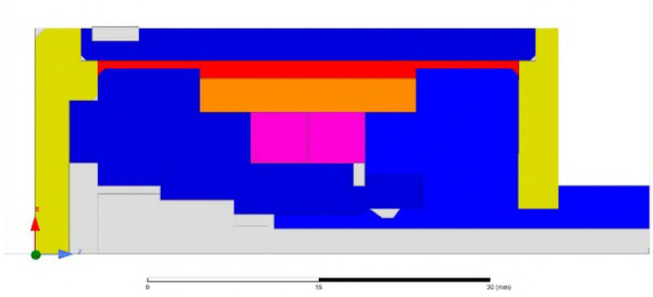

Figure 5. Simplified geometry of MR valve for the magnetic model; steel 11SMn30 (blue), MR fluid or Air (red), bronze (yellow), NdFe42 magnet (green), copper (orange) and air surrounding (white).

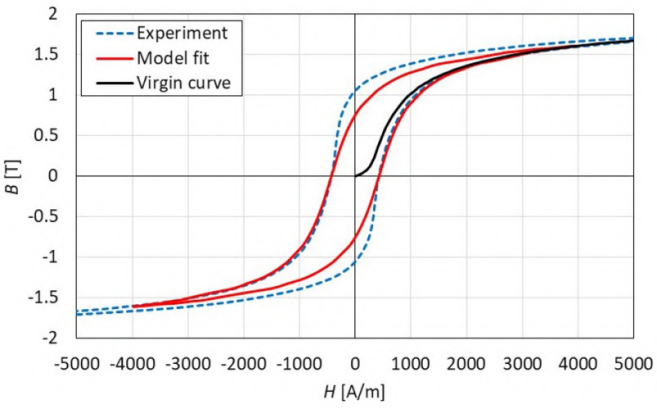

Figure 6. The virgin (black) and hysteresis magnetization curve for steel 11SMn30; experiment (blue), model fit on experimental data (red).

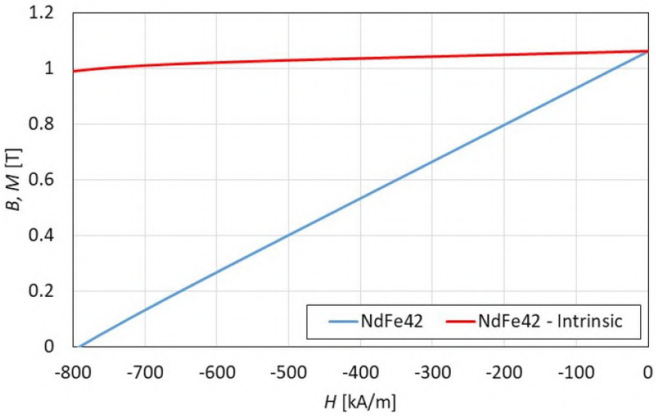

Figure 7. Magnetisation curve of NdFe42 permanent magnet.

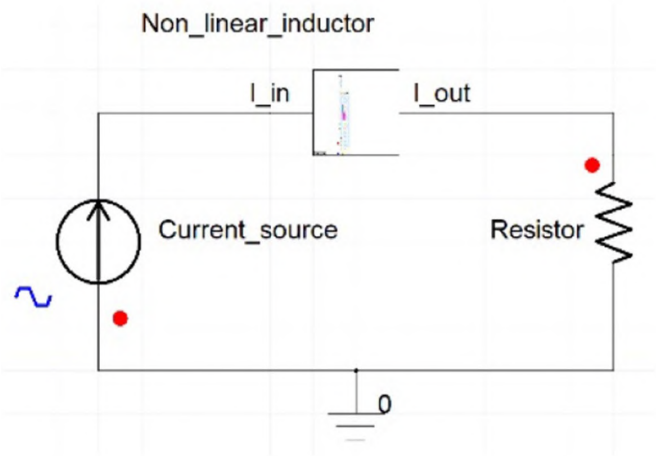

Figure 8. Lumped electric circuit (an external electric circuit).

2.3. *Magnetic model*

The FE magnetic model is necessary for the calculation of magnetic circuit properties including significant non-linearities (magnetization curve, magnetic hysteresis, etc). The analytical approach is considerably inaccurate due to the model complexity. The Ansys Electronics Desktop 2018 with co-simulation of Ansys Twin Builder 2018 was used for the presented models. We assumed the MR valve in the damper as asymmetric around the centerline Z in a cylindrical coordinate system. The simplified geometry of the MR valve for magnetic simulation is shown in figure 5.

The magnetic circuit (figure 3 (1–3)) was made of cutting steel 11SMn30. The virgin and hysteresis magnetization curve was experimentally determined for sample of this steel by system Remagraph C-500. Measured data is shown in figure 6. The coercivity and remanence were determined from the measured hysteresis loop: $H_c = 427$ A m^{-1} and $B_r = 1.05$ T.

The electric bulk conductivity $\sigma = 5.8$ MS m^{-1} was used. The lids were made of bronze with relative permeability $\mu_r = 1$ and electric bulk conductivity $\sigma = 10$ MS m^{-1}. The MRF 132-DG was used for models. The magnetic hysteresis of MR fluid was neglected. We applied the vector hysteresis modeling feature available in system Ansys on the electromagnetic model of the MR valve. A more detailed description of this model is in the publication [9]. The curve fit to the experimental hysteresis data for the steel 11SMn30 was created by Ansys software, see figure 6. The agreement is sufficient except for low magnetic field strength. The NdFe42 permanent magnet was used in the model, see the magnetization curve from magnet manufacture in figure 7. The exact geometry and magnet type were selected for availability on the market.

The magnetic model was coupled to the external electric circuit revealed in figure 8. The lumped electric circuit is composed of an ideal electric current source (control input), resistor (with the resistance of coil winding), and MR valve object (non-linear inductor).

The proposed magnetic model was used in two cases with different time scales to determine the quasi-static section 2.3.1 and transient section 2.3.2 behavior of the magnetic circuit.

2.3.1. Quasi-static magnetic model. This model was used to determine the hysteresis behavior of a magnetic circuit in two configurations: with air in the gap and with MRF in the gap. The effect of eddy currents was neglected due to slow changes in electric current. The setting of this model was used in these configurations:

(a) magnetic circuit with the electromagnetic coil (air in the gap; results in figure 11),
(b) magnetic circuit with electromagnetic coil and magnet (air and MRF in the gap; results in figures 12 and 13).

This model allows us to design a proper geometry of the magnetic circuit to maximize fail-safe magnetic flux and minimize the effect of the magnet in the gap in off-state.

2.3.2. Transient magnetic model. This model calculates the magnetic induction (flux density) course in the gap on step current input. The response times are determined from these data. The final value of the electric current (T_c) was reached at $T_c = 0.2$ ms. Therefore, it is assumed that it is the step control signal in the simulation. This value has been selected due to previous experimental experiences. The waveforms of electric current were different for different settings of this simulation. The constant simulation time step was set at 0.2 ms. The mesh was generated with refinement on the edges of the magnetic circuit due to the rapid creation of eddy current on these areas. The setting of this model was used in these configurations:

(a) magnetic circuit with electromagnetic coil and MRF in the gap (results in figure 16),
(b) magnetic circuit with an electromagnetic coil, permanent magnet and air in the gap (results in figure 15),
(c) magnetic circuit with an electromagnetic coil, permanent magnet, and MRF in the gap (results in figure 17).

2.4. Measurement setup of B–I map and magnetic circuit dynamics with the air gap

This measurement was carried out for verification of the modeling method. Measuring magnetic flux density with Hall probe can only be measured material in the gap with relative permeability $\mu_r = 1$ (air). It can be assumed, that the magnetic model verified with air in the gap will be valid for MR fluid in the gap as well. Four types of measurement with the almost identical configuration of measuring setup were carried out: (a) quasi-static properties of the magnetic circuit with permanent magnet and electromagnetic coil; (b) quasi-static properties of the magnetic circuit with electromagnetic coil; (c) response time of magnetic flux density on the electric current step in configuration with permanent magnet and electromagnetic coil; and (d) response time of magnetic flux density on the electric current step in configuration with an electromagnetic coil. For the response time measurement, the own patented current controller working with the overvoltage method was used [27]. The controller is supplied by laboratory supply and the input signal was generated from the Arduino control board. The increase in current took 0.2 ms. The experimental setup diagram can be seen in figure 9. The magnetic flux density was measured by a teslameter (F.W. Bell 5180) with an ultra-thin transverse probe (STB1X-0201). The course of electric current was measured by current clamp Fluke i30s. These two signal was measured with a sampling frequency of 200 kHz by font-end Dewetron USB-50. The measured data was processed by the software DeweSoft.

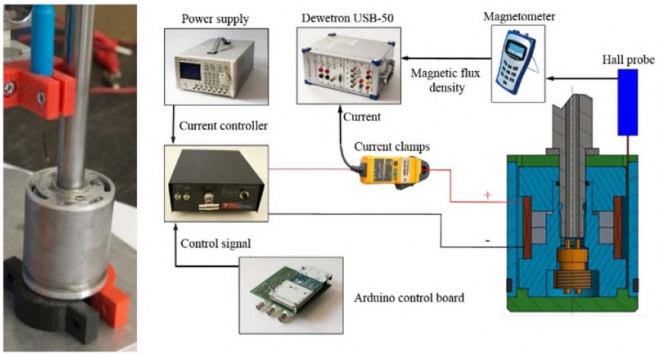

Figure 9. Experimental setup for magnetic behaviour measurement.

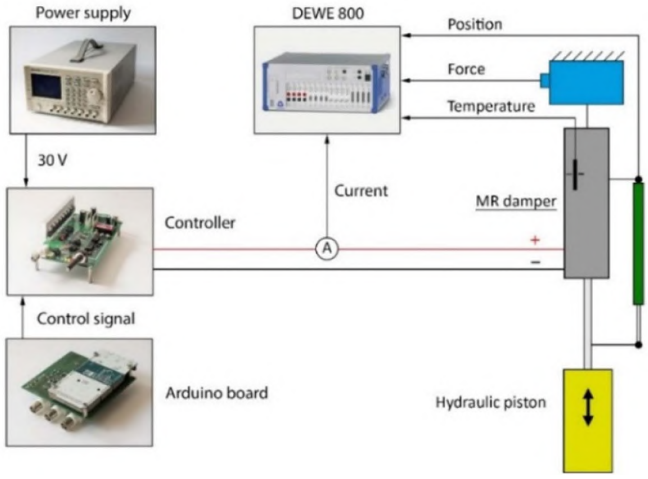

Figure 10. Experimental setup for F–v–I measurement.

2.5. Measurement setup of F–v–I map

The measurement of the F–v–I (force–velocity–electric current) map was performed on the hydraulic pulsator Inova, see figure 10. Logarithmic sweep with a constant amplitude of 25 mm was used as an excitation signal in the frequency range 0.05–1.91 Hz, therefore, the velocity was increasing during the test. The maximum velocity was 0.2 m s^{-1}. The load gauge 1730 ACK-50 kN was used for the force measurement, the position of piston-rod was measured by resistance sensor VLP15$A150, the current was calculated from the voltage drop on 0.1 Ω power shunt, and the temperature was measured by sensor PT35. The presented temperature was measured on the hydraulic tube surface of the MR damper in the range 37 °C–43 °C. These signals were recorded with a sampling frequency of 50 kHz by analyzer Dewe-800.

On the control board Arduino was set constant electric current 1 A, 2 A, 0 A(+) and with opposite polarity −1 A, −2 A, 0 A(−). The piston velocity was calculated by derivation of the piston position. The F–v–I map was calculated from measured data choosing the points with zero acceleration (center of the stroke).

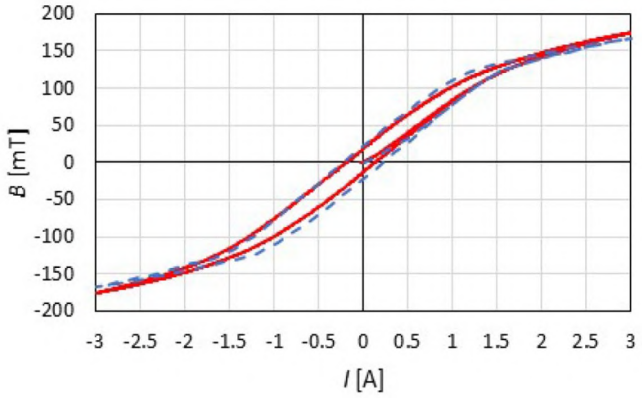

Figure 11. Comparison of the magnetic model (full line) and experiment (dotted line) for configuration without magnet and with air in the gap.

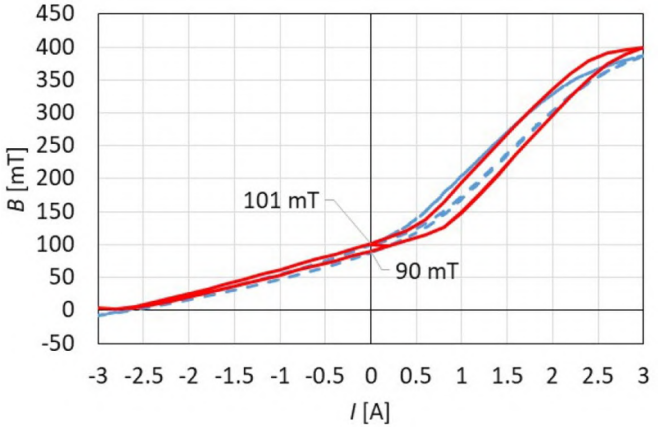

Figure 12. Comparison of the magnetic model (full line) and experiment (dotted line) for configuration with magnet and air in the gap.

2.6. Measurement setup of MR damper dynamics (force response time)

For the force response time measurement was used load gauge HBM U2AD1/2. The configuration of the measurement was the same as in chapter 2.4. The control signal was generated by the Inova control computer. This signal was input into the Arduino board and then to the current controller. The electric current was switched always after two strokes of the MR damper in the middle of the stroke. Measurement of transient response was carried out for piston velocity 0.2 m s^{-1} and electric currents 0.5 A, 1 A, 1.5 A, 2 A, and for the same values with opposite polarity. Measurement of the rise and drop of the force was performed 5× and the response time was determined as the average of these values for each electric current.

3. Results and discussion

3.1. Quasi-static magnetic behavior

This section aims to compare the magnetic model with an experiment for configuration with and without a permanent magnet. Figure 11 shows the comparison between the magnetic model (full line) and experiment (dotted line) for configuration without magnet and air in the gap. The magnetic circuit exhibits a remanent flux density of 22 mT in the gap. The agreement between model and experiment is very good. The maximum error is 15% at zero electric currents. This difference is probably given by an inaccurate fit of the hysteresis magnetization curve, see figure 6.

Figure 12 shows the comparison between the magnetic model (full line) and experiment (dotted line) for configuration with the magnet and air in the gap. Remanent flux density 101 mT and 90 mT were measured in the gap at zero electric currents. The accuracy of the model is good except for the low electric current.

The fail-safe magnetic flux density in the gap creates roughly one-fourth of the maximum. This experimentally verified model was used to determine magnetic behavior with MRF in the gap, see figure 13. The fail-safe magnetic flux density (B_{fail}) in the gap creates roughly one-third of the maximum flux density. However, the B_{fail} value is a magnetization history-dependent.

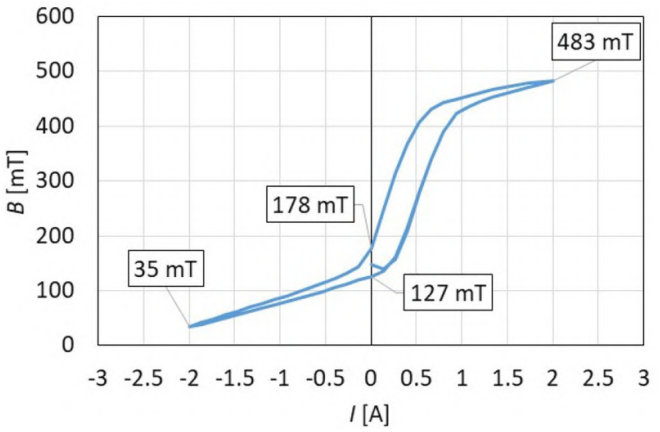

Figure 13. Hysteresis *B–I* curve of MR damper with MRF in the gap and permanent magnet.

3.2. Magnetic circuit dynamics

Magnetic flux response on a different input of electric current and a different configuration of magnetic circuit were compared for the magnetic model and experiment.

3.2.1. Magnetic circuit with air in the gap (magnet and coil).

This section is important for experimental verification of the transient magnetic model. Figure 14 shows the course of magnetic flux density determined from the magnetic model (red) and experiment (blue) for the electric current step from 0 A to −1 A. Measured data were normalized in the bottom diagram.

The difference in magnetic flux density *B* course from the model and the experiment is probably due to the slightly different electrical conductivity of the material uses in the model. The electric conductivity was used from the datasheet of the steel suppliers. The initial and final magnetic flux density data

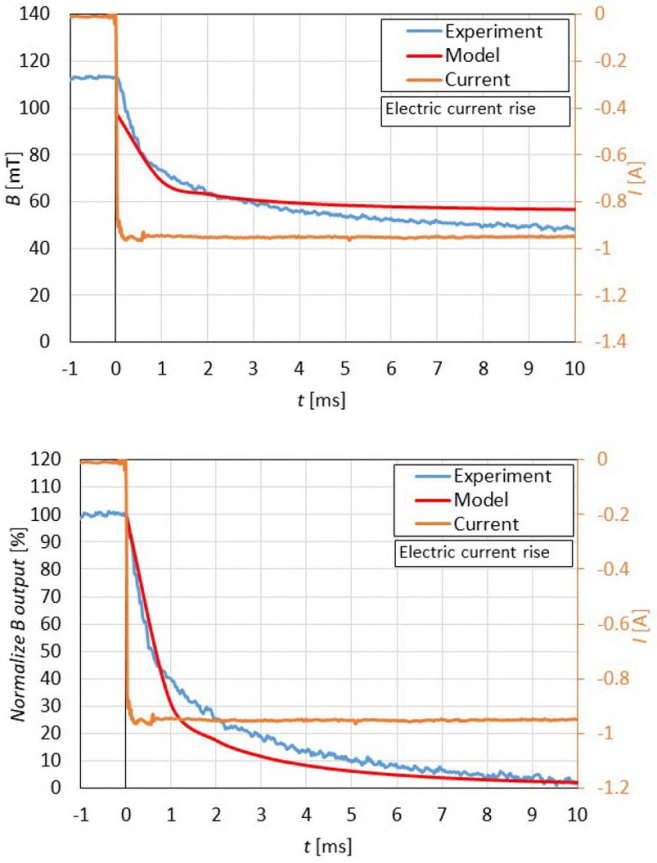

Figure 14. The course of magnetic flux density from the magnetic model and experiment.

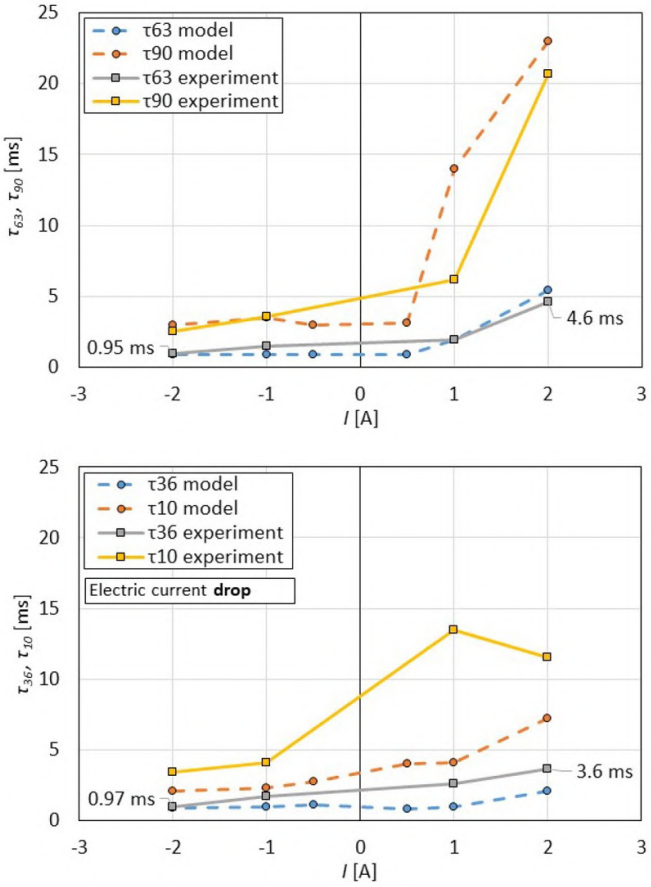

Figure 15. The primary and secondary response time for configuration with air in the gap.

from the model and experiment exhibits roughly 15% difference, see figure 14. This error is probably caused by the fitting of the hysteresis model to measured the hysteresis loop of magnetic circuit material, see figure 6. The accuracy of the magnetic model is very good in the context of many possible materials (slightly different chemical composition of steel, a measurement error of *B–H* curve, etc) inaccuracies. The primary and secondary response time dependency on the electric current are shown in figure 15. All values presented in diagram labelled 'rise' were measured for initial current in the coil I = 0 A (fail-safe state). On the other hand, the data presented in diagram labelled 'drop' were measured for final value of current I = 0 A. The presented response time values in the next text sections (if are available) are always experimental data. The response time for the negative polarity ($-I$) of electric current is significantly lower than positive polarity ($+I$). The primary response time for the electric current *rise* from 0 A to -2 A is $\tau_{63} = 0.95$ ms and for electric current *drop* from -2 A to 0 A is $\tau_{36} = 0.97$ ms. The primary response time for the electric current *rise* from 0 A to 2 A is $\tau_{63} = 4.6$ ms and for a *drop* from 2 A to 0 A is $\tau_{36} = 3.6$ ms. The magnetic flux density decrease in the gap is significantly faster than the increase. The *magnet* significantly *influences* the *dynamic behavior of the magnetic circuit*. The magnetic model describes the primary response time very well. The secondary response time exhibits greater variance, especially for the electric current drop. The magnetic model can be considered experimentally verified.

3.2.2. Magnetic circuit with MRF (coil). The experimentally verified magnetic model was used to determine the dynamic behavior of the magnetic circuit with MRF in the gap (no magnet). The response time for the electric current drop and rise are presented in figure 16. The response time dependency on electric current is non-linear. For electric current rise, the lower the electric current, the greater the response time. For electric current drop, the tendency is the opposite up to 0.5 A. Than the response time is stabilized. Thus, it can be stated that the response time is dependent on the final magnitude of the electric current. Similar results are published [32]. However, this dependence is probably related to the design of the magnetic circuit (geometry) and the magnetization characteristics of the used material. These trends are supported by several simulations and publications.

3.2.3. Magnetic circuit with MRF (magnet and coil). Figure 17 shows the dependence of the response time on step electric current drop and rise input. The response time for the current rise is increasing up to 0.5 A, then significantly decreases. The response time is $\tau_{63} = 17$ ms and $\tau_{90} = 53$ ms for the electric current rise from 0 A to 0.5 A. The trends are similar as in the case of configuration without magnet. In the opposite electric current polarity (−I), the primary and secondary time responses are almost independent of the magnitude

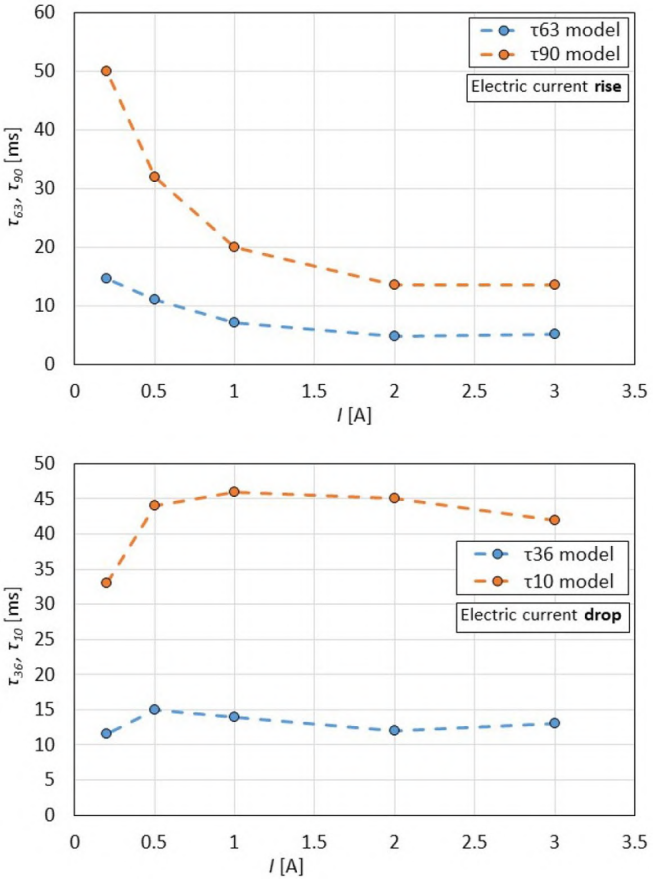

Figure 16. The response time dependency of electric current for configuration with the coil (no magnet) and MRF.

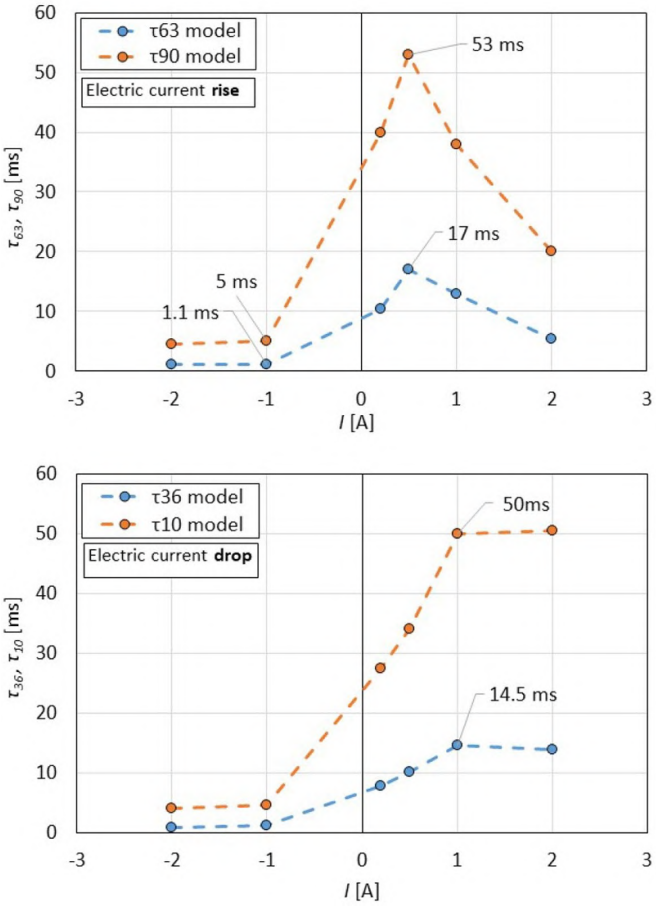

Figure 17. The response time dependency of electric current for configuration with an electromagnetic coil, magnet, and MRF.

of the electric current. The response time is $\tau_{63} = 1.1$ ms and $\tau_{90} = 5$ ms for electric current rise from 0 A to −1 A. The drop of magnetic induction in the gap is 15 times faster (primary response time) and 10 times faster (secondary response time) than the rise. The magnetic circuit dynamic is almost independent of the rising or dropping of electric current in opposite electric current polarity (−I). However, the rise and drop for electric current have a different tendency for positive polarity. The response time is $\tau_{36} = 14.5$ ms and $\tau_{10} = 50$ ms for electric current drop from 1 A to 0 A. The response time is stabilized after achieved 1 A. It can be deduced that the short response time of magnetic field formation with the negative polarity of electric current is not related to MR fluid because this effect was observed also in the magnetic circuit without MRF, see figure 15.

3.3. F–v–I map

Based on the methodology described in chapter 2.4, the force–velocity (F–v) maps were measured for 2 A, 1 A, 0 A (+), −1 A, −2 A and 0 A(-) electric currents, see figure 18. The F–v map for no electric current is affected by magnetization history (previous orientation of electric current). The damping force for zero electric current and change from higher damping forces (+0 A) is higher than the switch from lower damping forces (−0 A). The damping force for +0 A was 592 N and for −0 A was 505 N at piston velocity 0.1 m s^{-1}. This is a 15% decrease. This difference is due to the hysteresis behavior of the magnetic circuit itself, as described in figure 13. The force 505 N corresponds with magnetic induction 127 mT and force 592 N with magnetic induction 178 mT. This difference could be reduced by using another material of magnetic circuit (SMC, Vacoflux, etc) or by selecting a suitable heat treatment. Fail-safe damping force is approximately 1/3 of the maximum damping force (0.1 m s^{-1}).

The dynamic force range of damper was calculated from the maximum (+2 A) a minimum (−2 A) damping forces at given piston velocity, see figure 19. The maximum dynamic force range is 8.5 at the piston velocity of 0.06 m s^{-1}. The presented fail-safe MR damper achieves a comparable dynamic force range as the non-permanent magnet MR damper variants [3, 9, 16]. The dynamic force range of the damper is also one of the essential parameters for efficient S/A control [6].

3.4. MR damper dynamics (force response time)

The force courses on the step current input were measured according to the methodology described in chapter 2.5. Figure 20 shows the course of force (blue) and electric current

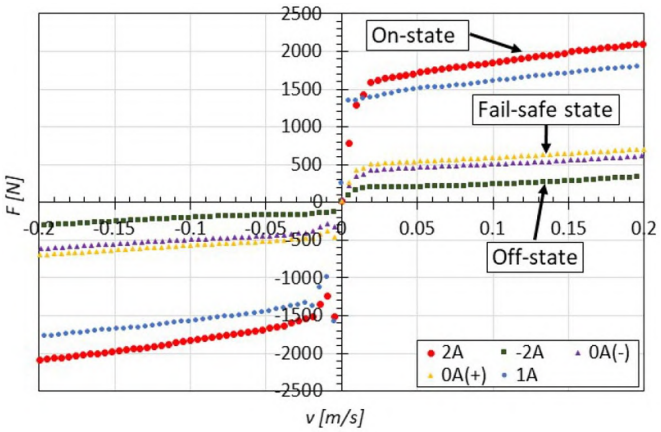

Figure 18. Force–velocity map of fail-safe MR damper.

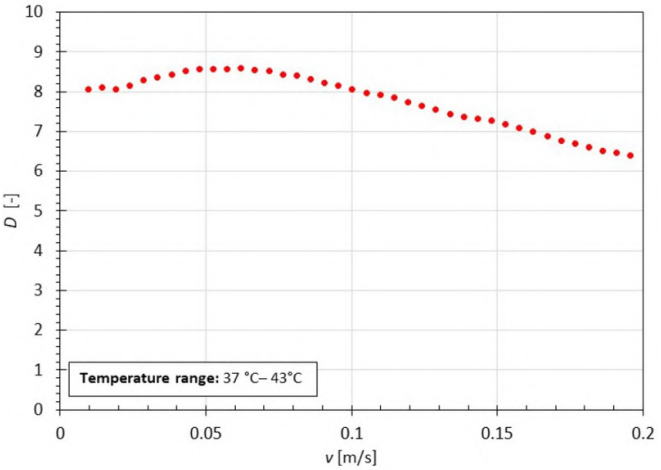

Figure 19. Dynamic force range of MR damper with magnet.

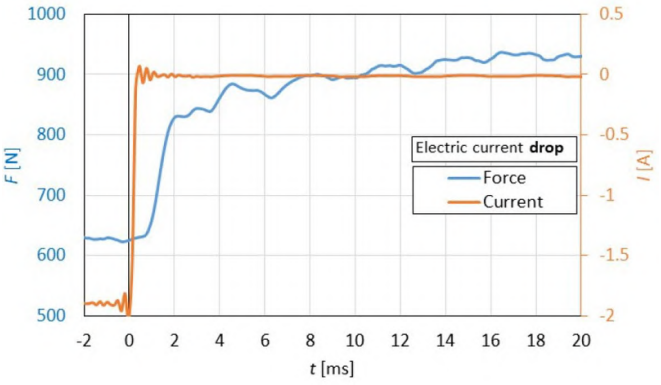

Figure 20. Example of the course of the force and electric current for unit-step electric current drop input at piston velocity 0.3 m s^{-1}.

(orange) for step current drop input from −2 A to 0 A at piston velocity 0.3 m s^{-1}. The measured force data was normalized, see figure 21. In all the measured data, it can be seen the time delay approximately 0.5–0.8 ms between the course of electric current and force. This time delay was *not* observed in the

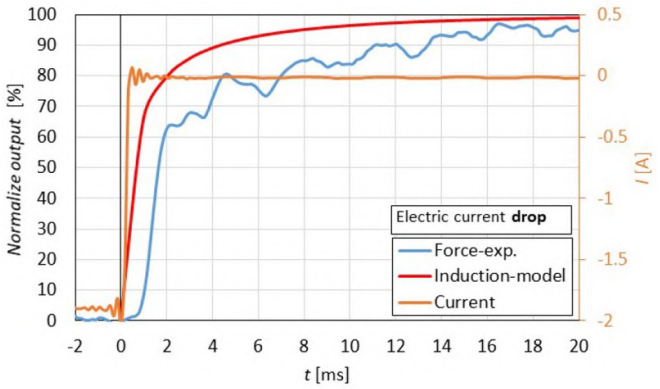

Figure 21. Normalize course of force and magnetic induction.

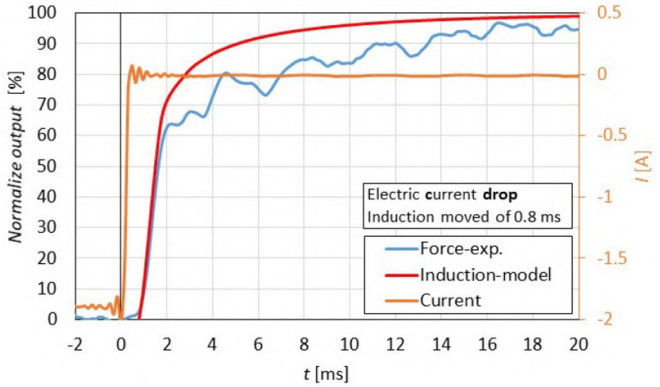

Figure 22. Normalize course of force and magnetic induction (moved of 0.8 ms).

course of magnetic induction, see figure 21, which means that it must be related to the hydraulic system.

It was checked that this time delay is not due to measurement devices or their settings. This time delay is probably caused by the response time of MR fluid itself or deformation of the rubber part of the damper (seal). Similar conclusions have been published in [17]. This phenomenon will be detailed studied in the following research.

The data from the magnetic model was moved of 0.8 ms due to the presented delay, see figure 22. The magnetic model well describes the initial course of force.

The force course exhibits significant pulsation due to the hydraulic system compliance [9]. Therefore, the determination of secondary response time is quite inaccurate and exhibits a large dispersion. The comparison of response time dependency on electric current from force measurement and magnetic model is presented in figures 23 and 24. The force measurement dispersion is presented by error bars that show maximum, minimum measured force value, and also average value.

3.4.1. Electric current step rise. The primary (τ_{63}) and secondary (τ_{90}) force response time is strongly dependent on electric current polarity and magnitude, see figure 23.

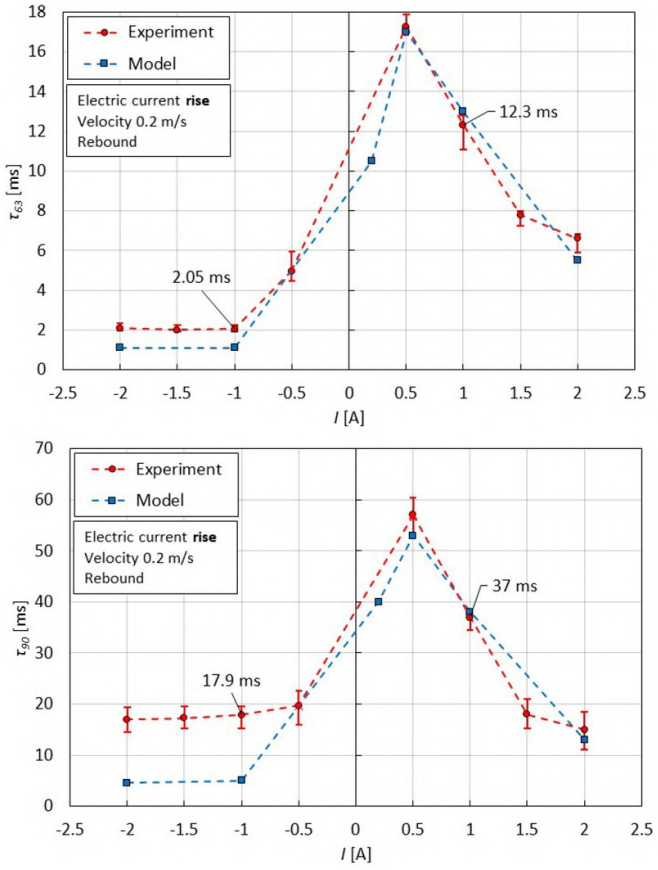

Figure 23. The course of primary and secondary response time on orientation and magnitude of electric current for configuration with electric current step rise; force data (red circle), magnetic model data (blue square).

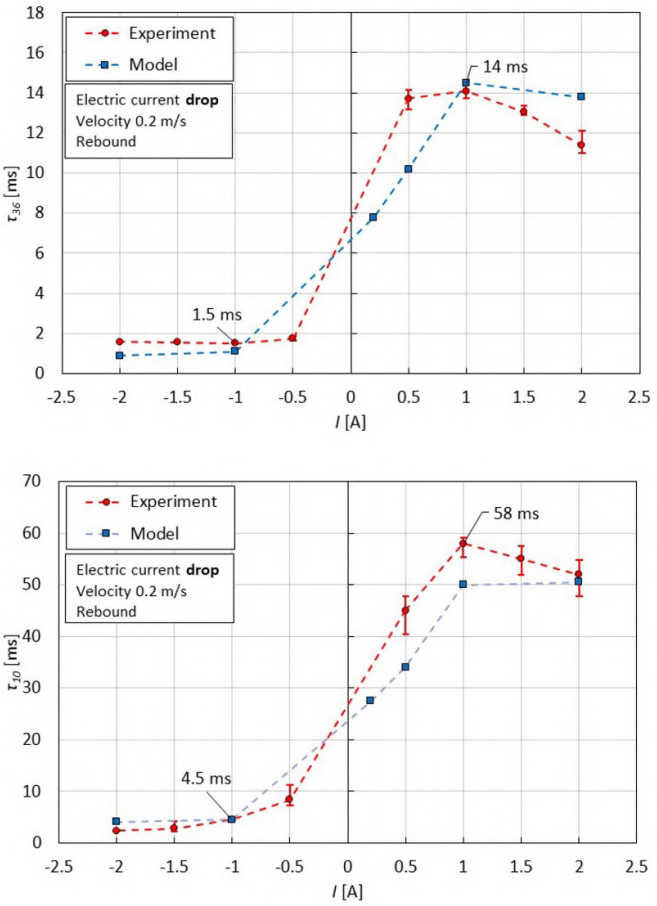

Figure 24. The course of primary and secondary response time on orientation and magnitude of electric current for configuration with electric current step drop; force data (red circle), magnetic model data (blue square).

The response time is significantly lower for the negative orientation of electric current (form 0 A to −1 A; force data $\tau_{63} = 2.05$ ms, $\tau_{90} = 17.9$ ms) than for positive orientation (from 0 A to 1 A; force data $\tau_{63} = 12.3$ ms, $\tau_{90} = 37$ ms). The drop of force is app. six times faster than rising. The primary response time determined from the magnetic model well fit experimental data, see figure 23. The secondary response time from the magnetic model also well fit experimental data except for the negative orientation of electric current. There is a significant difference.

3.4.2. Electric current step drop. The primary (τ_{63}) and secondary (τ_{90}) force response time is also strongly dependent on electric current orientation and magnitude, see figure 24.

It can be seen that negative orientation of electric current (from −1 A to 0 A; $\tau_{36} = 1.5$ ms, $\tau_{10} = 4.5$ ms) is significantly faster than positive orientation (from 1 A to 0 A; $\tau_{36} = 14$ ms, $\tau_{10} = 58$ ms). In this case, the magnetic model very well fit experimental data. It should be noted that the presented data are connected with the exact geometry and material configuration of the MR valve. It can be assumed that the exact value of response time will be dependent on the specific geometry and material configuration of the MR valve. However, the trend will be the same.

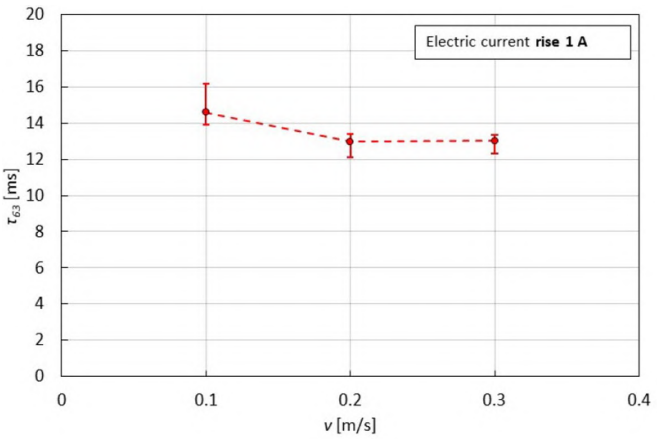

Figure 25. The influence of piston velocity on primary response time.

3.4.3. Influence of piston velocity on force response time. Figure 25 shows the influence piston velocity on primary response time for the rise of the damping force. The primary response time slightly increases at a piston velocity of 0.1 m s^{-1}. This increase is caused by the rigidity of the hydraulic system itself especially the rigidity of MR fluid. This phenomenon is also described in [9].

4. Conclusion

The optimal performance of a semi-active suspension system with fail-safe MR damper requires understanding its dynamic behavior. The knowledge of time delay between force and control signal is necessary for accurate control design study or vehicle dynamic simulations. This paper presented the dynamic behavior of MR damper with the permanent magnet. The conclusions from this paper are the following:

- The magnetic flux density in the gap at zero electric current creates roughly 1/4 of maximum and is magnetization history dependent due to hysteresis behaviour of magnetic circuit material.
- The magnetic flux density in the gap decreases significantly faster than increases on the electric current step. This is probably given by the effect of permanent magnet.
- The fail-safe damping force at zero electric current is also dependent on magnetization history and the achieved app. 1/3 of maximum damping force. The difference at fail-safe forces is due to the hysteresis behavior of the magnetic circuit.
- The dynamic force range of fail-safe MR damper achieved a value of 8.5 which similar to the common design of MR damper. The maximum damping forces are also comparable.
- The *decrease* in the *damping force* (negative polarity of electric current) from a fail-safe state to off-state is significantly faster than the increase from fail-safe state to on-state. The primary response time is roughly 2 ms. This short response time in probably given by the effect of the permanent magnet.
- The *increase* in the *damping force* (positive polarity of electric current) from fail-safe state to on-state is significantly slower than the decrease and strongly dependent on the magnitude of the electric current. The primary response time achieved roughly 12 ms at electric current 1 A.
- The initial time delay of 0.5–0.8 ms between the course of force and an electric current was observed. This delay was not observed in magnetic flux density measurement. Therefore, this delay is probably caused by hydraulic system compliance or response time MR fluid itself.
- The response time determined from the magnetic model well fitted experimental force data of MR damper. For this reason, a transient magnetic simulation is an effective tool for the determination of the dynamic behaviour of MR damper.

The following research will be focused on the durability of this type of damper and fail-safe behaviour dependency on temperature.

Acknowledgments

The authors wish to acknowledge the support of the Grant Nos. FEKT/FSI-J-20-6260, GAČR 20-23261Y and FSI-S-20-6247.

ORCID iDs

F Jeniš https://orcid.org/0000-0002-1753-1508
M Kubík https://orcid.org/0000-0003-0105-2921
Z Strecker https://orcid.org/0000-0002-1598-487X

References

[1] Westerhoff M 2018 ZF Vision magazine www.zf.com/site/magazine/en/home/magazine_homepage.html
[2] Karnopp D, Crosby M J and Harwood R A 1973 Vibration control using semi-active force generators *ASME Pap.* **96** 619–26
[3] Strecker Z, Mazůrek I, Roupec J and Klapka M 2015 Influence of MR damper response time on semiactive suspension control efficiency *Meccanica* **50** 1949–59
[4] Koo J H, Goncalves F D and Ahmadian M 2006 A comprehensive analysis of the response time of MR dampers *Smart Mater. Struct.* **15** 351–8
[5] Giua A, Melas M and Seatzu C 2004 Design of a control law for a semiactive suspension system using a solenoid valve damper *Proc. IEEE Int. Conf. Control Appl.* **2** pp 1467–72
[6] Machacek O, Kubik M and Novák P 2017 A new method of magnetorheological damper quality evaluation *Eng. Mech.* **2017** 594–7
[7] Qin Y, Zhao F, Wang Z, Gu L and Dong M 2017 Comprehensive analysis for influence of controllable damper time delay on semi-active suspension control strategies *J. Vib. Acoust. Trans. ASME* **139** 1–12
[8] Li P X, Su M and Zhang D B 2017 Response characteristic of high-speed on/off valve with double voltage driving circuit *IOP Conf. Ser. Mater. Sci. Eng* **220** 012028
[9] Kubík M and Goldasz J 2019 Multiphysics model of an mr damper including magnetic hysteresis *Shock Vib.* **2019** 1–21
[10] Roupec J, Berka P, Mazůrek I, Strecker Z, Kubík M, Macháček O and Andani M T 2017 A novel method for measurement of MR fluid sedimentation and its experimental verification *Smart Mater. Struct.* **26** 107001
[11] Cheng H, Wang M, Liu C and Wereley N M 2018 Improving sedimentation stability of magnetorheological fluids using an organic molecular particle coating *Smart Mater. Struct.* **27** 1–10
[12] Plachy T, Cvek M, Kozakova Z, Sedlacik M and Moucka R 2017 The enhanced MR performance of dimorphic MR suspensions containing either magnetic rods or their non-magnetic analogs *Smart Mater. Struct.* **26** 1–8
[13] Cvek M, Mrlik M, Ilcikova M, Plachy T, Sedlacik M, Mosnacek J and Pavlinek V 2015 A facile controllable coating of carbonyl iron particles with poly(glycidyl methacrylate): a tool for adjusting MR response and stability properties *J. Mater. Chem.* C **3** 4646–56
[14] Zheng J, Li Y and Wang J 2017 Design and multi-physics optimization of a novel magnetorheological damper with a variable resistance gap *Proc. Inst. Mech. Eng.* C **231** 3152–68
[15] Gołdasz J 2013 Electro-mechanical analysis of a magnetorheological damper with electrical steel laminations *Prz. Elektrotechniczny* **89** 8–12 (http://pe.org.pl/articles/2013/2a/2.pdf)
[16] Kubík M, Macháček O, Strecker Z, Roupec J and Mazůrek I 2017 Design and testing of magnetorheological valve with fast force response time and great dynamic force range *Smart Mater. Struct.* **26** 047002
[17] Strecker Z, Kubik M, Vitek P, Roupec J, Paloušek D and Šreibr V 2019 Structured magnetic circuit for

magnetorheological damper made by selective laser melting technology *Smart Mater. Struct.* **28** 1–13
[18] Goldasz J 2019 Magnetostatic study of a dual-gap MR valve *Proc. 2019: 20th Int. Conf. Res. Educ. Mechatronics, REM 2019* **5** pp 1–5
[19] Goldasz J 2013 Study of a magnetorheological fl uid damper with multiple annular flow gaps *Int. J. Veh. Des.* **62** 21–41
[20] Bai X X and Wereley N M 2014 A fail-safe magnetorheological energy absorber for shock and vibration isolation *J. Phys. D: Appl. Phys.* **115** 1–4
[21] Zhang H H, Liao C R, Yu M and Huang S L 2007 A study of an inner bypass magneto-rheological damper with magnetic bias *Smart Mater. Struct.* **16** N40–6
[22] Yan W, Ji J, Dong B and Ge H 2009 Theoretical and experimental studies on a new reversible magnetorheological damper *Struct. Control Health Monit.* **18** 1–19
[23] Du C, Wan F and Yu G 2011 A magnetic flux leakage study of a self-decoupling magnetorheological damper *Smart Mater. Struct.* **20** 065019
[24] Böse H and Ehrlich J 2012 Magnetorheological dampers with various designs of hybrid magnetic circuits *J. Intell. Mater. Syst. Struct.* **23** 979–87
[25] Bose H, Ehrlich J and Trendler A-M 2009 Performance of magnetorheological fluids in a novel damper with excellent fail-safe behavior *11th Conf. on Electrorheological Fluids and Magnetorheological Suspensions* p 5
[26] Takesue N, Kiyota Y and Furusho J 2002 Development of fast response MR-fluid actuator *Proc. 41st SICE Annual Conf. SICE* (Soc. Instrument & Control Eng. (SICE)) vol **2** pp 949–53
[27] Strecker Z, Roupec J, Mazurek I, Machacek O, Kubik M and Klapka M 2015 Design of magnetorheological damper with short time response *J. Intell. Mater. Syst. Struct.* **26** 1951–8
[28] Kostamo E, Kostamo J, Kajaste J and Pietola M 2012 Magnetorheological valve in servo applications *J. Intell. Mater. Syst. Struct.* **23** 1001–10
[29] Sahin H, Gordaninejad F, Wang X and Liu Y 2012 Response time of magnetorheological fluids and magnetorheological valves under various flow conditions *J. Intell. Mater. Syst. Struct.* **23** 949–57
[30] Lee T-H and Choi S-B 2019 On the response time of a new permanent magnet based magnetorheological damper: experimental investigation *Smart Mater. Struct.* **28** 014001
[31] Maas J and Güth D 2011 Experimental investigation of the transient behavior of MR fluids *Conf. on Smart Materials, Adaptive Structures and Intelligent Systems (ASME)* pp 229–38
[32] Wu G, Feng Z, Zhang G and Hou Z 2011 Experimental study on response time of magnetorheological damper *Int. Conf. on Artificial Intelligence, Management Science and Electronic Commerce* (IEEE) pp 3968–72
[33] Yoon D S, Park Y J and Choi S B 2019 An eddy current effect on the response time of a magnetorheological damper: analysis and experimental validation *Mech. Syst. Signal Process.* **127** 136–58

actuators

MDPI

Article

Effect of the Magnetorheological Damper Dynamic Behaviour on the Rail Vehicle Comfort: Hardware-in-the-Loop Simulation

Filip Jeniš [1,*], Michal Kubík [1], Tomáš Michálek [2], Zbyněk Strecker [1], Jiří Žáček [1] and Ivan Mazůrek [1]

[1] Institute of Machine and Industrial Design, Faculty of Mechanical Engineering, Brno University of Technology, Technicka 2, 616 69 Brno, Czech Republic
[2] Department of Transport Means and Diagnostics, Faculty of Transport Engineering, University of Pardubice, Studentska 95, 532 10 Pardubice, Czech Republic
* Correspondence: filip.jenis@vutbr.cz; Tel.: +420-541-143-216

Abstract: Many publications show that the ride comfort of a railway vehicle can be significantly improved using a semi-active damping control of the lateral secondary dampers. However, the control efficiency depends on the selection of the control algorithm and the damper dynamic behaviour, i.e., its force rise response time, force drop response time and force dynamic range. This paper examines the influence of these parameters of a magnetorheological (MR) damper on the efficiency of S/A control for several control algorithms. One new algorithm has been designed. Hardware-in-the-loop simulation with a real magnetorheological damper has been used to get close to reality. A key finding of this paper is that the highest efficiency of algorithms is not achieved with a minimal damper response time. Furthermore, the force drop response time has been more important than the force rise response time. The Acceleration Driven Damper Linear (ADD-L) algorithm achieves the highest efficiency. A reduction in vibration of 34% was achieved.

Keywords: hardware-in-the-loop; Acceleration Driven Damper; response time; dynamic range; semi-active; magnetorheological; damper; railway vehicle; lateral vibration

Citation: Jeniš, F.; Kubík, M.; Michálek, T.; Strecker, Z.; Žáček, J.; Mazůrek, I. Effect of the Magnetorheological Damper Dynamic Behaviour on the Rail Vehicle Comfort: Hardware-in-the-Loop Simulation. *Actuators* **2023**, *12*, 47. https://doi.org/10.3390/act12020047

Academic Editor: Norman M. Wereley

Received: 19 December 2022
Revised: 12 January 2023
Accepted: 17 January 2023
Published: 19 January 2023

1. Introduction

Rail transport has recently become increasingly important around the world. One of the most important parameters of a railway vehicle is comfort (carbody vibration). The damping system is primarily responsible for carbody vibration mitigation. Today, commonly-used passive dampers have limits and can no longer solve new problems. The carbody vibration can be reduced using a semi-active or active system. The active system contains actuators instead of springs and dampers. The actuator can precisely create the force required to dampen the sprung mass. The significant disadvantages of active systems are the relative complexity, high cost, energy consumption and difficulties in implementing a fail-safe system [1,2]. An alternative to an active system is a semi-active system. The semi-active damper can change the damping characteristic using data from various sensors [3,4]. Using magnetorheological (MR) dampers for semi-active (S/A) control is advisable because MR dampers have very good transient behaviour [5]. One of the advantages of the MR damper is the possibility of fail-safe behaviour using a permanent magnet [6].

In the case of railway vehicles, several publications have verified the potential benefits of semi-active control of lateral secondary MR dampers in reducing carbody vibrations. Codeca et al. [7] tested the semi-actively controlled lateral secondary dampers and their effect on the carbody vibrations on a laboratory stand. The experimental stand was excited by a signal obtained from a real measurement on the track when running at high speed. A combination of Skyhook and Acceleration Driven Damping algorithms achieved the highest efficiency, reducing vibrations by 34%, compared to passive damping. Lau and Liao [8] examined the effect of S/A control of the lateral secondary dampers on ride comfort. The semi-active algorithm is simple and switches between Low and High damping states

based on the magnitude of carbody lateral velocity. If the carbody velocity exceeds the critical speed, the damper switches to a High state. The simulations were performed on a complex railway vehicle dynamic model. The carbody lateral vibration was reduced by 39% compared to the passive damper. Shin et al. [9] dealt with the simulation and experimental verification of the secondary lateral damper semi-active control effect. A half-vehicle model with nine degrees of freedom was used for the simulation. For experimental validation, a 1:5 scale real simplified model was used. The Skyhook algorithm decreased vibration by 77% in the simulation compared to passive damping and 67% in the experiment. Hudha et al. [10] used two types of Skyhook algorithm: body-based and bogie-based for the lateral secondary MR dampers. The vehicle's body lateral deviation, yawing, and rolling motion were evaluated in a dynamic model of 17 degrees of freedom. The algorithms worked well, both improving all three criteria.

Papers [11,12] show that damper force response time is essential for the performance of semi-actively controlled damping systems. The shorter the response time, the better the S/A control performance. Paper [13] shows that the time response is further dependent on the piston velocity, the magnitude of the electric current change, the stiffness of the damper mounting and the control electronics. The response time is negatively affected by the formation of eddy currents in the piston core, but this problem can be solved by using a suitable core shape [5,14]. Response time also depends on the dwell time of Fe particles in the active-magnetic zone and the concentration of Fe particles in the carrier fluid [13]. Papers [5,7] show that force response time differs for force rise and drop. The damper dynamic range (the ratio of the damping force in the activated and non-activated state) is also essential for the efficiency of the S/A control [15].

The MR dampers exhibit highly non-linear behaviour, which is very difficult to model properly. The MR damper models used in simulations are always simplified and often do not correspond to the force generated by real MR damper for given working conditions, degrading the results from simulations of semi-active suspension. To avoid the problem, many teams used the Hardware-in-the-loop method to evaluate the semi-active algorithms. Choi et al. [16] used HILS to design a semi-active control seat for a truck vehicle, and Lee et al. [17] used it to study the S/A control of a car suspension. Misselhorn et al. [18] successfully tested HILS usability in suspension design, comparing HILS with a virtual simulation on a single corner model and a simplified physical model of motorcycle suspension. Kwak et al. [19] used HILS to verify the benefit of the Skyhook algorithm for the lateral movement of the railway vehicle carbody. Oh et al. [20] studied the active control of tramcars independently rotating wheels in HILS. This approach enables to use of force generated directly by the real MR damper excited by the pulsator. The pulsator position in the time is controlled by the output of a virtual model running on a suitable platform.

Problem Formulation

It is known that force response time and dynamic range have an essential effect on the effectiveness of S/A control but the impact of this effect on different S/A algorithms has not been directly investigated. It is also known that the response time is different for the force rise and force drop when the electric current changes but in the case of simulation with the implemented response time of the damper, the response time is considered to be the same for both force rise and force drop. It is not known whether this simplification is permissible. It can be assumed the longer response time and the lower dynamic range lead to the lower effectiveness of the strategy used, but it is not known what maximum response time is acceptable for different algorithms.

The paper's main aim is to investigate the effect of selected parameters of the MR damper on rail suspension performance in detail. The response time of damping force rise, damping force drop, and dynamic force range are studied separately. The hardware-in-the-loop simulation with a real MR damper will be used to accommodate several non-linearity in damper dynamics. Simulations are evaluated for several known S/A damper control algorithms and one newly-designed algorithm (Acceleration Driven Damper Linear).

2. Materials and Methods

2.1. Vehicle Model

A lateral motion model of a rail vehicle with two degrees of freedom has been developed. The model represents one wheelset, half of the bogie frame and a quarter of a carbody. The model layout can be seen in Figure 1, and the following equations describe the model:

$$m_2\ddot{y}_2 = -k_2\,(y_2 - y_1) + F_{mr} \tag{1}$$

$$m_1\ddot{y}_1 = k_2\,(y_2 - y_1) - F_{mr} - k_1\,(y_1 - y_0) - c_1\,(\dot{y}_1 - \dot{y}_0) \tag{2}$$

where F_{mr} is s force of MR damper and y_2, y_1 and y_0 are lateral displacements of carbody, bogie frame and wheelset. Other model parameters are listed in Table 1. The model parameters are derived from a four-axle locomotive weighing 90 tons. The lateral damper used is reduced in scale. Therefore the parameters of the vehicle model are also reduced by a ratio of 1:5.

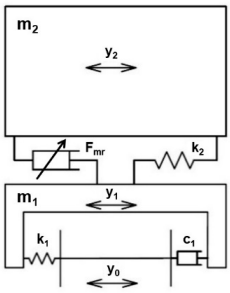

Figure 1. Railway vehicle simplified model schema.

Table 1. Model parameters.

Parameter	Symbol	Original	1:5 Scale
half bogie frame weight	m1	5000 kg	1000 kg
quarter carbody weight	m2	13,750 kg	2750 kg
wheelset-bogie frame bond stiffness	k1	10 kN/mm	2 kN/mm
bogie frame-carbody bond stiffness	k2	1 kN/mm	0.2 kN/mm
wheelset-bogie frame bond damping	c1	10 kNs/m	2 kNs/m

The model was excited by defined lateral wheelset motion y_0, which was obtained from a simulation of a complex multi-body model of a railway vehicle (electric locomotive) running on a straight track with irregularities at 160 km/h, which is the speed limit on Czech railways. This complex model with 58 degrees of freedom was created in the multi-body simulation tool "SJKV" [21]. The track irregularities were generated using PSD of track irregularities in Europe according to ORE B 176. The wheelset-track coupled dynamic is neglected, for a more objective comparison of the results of S/A algorithms, so excitation y_0 is still the same for every case. Figure 2 shows the wheelset lateral displacement course and the FFT analysis of this course. The duration of the excitation signal was 10 s. The excitation magnitude was at the original scale, so even the scale of the damper stroke corresponds to reality.

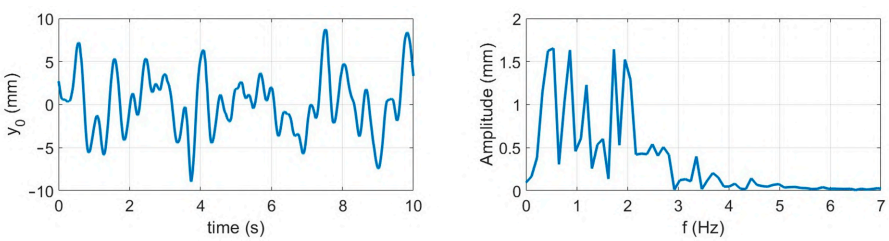

Figure 2. Excitation signal y_0 (**left**) and its FFT analysis (**right**).

2.2. Hardware-in-the-Loop Simulation

Mathematically describing the behaviour of a real damper is very difficult because it is necessary to include hysteresis (magnetic, hydraulic, etc.), temperature dependence, etc., in the model. For simplified models, it is difficult to say whether they neglect some essential property. Therefore, it is necessary to use HIL simulation to bring it closer to reality. This simulation allows the damper response time and the dynamic range effect on the S/A control to be investigated on a real MR damper without needing a real vehicle or physical model.

The damper is mounted in a hydraulic pulsator, controlled by a control system (dSpace RTI1104 in this case). A virtual railway vehicle model was built in Matlab/Simulink and transferred to the ControlDesk program, which controls the dSpace system. Based on the damper-measured force, the simulation calculates the virtual position of sprung and unsprung masses (y_2 and y_1) in real time. The calculated control signal 1 (see Figure 3 left) with the damper stroke $y_2 - y_1$ (see Figure 1) is sent to the hydraulic pulsator, which excites the MR damper. The control signal 2 with the desired current (see Figure 3 left) is also sent in real-time to the current controller, which excites the MR damper.

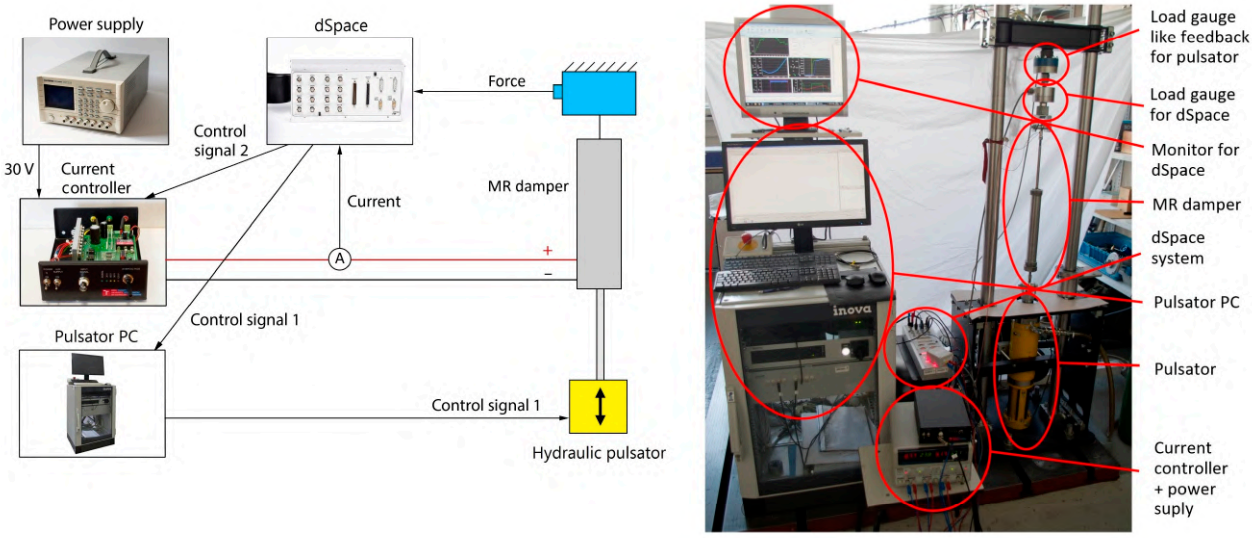

Figure 3. Experimental setup for HILS (**left**), HILS assembly (**right**).

The current controller is a self-made device that works in analogue voltage input-analogue current output mode. The highest achievable current is I = 3 A. The rise time of the electric current from 0 to 2 A is 1 ms as a response to input signal step 0–2 V, and the drop time from 2 to 0 A is 0.5 ms as a response to step 2–0 V. The pulsator assembly has a built-in load gauge HBM U2AD1/2 that measures the current damping force. Load gauge deflection at maximal damper force is 7 μm, so gauge mechanical response time is possible to neglect. The signal from the load gauge is amplified by an analogue bridge amplifier with no delay. The damping force data are input for the virtual model. The HILS schema is shown in Figure 3 left, and the HILS assembly is in Figure 3 right. It showed that the response time of the pulsator was significantly shorter than the response time of the damper, so it did not cause any problems.

2.3. Magnetorheological Damper

This study used a real MR damper with a stroke of 160 mm and a maximum damping force of 2000 N (at the piston velocity of 0.3 m/s). In the piston, the MR damper has one coil with an electric resistance of R = 1.39 Ω. The coil inductance in the damper electric circuit with MR fluid is L = 50 mH. The magnetic circuit is made of Sintex SMC material to achieve a fast transient response. The damper is described in more detail in the paper [5].

2.3.1. F-v-I Map

The F-v-I (force-velocity-electric current) map expresses the dependence of the damper force on the actual piston velocity and the electric current in the coil. The measurement of the F-v-I map was performed on the hydraulic pulsator in the configuration described in Figure 3. However, in the case of the F-v-I map measurement, the device did not work in HILS mode (pulsator stroke generated based on vehicle model simulations), but the course of the damper stroke was fixedly specified. The logarithmic sweep with a constant amplitude of 20 mm was used as an excitation signal in the frequency range of 0.05–1.6 Hz. Therefore, the velocity was increasing during the test. The maximum velocity was 0.2 m/s. The load gauge HBM U2AD1/2 was used. The electric current was measured by current clamps Fluke i30s. Signals were recorded by dSpace. The F-v-I map was calculated from measured data choosing the points with zero acceleration (centre of the stroke).

The measured F-v curves are shown in Figure 4. The damper F-v curves are symmetrical for both tension and compression, whereas the graph shows only the positive F-v curves part. The damper dynamic force range at piston velocity 0.1 ms^{-1} is dr = 7.6.

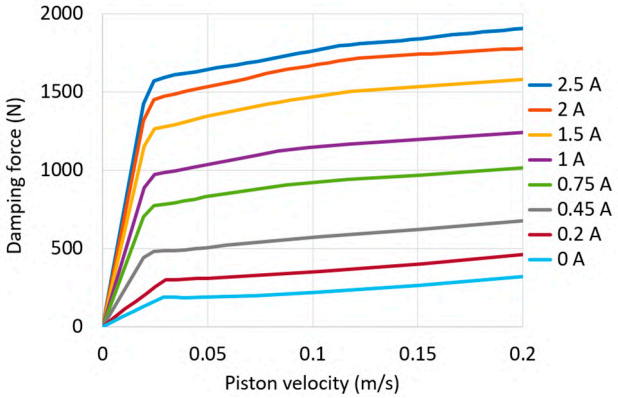

Figure 4. Measured F-v-I map of the used damper.

2.3.2. Response Time

The dynamic (transient) behaviour of the MR damper is usually assumed to be a first-order system, and the response time is usually defined as a time constant τ_{63} [22–24]. The force in time can then be described by the equation:

$$F(v,t) = F_0(v) + (F_1(v) - F_0(v)) \cdot \left(1 - e^{-\frac{t}{\tau_{63}}}\right) \quad (3)$$

where $F_0(v)$ is a force at $t = 0$, and $F_1(v)$ is force corresponding to the desired force for the given velocity and current, v is piston velocity, t is the time from the change of the control signal, and τ_{63} is the time constant.

The time constant τ_{63} means the time required to reach 63.2% of the final steady-state force (see Figure 5). Similarly, the time constant for the force drop τ_{36} expresses how long it takes for the force to drop back to 36.8% of the initial force. Response times for damper force rise τ_{63}, and for damper force drop τ_{63} on unit-step electric current rise and drop will be determined from measured data in this paper.

The measurement configuration was the same as described in the previous sections (Figure 3). The damper was tested without flexible silent blocks. The electric current was activated (to I = 2 A) and deactivated (to I = 0 A) when the damper was mid-stroke. The transient force response was measured for electric current change from 0 A to 2 A and from 2 A to 0 A, and for piston velocity of 0.1 m/s, approximately 70% of the highest piston velocity reached during simulations. The methodology is described in more detail in [25].

Damper force response time was measured at τ_{63} = 1.8 ms for force rise and τ_{36} = 1.1 ms for force drop (see Figure 5). Every response time value is an average of five measurements.

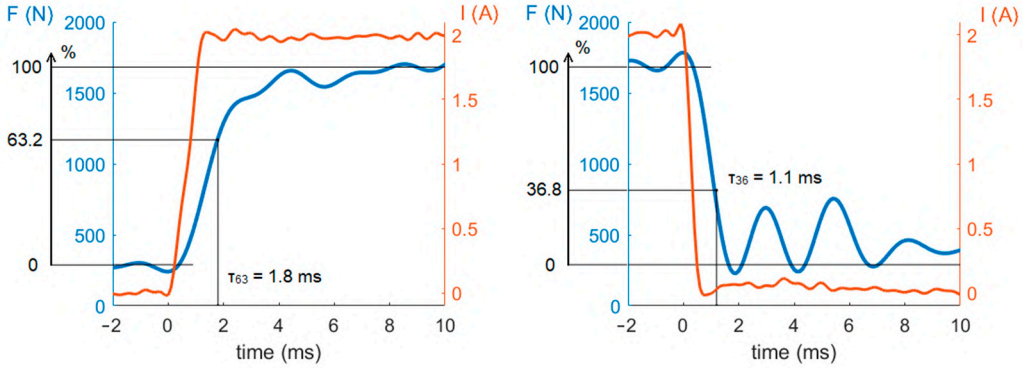

Figure 5. Example of measured response time for rise (**left**) and drop (**right**). I (A) is the measured electric current, and F (N) is the measured damping force.

2.4. Semi-Active Control

For evaluation of the response time impact on different control strategies, this research used passive mode, three well-known semi-active algorithms: Skyhook, Skyhook linear, and Acceleration Driven Damper and one newly designed: Acceleration Driven Damper Linear.

2.4.1. Skyhook

Skyhook with two states (SH-2) is a commonly used algorithm for comfort improvement. It was designed by Karnopp [26]. The control rule for this algorithm is based on two input signals: the carbody lateral velocity and the relative lateral velocity between the carbody and the bogie frame. If the carbody velocity is higher than the relative velocity between the carbody and the bogie frame, the damper is in the high damping state. Mathematically:

$$F(v) = \begin{cases} F_{max}(v), & \dot{y}_2(\dot{y}_2 - \dot{y}_1) \geq 0 \\ F_{min}(v), & \dot{y}_2(\dot{y}_2 - \dot{y}_1) < 0 \end{cases} \quad (4)$$

where $F(v)$ is a required damping force, $F_{max}(v)$ is damping force at a current of I_{max}, $F_{min}(v)$ is damping force at I_{min}, $\dot{y}_2$ is carbody lateral velocity, and $\dot{y}_1$ is bogie frame lateral velocity.

2.4.2. Skyhook Linear

The Skyhook Linear (SH-L) is an improved version of the ON/OFF Skyhook, published by Sammier [27]. This algorithm changes the damping characteristics continuously. Initially, the algorithm is designed as follows:

$$F(v) = \begin{cases} F_{min}(v), & \dot{y}_2(\dot{y}_2 - \dot{y}_1) \leq 0 \\ sat\left(\frac{\alpha \cdot F_{max}(v) \cdot (\dot{y}_2 - \dot{y}_1) + (1-\alpha) \cdot F_{max}(v) \cdot \dot{y}_2}{(\dot{y}_2 - \dot{y}_1)}\right), & \dot{y}_2(\dot{y}_2 - \dot{y}_1) > 0 \end{cases} \quad (5)$$

where $F(v)$ is a required damping force, $F_{max}(v)$ is damping force at a current of I_{max}, and $F_{min}(v)$ is damping force at I_{min}, $\dot{y}_2$ is carbody lateral velocity, $\dot{y}_1$ is bogie frame lateral velocity, $\alpha \in [0,1]$ is tuning, and *sat* denotes that $F_c \in [F_{min}(v),\ F_{max}(v)]$.

The algorithm has the best performance for $\alpha = 0$. For a simpler algorithm application, the damping force in the equation has been replaced by an electric current. So, the final calculation of the current looks as follows:

$$I = \begin{cases} sat\left(\frac{I_{max} \cdot \dot{y}_2}{(\dot{y}_2 - \dot{y}_1)}\right), & \dot{y}_2(\dot{y}_2 - \dot{y}_1) \geq 0 \\ I_{min}, & \dot{y}_2(\dot{y}_2 - \dot{y}_1) < 0 \end{cases} \quad (6)$$

where I is a required electric current, I_{max} is a maximal electric current, I_{min} is a minimal electric current, $\dot{y}_2$ is carbody lateral velocity, $\dot{y}_1$ is bogie frame lateral velocity, and *sat* denotes that $I \in [I_{min}(v),\ I_{max}(v)]$.

The damping force is not linearly dependent on the electric current but converting the damping force to electric current so that the force corresponds to the equation above would be unnecessarily demanding. Therefore, there is some bias in the algorithm from the original version, but the control strategy still works well.

2.4.3. Acceleration Driven Damper

Acceleration Driven Damper (ADD-2) was designed by Savaresi [28]. This algorithm works such as Skyhook but uses carbody acceleration instead of carbody velocity. So, its realisation is more accessible in practice. Mathematically:

$$F(v) = \begin{cases} F_{max}(v), & \ddot{y}_2(\dot{y}_2 - \dot{y}_1) \geq 0 \\ F_{min}(v), & \ddot{y}_2(\dot{y}_2 - \dot{y}_1) < 0 \end{cases} \tag{7}$$

where $F(v)$ is a required damping force, $F_{max}(v)$ is damping force at a current of I_{max}, $F_{min}(v)$ is damping force at I_{min}, $\ddot{y}_2$ is carbody lateral acceleration, $\dot{y}_2$ is carbody lateral velocity and $\dot{y}_1$ is bogie frame lateral velocity.

The algorithm has a problem with unwanted fast-switching behaviour. A rapid change in damping force when switching the state causes a change in the acceleration orientation, which again causes the state switch. Thus, the damper switches state very quickly at low piston velocity, reducing the damper's life. Savaresi also encountered this phenomenon of the problem of the fast-switching behaviour of ADD, but he did not deal with it [29]. However, this problem could be eliminated by switching the damper state only if the carbody lateral acceleration is larger than $\ddot{y}_2 > 0.2\ \mathrm{ms}^{-2}$. If $\ddot{y}_2 < 0.2\ \mathrm{ms}^{-2}$, the damper remains in the state from the previous step, regardless of the result of the equation $\ddot{y}_2(\dot{y}_2 - \dot{y}_1)$. This equation is solved only if $\ddot{y}_2 > 0.2\ \mathrm{ms}^{-2}$. Eliminating unwanted chattering behaviour further improved the efficiency of the algorithm.

2.4.4. Acceleration Driven Damper Linear

This variant of the algorithm Acceleration Driven Damper is new. It has not been described in the literature yet. The ADD algorithm was modified to a linear form according to the Skyhook linear pattern:

$$I = \begin{cases} sat\left(\frac{I_{max} \cdot \dot{y}_2}{(\dot{y}_2 - \dot{y}_1)}\right), & \ddot{y}_2(\dot{y}_2 - \dot{y}_1) \geq 0 \\ I_{min}, & \ddot{y}_2(\dot{y}_2 - \dot{y}_1) < 0 \end{cases} \tag{8}$$

where I is a required electric current, I_{max} is a maximal electric current, I_{min} is a minimal electric current, $\ddot{y}_2$ is carbody lateral acceleration, $\dot{y}_2$ is carbody lateral velocity, $\dot{y}_1$ is bogie frame lateral velocity, and *sat* denotes that $I \in [I_{min}(v), I_{max}(v)]$.

The new algorithm is called Acceleration Driven Damper Linear (ADD-L). This algorithm has the same problem with unwanted damping force oscillations as ADD-2. This problem has been solved similarly as in the previous case.

2.5. Plan of Experiments and Evaluation Method

The simulations of S/A control were performed in HIL mode (Section 2.2), where the damper stroke $y_2 - y_1$ is obtained based on the vehicle model simulation (Figure 1). Four case studies will be reported: (1) the influence of force rise response time, (2) the influence of force drop response time, (3) the influence of force rise and drop response time together in real proportions, and (4) the influence of dynamic force range. The variables for sensitivity analysis are in Table 2.

Table 2. The variables for sensitivity analysis.

Case	τ_{63} (ms)	τ_{36} (ms)	DR at 0.1 m/s (-)
1	1.8–56	*	7.6
2	*	1.1–56	7.6
3	1.8–56	$\tau_{63}/1.7$	7.6
4	*	*	2–7.6

* Ideal response time for the selected algorithm.

In case 3 the real damper does not have the same long response time for force rise and drop. The ratio between the force rise response time and force drop response time is about 1.7.

The influence of the response time was monitored from the shortest possible response times, determined by the damper design (τ_{63} = 1.8 ms and τ_{36} = 1.1 ms, see Section 2.3.2), to response times of 56 ms. The longer force response times, then 1.8 ms or 1.1 ms, were created using the current controller. The current rises (or drops) exponentially according to the equation:

$$I(t) = I_0 + (I_1 - I_0) \cdot \left(1 - e^{-\frac{t}{\tau}}\right) \quad (9)$$

where I_0 is an electric current at $t = 0$, I_1 is the desired current, t is the time from the step of the control signal, and τ is an artificial current response time that is adjusted as needed.

When response time was slowed down using the current ramp-up, its real value was measured by the methodology described in Section 2.3.2. The required dynamic force range (DR) was set by I_{min}. It showed that S/A algorithms have the best performance when the maximal electric current is I_{max} = 2 A, and passive damping has the best performance when the current is I = 0.5 A. Thus, these currents were used in HILS.

The lateral acceleration of the carbody testifies, above all, to ride comfort. The overall RMS of lateral acceleration in relevant track sections was used to evaluate the comfort of the railway vehicle in on-track tests. This evaluation is also used by the standard EN 14363 [30].

3. Results and Discussion

3.1. Response Time Effect

Figure 6 shows the dependence of carbody lateral acceleration overall RMS on the response time of damping force rise τ_{63} (case 1). The dependency is the same for all four algorithms. With decreasing τ_{63}, the vibrations decrease linearly to τ_{63} = 15 ms. After that, no significant improvement was observed for shorter response times. However, with a shorter time response, noise appears. The noise is caused by a large force impact during damper state switching. Enormous force impact is caused by a rapid change in damping force when a very short response time is used. We assume these force impacts cause unwanted vibrations and thus degrade the results for very short response times. The ideal force rise and drop response times for each algorithm are shown in Table 3. In case 1, the force drop response time was set statically, ideal for each algorithm, according to Table 3.

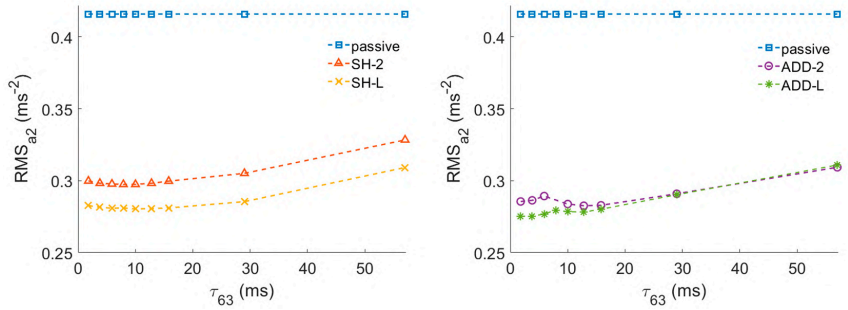

Figure 6. Damper force rise response time τ_{63} effect for passive mode, SH-2 and SH-L algorithms (left) and passive mode, ADD-2 and ADD-L algorithms (right), HILS results.

Table 3. Ideal response times for selected algorithm.

Algorithm	τ_{63} (ms)	τ_{36} (ms)
SH-2	7.9	1.1
SH-L	10	9.5
ADD-2	12.8	46
ADD-L	3.8	46

Figure 7 shows the effect of force drop response time τ_{36} on carbody lateral acceleration overall RMS (case 2). The response time trend on RMS for algorithm SH-2 decreases to τ_{36} = 1.1 ms. In the case of SH-L, the vibrations decrease linearly up to 20 ms, similarly to τ_{63}, and the lowest value is at τ_{36} = 9.5 ms (Figure 7 left). The performance of the ADD-2 and ADD-L algorithms is the best, surprisingly, for a force drop response time around τ_{36} = 46 ms, see Figure 7 right. The force rise response time τ_{63} was set statically, ideal for each algorithm, according to Table 3.

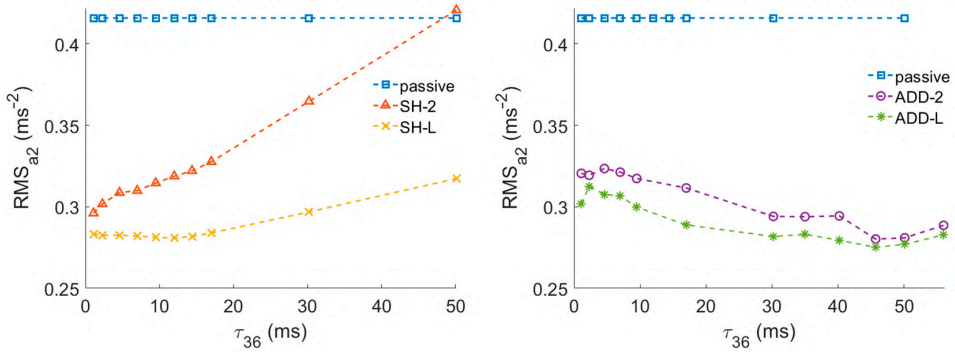

Figure 7. Damper force drop response time τ_{36} effect for passive mode, SH-2 and SH-L algorithms (left) and passive mode, ADD-2 and ADD-L algorithms (right), HILS results.

For SH-2 and SH-L algorithms, the response time for the damping force drop is significantly more critical than for the damping force rise. It is caused by the input electric current being switched to I_{max} = 2 A when the damper piston velocity $v_2 - v_1$ is zero (when the force for activated and non-activated states is 0 N) and switched to I_{min} = 0 A when the piston velocity and damping force are non-zero, see Figure 8 left. In Figure 8 right, it can be seen that the artificial long response time τ_{36} makes the function of the ADD-2 algorithm similar to the SH-L algorithm function. This similarity explains the importance of a long force drop response time for good results from the ADD-2 and ADD-L algorithms.

The effect of the response time of real damper (including response time for rise and drop) was tested (case 3), see Figure 9. It can be seen that the long response time significantly degrades the efficiency of the SH-2 algorithm. Dependency is linear. The shorter the response time, the lower RMS. However, the algorithm SH-L exhibits a significant improvement in RMS up until a response time of 30 ms. After exceeding this value, the improvement is not observed. For ADD-2 and ADD-L algorithms, it would be ideal to use a damper with a response time of around τ_{63} = 16 ms and the corresponding τ_{36} = 9.5 ms. When using the SH-L, ADD-2, or ADD-L algorithm, it is possible to achieve a vibration reduction of about 22% even with a response time of τ_{63} = 57 ms and the corresponding τ_{36} = 33.5 ms. Strecker et al. [31] wrote that a successful semi-active control requires a short response time of at least 20 ms, but they used the SH-2 algorithm, a different dynamic system for simulating, and an obstacle crossing as an excitation method. In this case, excitation with a relatively low frequency (2 Hz) is used, and more advanced algorithms for S/A control are used, so semi-active control works well even with a relatively long response time. Obviously, reducing the damper response time τ_{63} to less than 8 ms does not make sense for a lateral movement of rail vehicle carbody. Therefore, our MR damper for a railway vehicle with force rise response time of τ_{63} = 7.8 ms [32] is fast enough.

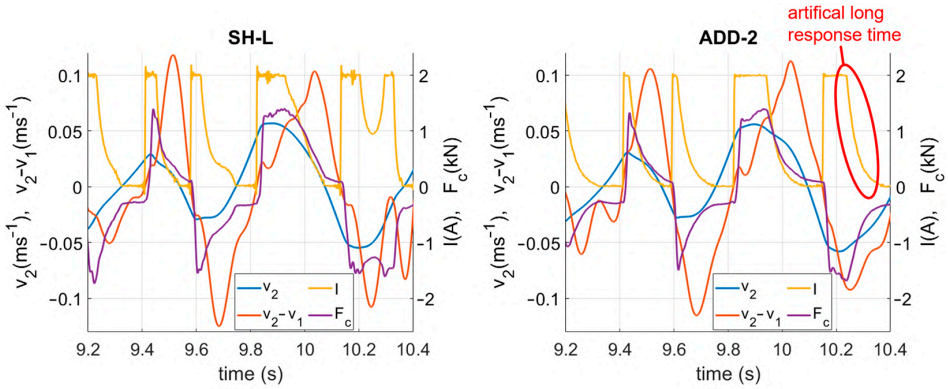

Figure 8. Course of v_2–carbody lateral velocity from the model, $v_2 - v_1$ damper piston velocity from the model, I –measured electric current in damper, F_c–measured damper force, for SH-L control (left) and ADD-2 control (right), HILS results.

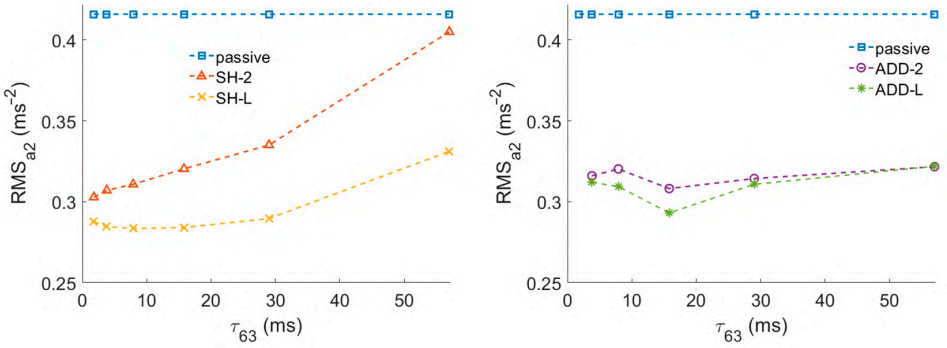

Figure 9. Damper force drop response time τ_{63} effect for passive mode, SH-2 and SH-L algorithms (**left**) and passive mode, ADD-2 and ADD-L algorithms (**right**), HILS results.

3.2. Dynamic Force Range Effect

Figure 10 shows the dependence of the S/A control efficiency on the force dynamic range of the damper (at piston velocity 0.1 ms^{-1}). The vibration maximum RMS value increases with decreasing dynamic range for all algorithms. The Skyhook algorithm is more sensitive than other algorithms. It would be appropriate to change the damper design and make the dynamic range higher than 7.6 to achieve better results. It is possible to achieve a dynamic range of around 12 [33]. From the dependence course, it seems that the ideal value of the dynamic range could be around 10. The force rise and drop response times were set statically, ideal for each algorithm, according to Table 3. All cases of S/A control, except SH-2 with the dynamic range of 2, reduced carbody vibration.

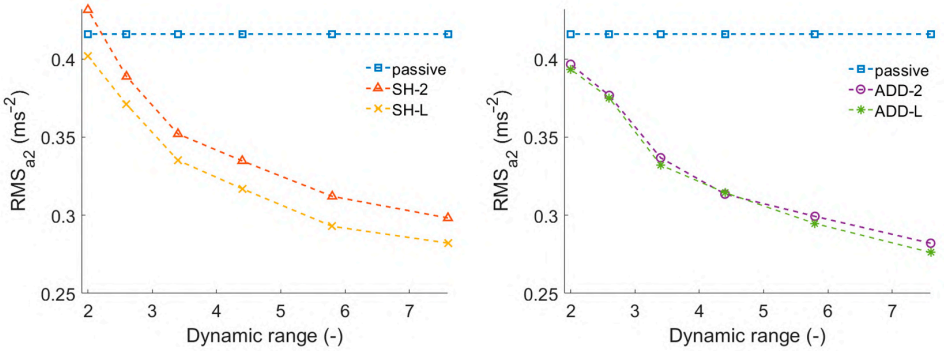

Figure 10. Damper dynamic range *DR* effect for passive mode, SH-2 and SH-L algorithms (left) and for passive mode, ADD-2 and ADD-L algorithms (right), HILS results.

3.3. Benefits of Each Algorithm

Table 4 shows the overall RMS of the lateral carbody vibrations determined by ideal response times. The most significant vibration reduction was performed by the ADD-L algorithm–33.6%. This value corresponds to the results of most previous research, e.g., [4,9].

Table 4. Carbody lateral acceleration RMS (ms^{-2}) for each mode and percentage reduction compared to passive mode.

Mode	RMS (ms^{-2})	Improvement (%)
passive	0.416	0
SH-2	0.298	28.3
SH-L	0.282	32.2
ADD-2	0.282	32.2
ADD-L	0.276	33.6

In relation to this, SH-L achieved the same result as ADD-2, which was 32.2%. It is an important finding because ADD-2 is easier to apply to a real control system. Only an accelerometer for measuring the sprung mass acceleration and a displacement sensor for measuring the damper piston velocity are required for the ADD-2 application. When using the SH-2 or SH-L algorithm, it is necessary to integrate the sprung mass acceleration to obtain the sprung mass velocity, which leads to problems with the integration constant. The same problem must be solved for the ADD-L algorithm.

Courses of lateral acceleration of vehicle body in the time domain for selected results are shown in Figure 11.

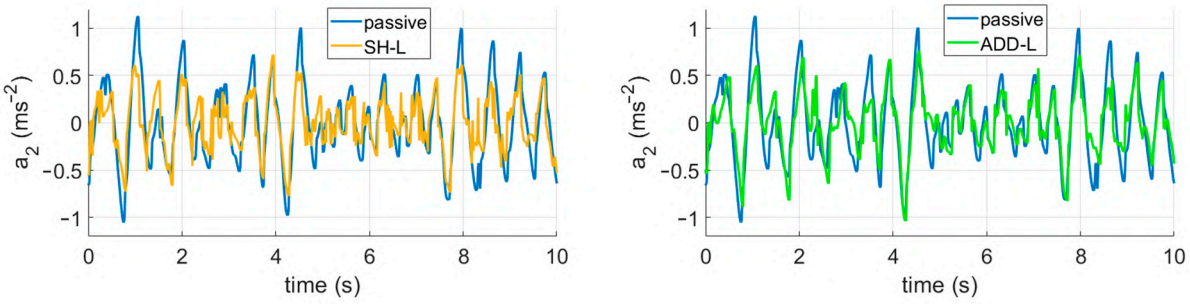

Figure 11. Courses of lateral body acceleration in the time domain for passive mode, SH-L control (**left**) and ADD-L control (**right**), HILS results.

4. Conclusions

The paper deals with the dynamic MR damper behaviour and its influence on the efficiency of four algorithms for semi-active control. A simple model of the lateral movement of a railway vehicle carbody with two degrees of freedom was used for the study. The Hardware-in-the-loop simulation was used. It has been confirmed that S/A control of dampers can significantly reduce carbody vibrations and increase crew comfort. For the selected dynamic system, the chosen excitation method and four selected control strategies, the key findings of this study can be summarised as follows:

- Force drop response time is more important than force rise response time for S/A control performance.
- In this dynamic system, there is no point in shortening the response time to less than τ_{63} = 8 ms.
- The newly designed Acceleration Driven Damper Linear algorithm is best suited for damping the railway vehicle's carbody lateral movement.
- Under ideal conditions, vibrations were reduced by 34%.
- Acceleration Driven Damper (two states) achieves the same effectiveness as Skyhook Linear, but Acceleration Driven Damper is easier to implement in real vehicles.

- For better results, it would be appropriate to increase the dynamic range by at least 10.

In this research, the damper was mounted in the pulsator without silentblocks, which will probably not be possible in practice. However, the damper's soft mounting will worsen the system's hysteretic behaviour and reduce the effectiveness of the S/A control. Silentblocks of various stiffnesses are produced. It would be appropriate to investigate the dependence of the S/A control effectiveness on the damper mounting stiffness and determine what stiffness of the silentblock is acceptable for the S/A control. It will be part of follow-up research.

Author Contributions: Conceptualisation, F.J., M.K., Z.S.; methodology, F.J., Z.S.; software, F.J., T.M., J.Ž.; validation, F.J., J.Ž.; formal analysis, M.K., Z.S.; investigation, F.J., M.K., J.Ž.; data curation, F.J., T.M.; writing—original draft preparation, F.J., T.M.; writing—review and editing, F.J., M.K., T.M., Z.S., J.Ž., I.M.; visualisation, F.J., M.K.; supervision, M.K., Z.S., I.M.; project administration, M.K., I.M.; funding acquisition, M.K., I.M. All authors have read and agreed to the published version of the manuscript.

Funding: This work was supported partly by Czech Science Foundation under Grant GF21-45236L, partly by Technology Agency of the Czech Republic under Grant CK03000052 and party by Brno University of Technology under Grant FSI-S-20-6247.

Institutional Review Board Statement: Not applicable.

Informed Consent Statement: Not applicable.

Data Availability Statement: The data presented in this study are available on request from the corresponding author.

Conflicts of Interest: The authors declare no conflict of interest.

References

1. Goodall, R.M. Control Engineering Challengs for Railway Trains of the Future. *Meas. Control* **2011**, *44*, 16–24. [CrossRef]
2. Pérez, J.; Busturia, J.M.; Goodall, R.M. Control Strategies for Active Steering of Bogie-Based Railway Vehicles. *Control Eng. Pract.* **2002**, *10*, 1005–1012. [CrossRef]
3. Shin, Y.J.; You, W.H.; Hur, H.M.; Park, J.H. Semi-Active Control to Reduce Carbody Vibration of Railway Vehicle by Using Scaled Roller Rig. *J. Mech. Sci. Technol.* **2012**, *26*, 3423–3431. [CrossRef]
4. Codecà, F.; Savaresi, S.M.; Spelta, C.; Montiglio, M.; Ieluzzi, M. Semiactive Control of a Secondary Train Suspension. In Proceedings of the 2007 IEEE/ASME International Conference on Advanced Intelligent Mechatronics, Zurich, Switzerland, 4–7 September 2007. [CrossRef]
5. Strecker, Z.; Jeniš, F.; Kubík, M.; Macháček, O.; Choi, S.B. Novel Approaches to the Design of an Ultra-Fast Magnetorheological Valve for Semi-Active Control. *Materials* **2021**, *14*, 2500. [CrossRef] [PubMed]
6. Jeniš, F.; Kubík, M.; Macháček, O.; Šebesta, K.; Strecker, Z. Insight into the Response Time of Fail-Safe Magnetorheological Damper. *Smart Mater. Struct.* **2021**, *30*, 017004. [CrossRef]
7. Spelta, C.; Savaresi, S.M.; Codecà, F.; Montiglio, M.; Ieluzzi, M. Smart-Bogie: Semi-Active Lateral Control of Railway Vehicles. *Asian J. Control* **2012**, *14*, 875–890. [CrossRef]
8. Lau, Y.K.; Liao, W.H. Design and Analysis of Magnetorheological Dampers for Train Suspension. *Proc. Inst. Mech. Eng. Part F J. Rail Rapid Transit* **2005**, *219*, 261–276. [CrossRef]
9. Shin, Y.-J.; You, W.-H.; Hur, H.-M.; Park, J.-H.; Lee, G.-S. Improvement of Ride Quality of Railway Vehicle by Semiactive Secondary Suspension System on Roller Rig Using Magnetorheological Damper. *Adv. Mech. Eng.* **2014**, *6*, 298382. [CrossRef]
10. Hudha, K.; Harun, M.H.; Harun, M.H.; Jamaluddin, H. Lateral Suspension Control of Railway Vehicle Using Semi-Active Magnetorheological Damper. In Proceedings of the 2011 IEEE Intelligent Vehicles Symposium (IV), Baden-Baden, Germany, 5–9 June 2011; pp. 728–733. [CrossRef]
11. Žáček, J.; Šebesta, K.; Mohammad, H.; Jeniš, F.; Strecker, Z.; Kubík, M. Experimental Evaluation of Modified Groundhook Car Suspension with Fast Magnetorheological Damper. *Actuators* **2022**, *11*, 354. [CrossRef]
12. Jeyasenthil, R.; Yoon, D.S.; Choi, S.B. Response Time Effect of Magnetorheological Dampers in a Semi-Active Vehicle Suspension System: Performance Assessment with Quantitative Feedback Theory. *Smart Mater. Struct.* **2019**, *28*, 054001. [CrossRef]
13. Koo, J.H.; Goncalves, F.D.; Ahmadian, M. A Comprehensive Analysis of the Response Time of MR Dampers. *Smart Mater. Struct.* **2006**, *15*, 351–358. [CrossRef]
14. Yoon, D.S.; Park, Y.J.; Choi, S.B. An Eddy Current Effect on the Response Time of a Magnetorheological Damper: Analysis and Experimental Validation. *Mech. Syst. Signal Process.* **2019**, *127*, 136–158. [CrossRef]

15. Macháček, O.; Kubík, M.; Strecker, Z.; Roupec, J.; Mazůrek, I. Design of a Frictionless Magnetorheological Damper with a High Dynamic Force Range. *Adv. Mech. Eng.* **2019**, *11*, 1687814019827440. [CrossRef]
16. Choi, S.B.; Nam, M.H.; Lee, B.K. Vibration Control of a MR Seat Damper for Commercial Vehicles. *J. Intell. Mater. Syst. Struct.* **2001**, *11*, 936–944. [CrossRef]
17. Lee, H.S.; Choi, S.B. Control and Response Characteristics of a Magneto-Rheological Fluid Damper for Passenger Vehicles. *J. Intell. Mater. Syst. Struct.* **2000**, *11*, 80–87. [CrossRef]
18. Misselhorn, W.E.; Theron, N.J.; Els, P.S. Investigation of Hardware-in-the-Loop for Use in Suspension Development. *Veh. Syst. Dyn.* **2006**, *44*, 65–81. [CrossRef]
19. Kwak, M.K.; Lee, J.H.; Yang, D.H.; You, W.H. Hardware-in-the-Loop Simulation Experiment for Semi-Active Vibration Control of Lateral Vibrations of Railway Vehicle by Magneto-Rheological Fluid Damper. *Veh. Syst. Dyn.* **2014**, *52*, 891–908. [CrossRef]
20. Oh, Y.J.; Lee, J.K.; Liu, H.C.; Cho, S.; Lee, J.; Lee, H.J. Hardware-in-the-Loop Simulation for Active Control of Tramcars with Independently Rotating Wheels. *IEEE Access* **2019**, *7*, 71252–71261. [CrossRef]
21. Zelenka, J.; Michalek, T.; Kohout, M. Comparative Simulations of Guiding Behaviour of an Electric Locomotive. In Proceedings of the 20th International Conference Engineering Mechanics 2014, Svratka, Czech Republic, 12–15 May 2014; pp. 740–743.
22. Goncalves, F.D.; Koo, J.H.; Ahmadian, M. Experimental Approach for Finding the Response Time of Mr Dampers for Vehicle Applications. In *Proceedings of the ASME Design Engineering Technical Conference*; ASME: New York, NY, USA, 2003; Volume 5 A, pp. 425–430.
23. Guan, X.; Guo, P.; Ou, J. Study of the Response Time of MR Dampers. In Proceedings of the Second International Conference on Smart Materials and Nanotechnology in Engineering, Weihai, China, 8–11 July 2009; Volume 7493, p. 74930U. [CrossRef]
24. Koo, J.-H.; Goncalves, F.D.; Ahmadian, M. Investigation of the Response Time of Magnetorheological Fluid Dampers. In *Smart Structures and Materials 2004: Damping and Isolation*; SPIE: Bellingham, WA, USA, 2004; Volume 5386, p. 63. [CrossRef]
25. Strecker, Z.; Roupec, J.; Mazurek, I.; Machacek, O.; Kubik, M.; Klapka, M. Design of Magnetorheological Damper with Short Time Response. *J. Intell. Mater. Syst. Struct.* **2015**, *26*, 1951–1958. [CrossRef]
26. Karnopp, D.; Crosby, M.J.; Harwood, R.A. Vibration Control Using Semi-Active Force Generators. *J. Eng. Ind.* **1974**, *96*, 619. [CrossRef]
27. Sammier, D.; Sename, O.; Dugard, L. Skyhook and H∞ Control of Semi-Active Suspensions: Some Practical Aspects. *Veh. Syst. Dyn.* **2003**, *39*, 279–308. [CrossRef]
28. Savaresi, S.M.; Silani, E.; Bittanti, S. Acceleration-Driven-Damper (ADD): An Optimal Control Algorithm for Comfort-Oriented Semiactive Suspensions. *J. Dyn. Syst. Meas. Control. Trans. ASME* **2005**, *127*, 218–229. [CrossRef]
29. Savaresi, S.M.; Spelta, C. Mixed Sky-Hook and ADD: Approaching the Filtering Limits of a Semi-Active Suspension. *J. Dyn. Syst. Meas. Control. Trans. ASME* **2007**, *129*, 382–392. [CrossRef]
30. *EN 14363:2016+A1*; Railway Applications—Testing and Simulation for the Acceptance of Running Characteristics of Railway Vehicles—Running Behaviour and Stationary Tests. CEN (European Committee for Standardization): Brusel, Belgium, 2020.
31. Strecker, Z.; Mazůrek, I.; Roupec, J.; Klapka, M. Influence of MR Damper Response Time on Semiactive Suspension Control Efficiency. *Meccanica* **2015**, *50*, 1949–1959. [CrossRef]
32. Kubík, M.; Strecker, Z.; Jeniš, F.; Macháček, O.; Přikryl, M.; Špalek, P. Magnetorheological Yaw Damper with Short Response Time for Rail- Way Vehicle Bogie. In Proceedings of the International Conference and Exhibition on New Actuator Systems and Applications 2021, Online, 17–19 February 2021; Volume 36, pp. 373–376.
33. Yang, G.; Spencer, B.F.; Carlson, J.D.; Sain, M.K. Large-Scale MR Fluid Dampers: Modeling and Dynamic Performance Considerations. *Eng. Struct.* **2002**, *24*, 309–323. [CrossRef]

7 CONCLUSION

This dissertation thesis has investigated in detail the influence of the material and shape of the MR damper magnetic circuit on the damper dynamic behaviour, the influence of the additional permanent magnet in the magnetic circuit of the MR damper, and the effect of damper dynamic behaviour on the performance of the semi-actively controlled lateral suspension of railway vehicles.

In the first part of the thesis, the possibilities of improving the dynamic behaviour of the MR damper were investigated. The material and the shape approaches were used. The thesis evaluated the proposed variants based on the length of the force response time and the value of the dynamic force range. A transient simulation of the magnetic circuit was used for material selection or groove design. The output of the magnetic model is the time history of the magnetic flux density when the electric current is switched on (step signal). The response time of the magnetic flux density can be determined. The simulation was carried out for six magnetic circuit materials and two grooved variants to obtain the shortest response time and high dynamic range. Simulated variants have been verified by magnetic field measurements. The MR valve was designed for use in an MR damper, so the response time of the damping force was also measured. The key findings of this thesis part can be summarised as follows:

- MR valves made from ferrite and Sintex (SMC) materials have the fastest response time in terms of magnetic flux density and damper force. A damping force response time of approximately 1.3 ms can be achieved, while the dynamic force range is 4.
- The highest dynamic range can be achieved with the piston made of Hiperco/Vacoflux. The dynamic range is approximately 6.
- For MR valves made of 11SMn30 cutting steel, 6 grooves reduce the force response time 6 times to 1.7 ms, while the dynamic force range is 5.
- In comparison, the MR damper with a structured piston made from pure iron by SLM achieves a damper force response time of 1.3 ms and a dynamic force range of 5.1 [59].

The best option would, therefore, be a damper piston made of grooved Vacoflux or a structured piston made from pure iron made by SLM [59]. However, well-usable variants are also SMC piston and piston from grooved 11SMn30 steel.

The second part of the thesis investigates the dynamic behaviour of the fail-safe MR damper with a permanent magnet in the valve core. The magnetic circuit of the damper was made of 11SMn30 cutting steel. Two ring neodymium magnets are placed in the MR valve core to provide a fail-safe magnetic field. The response time of the magnetic field and force on the

step of the control signal were determined experimentally and by virtual simulation using the magnetic models. The key findings of this thesis part can be summarised as follows:

- The fail-safe damping force at zero electric current depends on the magnetisation history and reaches approximately 1/3 of the maximum damping force.
- The dynamic force range of the fail-safe MR damper reaches a value of 8.5.
- The damping force rise from the fail-safe state to the on-state is faster than the drop from the on-state back to the fail-safe state.
- The response time of the force rise from the fail-safe state to the on-state is strongly dependent on the magnitude of the electric current.
- The damping force rise from the off-state to the fail-safe state is faster than the drop from the fail-safe state back to the off-state and independent of the magnitude of the electric current.
- The changes between off-state and failsafe forces are significantly faster than changes between on-state and failsafe forces.
- The permanent magnet does not degrade the transient behaviour of the MR damper.

It should be noted that the response time of this fail-safe damper is quite long. This is due to the use of 11SMn30 cutting steel for the magnetic circuit of the MR valve. The force response time of this failsafe damper is comparable to the force response time of the damper with a piston made of 11SMn30 steel without grooves from the previous article. If we want a fail-safe damper with a shorter force response time, it is possible to groove the damper piston, which should reduce the response time by about 6 times.

In the third part, the influence of the behaviour of a semi-actively controlled MR secondary lateral damper on railway vehicle comfort was investigated in detail. The response time of the damping force rise, the damping force drop, and the dynamic force range were investigated separately. Hardware-in-the-loop simulation with a real MR damper was used to account for non-linearity in the damper dynamics. The key findings of this part can be summarised as follows:

- The force drop response time is more important than the force rise response time for S/A control performance.
- In this dynamic system, it does not make sense to reduce the response time to less than τ_{63} = 8 ms.
- The newly designed Acceleration Driven Damper Linear algorithm is best suited for damping the lateral motion of the railway vehicle body.
- Under ideal conditions, vibrations can be reduced by 34%.
- For better results, it would be appropriate to increase the dynamic range by at least 10.

With regard to the hypotheses tested, the results obtained are summarised in the following remarks:

Q1: How does the material and geometry of the MR damper magnetic circuit affect force response time and dynamic range? Is a shorter damper force response time always associated with a smaller force dynamic range?

It can be seen that a shorter damper force response time is associated with a smaller force dynamic range when a material-only or shape-only approach is used. Combining both approaches makes it possible to reduce the force response time while maintaining a high dynamic force range. Due to their high electrical resistivity, Ferrite and SMC materials give the shortest force response time. Due to its high magnetic saturation limit, Hiperco/Vacoflux gives the highest dynamic range. Grooves in magnetic circuits (shape approach) can 6 times speed up the force response time of MR valves. The shortest response time achieved is 1.28 ms. These are all facts that have been assumed. **Thus, the first hypothesis has been verified**.

Q2: Will the permanent magnet in the MR valve affect the response time of the MR damper? Will the response time of the damping force be different as the damping force rises and drops?

The force response time for force rise and force drop is different. However, contrary to the hypothesis, the force rise is faster than the force drop. This is true for the increase from off-state force to fail-safe force and the decrease back, as well as for the increase from failsafe force to on-state force and the decrease back. This is obviously caused by a permanent magnet, and it was not assumed. **Thus, the second hypothesis was not verified**.

<u>An alternative hypothesis was stated:</u>

H2.2: In this research, an MR valve made of 11SMn30 cutting steel was used. This steel has relatively poor characteristics in terms of the magnetic circuit, which causes excessive eddy current development and, therefore, a longer response time. A combination of the eddy current effect and the permanent magnet effect probably causes the behaviour described. We assume that the response time could behave as hypothesis H2, i.e., the force drop could be faster than the force rise if the 11SMn30 cutting steel was grooved or if the magnetic circuit was made of a material more resistant to eddy currents, such as SMC

Q3: How does damper force rise response time, force drop response time, and dynamic range affect the effectiveness of S/A control of railway vehicle lateral secondary MR dampers? Is there a difference between the effect of the force rise response time and the effect of the force drop response time on the efficiency of S/A control? What is the acceptable value of damper force response time and dynamic range for this control?

It was found that the response times of force drop and force rise are different, and the force drop response time has a greater influence than the force rise response time. Therefore, when modelling the MR damper, it is necessary to model each response time separately, as expected. An acceptable response time length for this application can be considered to be τ = 8 ms for both rise and drop. In the case of the force dynamic range, it is 10. These are approximately the values that were assumed. **Thus, the third hypothesis has been verified**.

It has been shown that semi-active control of lateral secondary dampers can significantly improve passenger comfort on railway vehicles. For maximum benefit, it is necessary to use the MR damper with a sufficiently short force response time and a sufficiently high dynamic force range. It has been shown that this can be achieved by a combination of the material and the shape approach to eliminate eddy currents in the MR valve magnetic circuit. At the same time, it is necessary to ensure the fail-safe behaviour of the MR damper in the case of a power failure. It has been shown that placing a permanent magnet in the damper core to provide fail-safe behaviour does not degrade the transient behaviour of the damper. Replacing the lateral secondary dampers (but also the vertical or yaw dampers) with semi-actively controlled dampers is relatively simple (Fig. 7-3 – right). It can be done without making any structural changes to the vehicle. This technology can, therefore, be easily applied to current railway vehicles that want to improve comfort, and it can also be applied to the new generation of high-speed railway vehicles.

It is important to note that the damper used in this research is approximately 1/5 scale. A larger damper with higher forces would be required for a railway vehicle application. It can be expected that increasing the damper force will result in a longer response time. Based on the results of this research, an MR damper for a railway vehicle has been designed and manufactured [108], see Fig. 7-1 (left). A magnetic circuit of this MR damper is made of low carbon cutting steel 11SMn30, and it is grooved, see Fig. 7-1 (right).

Fig. 7-1 MR damper for railway vehicle application (left) and its grooved magnetic circuit (right) [108]

The maximum damping force of this MR damper is 15.6 kN (0,2 m/s), see Fig. 7-2 (left). The dynamic force range of this damper is 25-8.5, depending on the piston velocity. The damper force response time is 7.8 ms for force rise (see Fig. 7-2 – right) and 4.5 ms

for force drop. So, based on the previous research, it is clear that this damper is suitable for use on a railway vehicle in terms of time response and dynamic range.

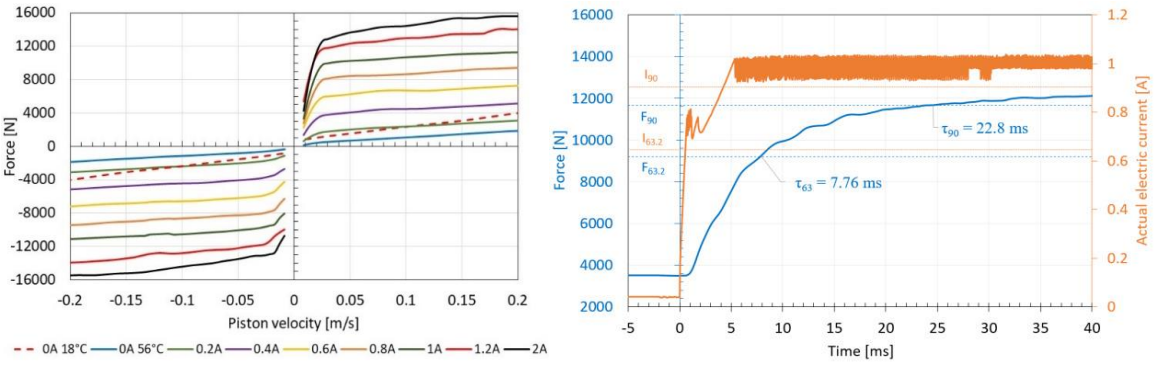

Fig. 7-2 F-v curves (left) and force response time (right) of MR damper for railway vehicle application [108]

This damper has been designed as a bogie yaw damper to resolve the contradiction between the requirements of the suspension system when running at high speed on a straight track and, on the other hand, when negotiating a curve with a small radius. Based on simulations and running tests (Fig. 7-3 – left), it has been shown that the MR yaw damper can improve the behaviour of a railway vehicle both when running at high speed on a straight track [115] and when negotiating a curve with a small radius [108, 116]. These results should be published in journals with an impact factor in the near future.

Fig. 7-3 Running test (left); mounting of the MR damper to railway vehicle (right)

Another follow-up to the research carried out is a project to develop a complete damping system for an intercity low-floor railway unit. The aim is to develop and manufacture a semi-actively controlled vertical (Fig. 7-3 – right) and lateral damping system (including designing and manufacturing MR dampers, control units and control algorithms) and test it on a real vehicle under real conditions on a track. The first test runs are planned for May 2024.

8 LIST OF PUBLICATIONS

8.1 Papers published in journals with impact factor

Realated to dissertation thesis:

JENIŠ, Filip; KUBÍK, Michal; MICHÁLEK, Tomáš; STRECKER, Zbyněk; ŽÁČEK, Jiří; MAZŮREK, Ivan. Effect of the magnetorheological damper dynamic behaviour on the rail vehicle comfort: hardware-in-the-loop simulation. *Actuators*, 2023, **12**(47), 1-14. **(IF 2.6)**

STRECKER, Zbyněk; JENIŠ, Filip; KUBÍK, Michal; MACHÁČEK, Ondřej; CHOI, Seung Bok. Novel Approaches to the Design of an Ultra-Fast Magnetorheological Valve for Semi-Active Control. *Materials, 2021*, **14**(10), 1-20. **(IF 3.4)**

JENIŠ, Filip; KUBÍK, Michal; MACHÁČEK, Ondřej; ŠEBESTA, Karel; STRECKER, Zbyněk. Insight into the response time of fail-safe magnetorheological damper. *Smart Materials and Structures*, 2020, **30**(1), 1-13. **(IF 4.1)**

Others:

ŽÁČEK, Jiří; ŠEBESTA, Karel; MOHAMMAD, Housam; JENIŠ, Filip; STRECKER, Zbyněk; KUBÍK, Michal. Experimental Evaluation of Modified Groundhook Car Suspension with Fast Magnetorheological Damper. *Actuators*, 2022, **11**(12), 1-14. **(IF 2.6)**

KUBÍK, Michal; VÁLEK, Josef; ŽÁČEK, Jiří; JENIŠ, Filip; BORIN, Dmitry; STRECKER, Zbyněk; MAZŮREK, Ivan. Transient response of magnetorheological fluid on rapid change of magnetic field in shear mode. *Scientific Reports*, 2022, **12**(1), 1-10. **(IF 4.6)**

KUBÍK, Michal; ŠEBESTA, Karel; STRECKER, Zbyněk; JENIŠ, Filip; GOLDASZ, Janusz; MAZŮREK, Ivan. Hydrodynamic response time of magnetorheological fluid in valve mode: model and experimental verification. *Smart Materials and Structures*, 2021, **30**(12), 1-13. **(IF 4.1)**

ROUPEC, Jakub; JENIŠ, Filip; STRECKER, Zbyněk; KUBÍK, Michal; MACHÁČEK, Ondřej. Stribeck Curve of Magnetorheological Fluid within Pin-on-Disc Configuration: An Experimental Investigation. *Materials*, 2020, **13**(20), 1-11. **(IF 3.4)**

8.2 Papers in conference proceedings

MICHÁLEK, Tomáš; JENIŠ, Filip. Modelling of secondary suspension for electric multiple unit. In. *Computational Mechanics 2023, 38th conference with international participation*. Srní: University of West Bohemia. s. 116-118.

JENIŠ, Filip; MICHÁLEK, Tomáš. The effect of semi-active control of bogie yaw dampers on the railway vehicle critical speed. In, *26th International Conference Current Problems in Rail Vehicles 2023.* Žilina: Scientific and Technical Society at the University of Žilina. s. 213-220. (expected WOS)

BASARGAN, Hakan; JENIŠ, Filip; MIHÁLY, András; GÁSPÁR, Péter. Fault-tolerant control of semi-active suspension in case of oil leakage of magnetorheological damper. In *2023 EUROPEAN CONTROL CONFERENCE, ECC*. Bucharest, Romania: IEEE, 2023. **(WOS)**

KUBÍK, Michal; STRECKER, Zbyněk; JENIŠ, Filip; MACHÁČEK, Ondřej; PŘIKRYL, Matěj; ŠPALEK, Petr. Magnetorheological Yaw Damper with Short Response Time for Railway Vehicle Bogie. In *Actuators 2021*. BERLIN: VDE VERLAG GMBH, 2021. s. 1-4. **(Scopus)**

JENIŠ, Filip; MICHÁLEK, Tomáš; MAZŮREK, Ivan. Benefit of a semi-actively conntroled magnetorheological damper for a railway vehicle. In *Current Problems in Rail Vehicles 2021, 25th conference with international participation.* Pardubice: Faculty of transport engineering University of Pardubice, 2021. s. 85-92. (expected WOS)

JENIS, Filip; STRECKER, Zbyněk; MAZUREK, Ivan. A new method for on-board car suspension testing. In *Proceedings of the Engineering Mechanics 2020*. Brno: Brno University of Technology Institute of Solid Mechanics, Mechatronics and Biomechanics, 2020. s. 238-241. **(WOS)**

ZINDULKA, Martin; STRECKER, Zbyněk; JENIŠ, Filip. *Semiactive seat suspension for agricultural machines*. In Proceedings of the Engineering Mechanics 2020. Brno: Brno University of Technology Institute of Solid Mechanics, Mechatronics and Biomechanics, 2020. s. 548-551. **(WOS)**

JENIŠ, Filip; MAZŮREK, Ivan. Sprung mass positioning by semi-actively controlled damper. In *MATBUD'2020 – Scientific-Technical Conference: E-mobility, Sustainable Materials and Technologies.* MATEC Web of Conferences. EDP Sciences, 2020. s. 1-8.

KUBÍK, Michal; JENIŠ, Filip; HAŠLÍK, Igor. The magnetic circuit dynamics of a magnetorheological valve with a permanent magnet. In *MATBUD'2020 – Scientific-Technical Conference: E-mobility, Sustainable Materials and Technologies*. MATEC Web of Conferences. EDP Sciences, 2020. s. 1-8.

KUBÍK, Michal; ROUPEC, Jakub; JENIŠ, Filip; MAZŮREK, Ivan. *The settings of CFD model with magnetorheological fluid and its influence on the results*. In Engineering Mechanics 2019, 25th International Conference. Praha: Institute of Thermomechanics of the Czech Academy of Sciences, 2019. s. 223-226. **(WOS)**

JENIŠ, Filip; ROUPEC, Jakub; ŽÁČEK, Jiří; KUBÍK, Michal; MACHÁČEK, O.; SMILEK, J.; SMILKOVÁ, M.; MAZŮREK, Ivan. *Abrasion of Magnetorheological Fluids.* In Engineering Mechanics 2019, 25th International Conference. Praha: Institute of Thermomechanics of the Czech Academy of Sciences, 2019. s. 169-172. **(WOS)**

JENIS, Filip; MAZUREK, Ivan. Mechatronicaly controlled bogie of high speed train. In *Conference proceedings of the 60th International Conference of Machine Design Departments. Brno Universtiy of Technology*, 2019.

8.3 Other results

JENIŠ, Filip; DANIEL, Pavel; MAZŮREK, Ivan: SW Demo; *Program for semi-active MR damper regulation*. Functional specimen (RIV-G)

STRECKER, Zbyněk; MAZŮREK, Ivan; MACHÁČEK, Ondřej; JENIŠ, Filip: C*ontroller for the semi-active MR damper.* Functional specimen (RIV-G)

JENIŠ, Filip; ŠEBESTA, Karel; DANIEL, Pavel; MAZŮREK, Ivan: *Demonstrator for verifying the functionality of a fast-response MR damper.* Functional specimen (RIV-G)

JENIŠ, Filip; MAZŮREK, Ivan: *Simulation model of the dynamic structure of the vehicle suspension during the over-crossing test.* Software (RIV-R)

JENIŠ, Filip; MAZŮREK, Ivan; SKUHRAVÝ, Pavel: *Control and analysis program of the over-crossing tester.* Software (RIV-R)

MAZŮREK, Ivan; JENIŠ, Filip; SKUHRAVÝ, Pavel: *Inertial measurement unit for sensing carbody movement*. Functional specimen (RIV-G)

MAZŮREK, Ivan; JENIŠ, Filip; SKUHRAVÝ, Pavel: *Universal over-crossing obstacle.* Functional specimen (RIV-G)

9 LITERATURE

[1] MICHÁLEK, Tomáš a Jaromír ZELENKA. The effect of spring pads in the secondary suspension of railway vehicles on bogie yaw resistance. *Vehicle System Dynamics*. 2015, **53**(12), 1952–1964.

[2] FOTOOHI, Abbas a Aghil YOUSEFI-KOMA. Improve Hunting of a Railway Vehicle Using Semi-Active Primary Suspension. In: *Volume 3: Dynamic Systems and Controls, Symposium on Design and Analysis of Advanced Structures, and Tribology*. B.m.: ASMEDC, 2006, 557–564.

[3] WEI, Xiukun, Ming ZHU a Limin JIA. A semi-active control suspension system for railway vehicles with magnetorheological fluid dampers. *Vehicle System Dynamics*. 2016, **54** (7), 982–1003.

[4] *Bombardier equipment for urban vehicles*. 2019 [accesed. 2019-5-20]. Available at: https://rail.bombardier.com/en/solutions-and-technologies/equipment/urban-equipment.html

[5] TRANSPORTATION, Bombardier. *FLEXX Tronic Technoligy*. 2008 [accesed. 2019-5-20]. Available at: https://www.bombardier.com/content/dam/Websites/bombardiercom/supporting-documents/BT/Bombardier-Transportation-ECO4-FLEXX_Tronic-EN.pdf

[6] *Tlumiče pro budoucnost*. [accesed. 2019-5-20] Available at: http://www.st-os.cz/tlumice/

[7] CODECÀ, Fabio, Sergio M. SAVARESI, Cristiano SPELTA, Mauro MONTIGLIO a Michele IELUZZI. Semiactive control of a secondary train suspension. *IEEE/ASME International Conference on Advanced Intelligent Mechatronics, AIM*. 2007.

[8] SPELTA, Cristiano, Sergio M. SAVARESI, Fabio CODECÀ, Mauro MONTIGLIO a Michele IELUZZI. Smart-bogie: Semi-active lateral control of railway vehicles. *Asian Journal of Control*. 2012, **14**(4), 875–890. ISSN 15618625.

[9] LAU, Y. K. a W. H. LIAO. Design and analysis of magnetorheological dampers for train suspension. *Proceedings of the Institution of Mechanical Engineers, Part F: Journal of Rail and Rapid Transit*. 2005, **219(**4), 261–276.

[10] SHIN, Yu Jeong, Won Hee YOU, Hyun Moo HUR a Joon Hyuk PARK. H∞ control of railway vehicle suspension with MR damper using scaled roller rig. *Smart Materials and Structures*. 2014, **23**(9).

[11] SHIN, Yu Jeong, Won Hee YOU, Hyun Moo HUR, Joon Hyuk PARK a Gyu Seop LEE. Improvement of Ride Quality of Railway Vehicle by Semiactive Secondary Suspension System on Roller Rig Using Magnetorheological Damper. *Advances in Mechanical Engineering*. 2014, **2014**(11).

[12] SHIN, Yu Jeong, Won Hee YOU, Hyun Moo HUR a Joon Hyuk PARK. Semi-active control to reduce carbody vibration of railway vehicle by using scaled roller rig. *Journal of Mechanical Science and Technology*. 2012, **26**(11), 3423–3431.

[13] HUDHA, Khisbullah, M. Hafiz HARUN, M. Hanif HARUN a Hishamuddin JAMALUDDIN. Lateral suspension control of railway vehicle using semi-active magnetorheological damper. *IEEE Intelligent Vehicles Symposium, Proceedings*. 2011, 728–733.

[14] MAZILU, Traian. An analysis of bogie hunting instability. *UPB Scientific Bulletin, Series D: Mechanical Engineering*. 2009, **71**(2), 63–78.

[15] ALONSO, A., J. G. GIMÉNEZ a E. GOMEZ. Yaw damper modelling and its influence on railway dynamic stability. *Vehicle System Dynamics*. 2011, **49**(9), 1367–1387.

[16] KLINGEL, W. Über den Lauf der Eisenbahnwagen auf gerader Bahn. *Organ für die Fortschritte des Eisenbahnwesens*. 1883, **20**(21), 113–123.

[17] SHEN, Gang a Roger M. GOODALL. Active Yaw Relaxation For Improved Bogie Performance. *Vehicle System Dynamics*. 1997, **28**(4–5), 273–289.

[18] MEI, T. X., Z NAGY, Roger M. GOODALL a A. H. WICKENS. Mechatronic solutions for high-speed railway vehicles. *Control Engineering Practice*. 2002, **10**, 1023–1028.

[19] DUKKIPATI, R. V., S. Narayana SWAMY a M. O.M. OSMAN. Independently Rotating Wheel Systems for Railway Vehicles - A State of the Art Review. *Vehicle System Dynamics*. 1992, **21**(1), 297–330.

[20] BRAGHIN, Francesco, Stefano BRUNI a Ferruccio RESTA. Active yaw damper for the improvement of railway vehicle stability and curving performances: Simulations and experimental results. *Vehicle System Dynamics*. 2006, **44**(11), s. 857–869.

[21] MATSUMOTO, Akira, Yasuhiro SATO, Hiroyuki OHNO, Yoshihiro SUDA, Yohei MICHITSUJI, Makoto KOMIYAMA, Naoki MIYAJIMA, Masuhisa TANIMOTO, Yasushi KISHIMOTO, Yoshi SATO a Takuji NAKAI. Curving performance evaluation for active-bogie-steering bogie with multibody dynamics simulation and experiment on test stand. *Vehicle System Dynamics*. 2008, **46(**1), 191–199.

[22] SUN, Shuaishuai, Huaxia DENG, Weihua LI, Haiping DU, Yi Qing NI, Jin ZHANG a Jian YANG. Improving the critical speeds of high-speed trains using magnetorheological technology. *Smart Materials and Structures*. 2013, **22**(11).

[23] GOODALL, Roger M., C.P. WARD, D. PRANDI a S. BRUNI. Railway bogie stability control from secondary yaw actuators. *The Dynamics of Vehicles on Roads and Tracks - Proceedings of the 24th Symposium of the International Association for Vehicle System Dynamics, IAVSD 2015*. 2016.

[24] WANG, Xu, Binbin LIU, Egidio DI GIALLEONARDO, Ivo KOVACIC a Stefano BRUNI. Application of semi-active yaw dampers for the improvement of the stability of high-speed rail vehicles: mathematical models and numerical simulation. *Vehicle System Dynamics*. 2021.

[25] GAILE, Anton a Yuan LUE. Electro Hydraulic Actuation (EHA) systems for primary flight control, landing gear and other type of actuation. *AUS 2016 - 2016 IEEE/CSAA International Conference on Aircraft Utility Systems*. 2016, 723–728.

[26] SÁNCHEZ-BORRÀS, Marta a Andrés LÓPEZ-PITA. Rail infrastructure charging systems for high-speed lines in Europe. *Transport Reviews*. 2011, **31**(1), 49–68.

[27] SINCHOLD PORT ENGINEERING CO., Ltd. *Train track safety: steel rail*. 2017. Available at: http://cz.sincholdrail.org/info/how-to-ensure-train-track-security-and-keep-it-19994320.html

[28] BRAGHIN, Francesco, Stefano BRUNI a R. LEWIS. 6 - Railway wheel wear. In: *Wheel–Rail Interface Handbook*. B.m.: Woodhead Publishing, 2009, 172–210.

[29] GOODALL, Roger M. Control engineering challengs for railway trains of the future. *Measurement and Control*. 2011, **44**(1), 16–24.

[30] PÉREZ, J., J. M. BUSTURIA a Roger M. GOODALL. Control strategies for active steering of bogie-based railway vehicles. *Control Engineering Practice*. 2002, **10**(9), 1005–1012.

[31] BRAGHIN, F., F. RESTA a E. SABBIONI. A modal control for active/semi-active suspension systems. *IEEE/ASME International Conference on Advanced Intelligent Mechatronics, AIM*. 2007.

[32] SPENCER, B.F. Phenomenological Model for Magnetorheological Dampers. *Journal of Engineering Machanics*. 1997, **123**(3), 230–238.

[33] KARNOPP, Dean. Active Damping in Road Vehicle Suspension Systems. *Vehicle System Dynamics*. 1983, **12**(6), 291–311.

[34] CREWS, John H., Michael G. MATTSON a Gregory D. BUCKNER. Multi-objective control optimization for semi-active vehicle suspensions. *Journal of Sound and Vibration*. 2011, **330**(23), 5502–5516.

[35] SONG, Xubin, Mehdi AHMADIAN, Steve SOUTHWARD a Lane R. MILLER. An adaptive semiactive control algorithm for magnetorheological suspension systems. *Journal of Vibration and Acoustics*. 2005, **127**(5), 493–502.

[36] SEONG, Min-Sang, Seung-Bok CHOI a Kum-Gil SUNG. Control Strategies for Vehicle Suspension System Featuring Magnetorheological (MR) Damper. *Vibration Analysis and Control - New Trends and Developments*. 2011.

[37] GOLDASZ, Janusz. Study of a modular magnetorheological valve. *2017 18th International Carpathian Control Conference, ICCC 2017*. 2017, **63**, 306–309.

[38] GOŁDASZ, J. a S. DZIERZEK. Parametric study on the performance of automotive MR shock absorbers. *IOP Conference Series: Materials Science and Engineering*. 2016, **148**(1).

[39] CARLSON, J.D., D.M. CATANZARITE a K.A. ST. CLAIR. Commercial magneto-rheological fluid devices. *International Journal of Modern Physics B*. 1996, **10**, 2857–2865.

[40] WU, X. a M. J. GRIFFIN. A semi-active control policy to reduce the occurrence and severity of end-stop impacts in a suspension seat with an electrorheological fluid damper. *Journal of Sound and Vibration*. 1997, **203**(5), 781–793.

[41] CHOI, S. B., M. H. NAM a B. K. LEE. Vibration control of a MR seat damper for commercial vehicles. *Journal of Intelligent Material Systems and Structures*. 2001, **11**(12), 936–944.

[42] MCMANUS, S. J., K. A. ST. CLAIR, P. É BOILEAU, J. BOUTIN a S. RAKHEJA. Evaluation of vibration and shock attenuation performance of a suspension seat with a semi-active magnetorheological fluid damper. *Journal of Sound and Vibration*. 2002, **253**(1), 313–327.

[43] CHOI, Y. T. a N. M. WERELEY. Mitigation of biodynamic response to vibratory and blast-induced shock loads using magnetorheological seat suspensions. *Proceedings of the Institution of Mechanical Engineers, Part D: Journal of Automobile Engineering*. 2005, **219**(6), 741–753.

[44] DYKE, S. J., B. F. SPENCER, M. K. SAIN a J. D. CARLSON. An experimental study of MR dampers for seismic protection. *Smart Materials and Structures*. 1998, **7**(5), 693–703.

[45] LI, Hui a Jian WANG. Experimental investigation of the seismic control of a nonlinear soil-structure system using MR dampers. *Smart Materials and Structures*. 2011, **20**(8).

[46] DYKE, S. J., B. F. SPENCER, M. K. SAIN a J. D. CARLSON. Modeling and control of magnetorheological dampers for seismic response reduction. *Smart Materials and Structures*. 1996, **5**(5), 565–575.

[47] YANG, G., B. F. SPENCER, J. D. CARLSON a M. K. SAIN. Large-scale MR fluid dampers: Modeling and dynamic performance considerations. *Engineering Structures*. 2002, **24**(3), 309–323.

[48] OK, Seung Yong, Dong Seok KIM, Kwan Soon PARK a Hyun Moo KOH. Semi-active fuzzy control of cable-stayed bridges using magneto-rheological dampers. *Engineering Structures*. 2007, **29**(5), 776–788.

[49] KIM, In Ho, Hyung Jo JUNG a Jeong Hoi KOO. Experimental evaluation of a self-powered smart damping system in reducing vibrations of a full-scale stay cable. *Smart Materials and Structures*. 2010, **19**(11).

[50] GONCALVES, Fernando D., Jeong Hoi KOO a Mehdi AHMADIAN. Experimental approach for finding the response time of mr dampers for vehicle applications. In: *Proceedings of the ASME Design Engineering Technical Conference*. B.m.: ASME, 2003, 425–430.

[51] GUAN, Xinchun, Pengfei GUO and Jinping OU. 2009. Study of the response time of MR dampers. *In: Proceedings of SPIE* [online]. Bellingham, Wash: SPIE, **7493**(1), 74930U-74930U-9.

[52] KOO, Jeong-hoi, Fernando D GONCALVES and Mehdi AHMADIAN. 2004. Investigation of the response time of magnetorheological fluid dampers. In: *Proceedings of SPIE* [online]. Bellingham WA: SPIE, **5386**(1), p. 63-71.

[53] KUBÍK, M. and J. GOLDASZ. 2019. Multiphysics Model of an MR Damper including Magnetic Hysteresis. *Shock and vibration* [online]. LONDON: Hindawi, 2019, 1-20.

[54] STRECKER, Zbynek, Jakub ROUPEC, Ivan MAZUREK, Ondrej MACHACEK, Michal KUBIK a Milan KLAPKA. Design of magnetorheological damper with short time response. *Journal of Intelligent Material Systems and Structures*. 2015, **26**(14), 1951–1958.

[55] KUBÍK, M., O. MACHÁČEK, Z. STRECKER, J. ROUPEC a I. MAZŮREK. Design and testing of magnetorheological valve with fast force response time and great dynamic force range. *Smart Materials and Structures*. 2017, roč. 26, č. 4.

[56] WU, Guangbin, Zhimin FENG, GANG ZHANG a Zhenning HOU. Experimental study on response time of magnetorheological damper. In: *International Conference on Artificial Intelligence, Management Science and Electronic Commerce*. B.m.: IEEE, 2011, 3968–3972.

[57] MAAS, Jürgen and Dirk GÜTH. 2011. Experimental Investigation of the Transient Behavior of MR Fluids. In: *ASME 2011 Conference on Smart Materials, Adaptive Structures and Intelligent Systems, SMASIS 2011* [online]. ASMEDC, **1**, p. 229-238.

[58] KOO, Jeong Hoi, Fernando D. GONCALVES a Mehdi AHMADIAN. A comprehensive analysis of the response time of MR dampers. *Smart Materials and Structures*. 2006, **15**(2), 351–358.

[59] STRECKER, Zbyněk, Michal KUBIK, Petr VITEK, Jakub ROUPEC, David PALOUŠEK a Vit ŠREIBR. Structured magnetic circuit for magnetorheological damper made by selective laser melting technology. *Smart Materials and Structures*. 2019, **28**(5).

[60] LEE, Tae-Hoon a Seung-Bok CHOI. On the response time of a new permanent magnet based magnetorheological damper: experimental investigation. *Smart Materials and Structures*. 2019, **28**(1), 14001.

[61] STRECKER, Zbyněk, Ivan MAZŮREK, Jakub ROUPEC a Milan KLAPKA. Influence of MR damper response time on semiactive suspension control efficiency. *Meccanica*. 2015, **50**(8), 1949–1959.

[62] YANG, Baokun, Jinglin LUO a Longlei DONG. Magnetic circuit FEM analysis and optimum design for MR damper. *International Journal of Applied Electromagnetics and Mechanics*. 2010, **33**(1–2), 207–216.

[63] ZHU, Xiaohua a Chunlin LAI. Design and performance analysis of a magnetorheological fluid damper for drillstring. *International Journal of Applied Electromagnetics and Mechanics*. 2012, **40**(1), 67–83.

[64] NGUYEN, Quoc Hung a Seung Bok CHOI. Optimal design of MR shock absorber and application to vehicle suspension. *Smart Materials and Structures*. 2009, **18**(3).

[65] ŽÁČEK, Jiří, Karel ŠEBESTA, Housam MOHAMMAD, Filip JENIŠ, Zbyněk STRECKER a Michal KUBÍK. Experimental Evaluation of Modified Groundhook Car Suspension with Fast Magnetorheological Damper. *Actuators*. 2022, **11**(354).

[66] JEYASENTHIL, R., Dal Seong YOON a Senug Bok CHOI. Response time effect of magnetorheological dampers in a semi-active vehicle suspension system: Performance assessment with quantitative feedback theory. *Smart Materials and Structures*. 2019, **28**(5).

[67] YOON, Dal Seong, Yu Jin PARK a Seung Bok CHOI. An eddy current effect on the response time of a magnetorheological damper: Analysis and experimental validation. *Mechanical Systems and Signal Processing*. 2019, **127**, 136–158.

[68] MACHÁČEK, Ondřej, Michal KUBÍK, Zbyněk STRECKER, Jakub ROUPEC a Ivan MAZŮREK. Design of a frictionless magnetorheological damper with a high dynamic force range. *Advances in Mechanical Engineering*. 2019, **11**(3), 1–8.

[69] LEE, Sen Yung a Yung Chang CHENG. Hunting stability analysis of high-speed railway vehicle trucks on tangent tracks. *Journal of Sound and Vibration*. 2005, **282**(3–5), 881–898.

[70] ZELENKA, Jaromír, T MICHÁLEK a M KOHOUT. Comparative simulations of guiding behaviour of an electric locomotive. In: *20th International Conference Engineering Mechanics 2014*. 2014, 740–743.

[71] FOTOUHI, Abbas a Aghil YOUSEFI-KOMA. Semi-active train bogie suspension using skyhook dampers. In: *The Thirteenth International Congres on Sound and Vibration*. 2006.

[72] LEE, Hwan Soo a Seung Bok CHOI. Control and response characteristics of a magneto-rheological fluid damper for passenger vehicles. *Journal of Intelligent Material Systems and Structures*. 2000, **11**(1), 80–87.

[73] MISSELHORN, W. E., N. J. THERON a P. S. ELS. Investigation of hardware-in-the-loop for use in suspension development. *Vehicle System Dynamics*. 2006, **44**(1), 65–81.

[74] KWAK, Moon K., Jae Ha LEE, Dong Ho YANG a Won Hee YOU. Hardware-in-the-loop simulation experiment for semi-active vibration control of lateral vibrations of railway vehicle by magneto-rheological fluid damper. *Vehicle System Dynamics*. 2014, **52**(7), 891–908.

[75] OH, Ye Jun, Jae Kwang LEE, Huai Cong LIU, Sooyoung CHO, Ju LEE a Ho Joon LEE. Hardware-in-the-Loop Simulation for Active Control of Tramcars with Independently Rotating Wheels. *IEEE Access*. 2019, **7**, 71252–71261.

[76] STRECKER, Z., J. ROUPEC, I. MAZŮREK a M. KLAPKA. Limiting factors of the response time of the magnetorheological damper. *International Journal of Applied Electromagnetics and Mechanics*. 2015, **47**(2), 541–550.

[77] *Eddy Current*. 2023. [accesed. 2023-12-20] Available at: https://www.sciencefacts.net/eddy-current.html

[78] FIORILLO, Fausto, Cinzia BEATRICE, Oriano BOTTAUSCIO a Enrico CARMI. Eddy-current losses in Mn-Zn ferrites. *IEEE Transactions on Magnetics*. 2014, **50**(1).

[79] POŠKOVIĆ, Emir, Fausto FRANCHINI a Luca FERRARIS. Effect of the Insulating Layer on the Properties of SMC Inductors. *Applied Sciences (Switzerland)*. 2022, **12**(17).

[80] BHALLA, Deepak, DK. SINGH, Swati SINGH a Dipti SETH. Material Processing Technology for Soft Ferrites Manufacturing. *American Journal of Materials Science*. 2013, **2**(6), 165–170.

[81] SHOKROLLAHI, H. The magnetic and structural properties of the most important alloys of iron produced by mechanical alloying. *Materials and Design*. 2009, **30**(9), 3374–3387.

[82] SHOKROLLAHI, H. a K. JANGHORBAN. Soft magnetic composite materials (SMCs). *Journal of Materials Processing Technology*. 2007, **189**(1–3), 1–12.

[83] STRECKER, Zbyněk, Jakub ROUPEC, Ivan MAZŮREK, Ondřej MACHÁČEK a Michal KUBÍK. Influence of response time of magnetorheological valve in Skyhook controlled three-parameter damping system. *Advances in Mechanical Engineering*. 2018, **10**(11), 1–8.

[84] FEELEY, Joseph J. A simple dynamic model for eddy currents in a magnetic actuator. *IEEE Transactions on Magnetics*. 1996, **32**(2), 453–458.

[85] HECK, Carl. *Magnetic Materials and their Applications*. London, UK: Butterworth, 1974.

[86] MUKERJI, S. K., M. GEORGE, M. B. RAMAMURTHY a K. ASADUZZAMAN. Eddy currents in laminated rectangular cores. *Progress in Electromagnetics Research*. 2008, **83**, 435–445.

[87] KOSTAMO, Esa, Jari KOSTAMO, Jyrki KAJASTE a Matti PIETOLA. Magnetorheological valve in servo applications. In: *Journal of Intelligent Material Systems and Structures*. 2012, 1001–1010.

[88] GOŁDASZ, Janusz. Electro-mechanical analysis of a magnetorheological damper with electrical steel laminations. *Przeglad Elektrotechniczny*. 2013, **89** (2A), 8–12.

[89] OMEKANDA, Avoki M., Thomas W. NEHL, Chandra S. NAMUDURI a Suresh GOPALAKRISHNAN. Electromagnetic Actuator Structure. U.S. Patent 10480674B2. 2015.

[90] BOESE, Holger a Johannes EHRLICH. Performance of magnetorheological fluids in a novel damper with excellent fail-safe behavior. *Journal of Intelligent Material Systems and Structures*. 2010, **21**(15), 1537–1542.

[91] ZHANG, H. H., C. R. LIAO, M. YU a S. L. HUANG. A study of an inner bypass magneto-rheological damper with magnetic bias. *Smart Materials and Structures*. 2007, **16**(5).

[92] XIAO, Ping, Hong GAO a Limin NIU. Research on magnetorheological damper suspension with permanent magnet and magnetic valve based on developed FOA-optimal control algorithm. *Journal of Mechanical Science and Technology*. 2017, **31**(7), 3109–3119.

[93] YAN, Wei-ming, Jin-bao JI, Bin DONG and Hui-juan GE. Theoretical and experimental studies on a new reversible magnetorheological damper. *Structural control and health monitoring*. 2011, **18**(1), 1-19.

[94] DU, Chengbin, Faxue WAN a Guojun YU. A magnetic flux leakage study of a self-decoupling magnetorheological damper. *Smart Materials and Structures*. 2011, **20**(6).

[95] BÖSE, Holger a Johannes EHRLICH. Magnetorheological dampers with various designs of hybrid magnetic circuits. *Journal of Intelligent Material Systems and Structures*. 2012, **23**(9), 979–987.

[96] SAPINSKI, Bogdan. Magnetorheological fluid damper with radially shaped gap and contact less sealing. *Journal of Theoretical and Applied Mechanics*. 2005, **43**(3), 223-240.

[97] ALLAUDDIN, Ansar, Deepak RAJENDRA a S N JALWADI. Performance Analysis of Skyhook , Groundhook and Hybrid Control Strategies on Semiactive Suspension System. *International Journal of Current Engineering and Technology*. 2014, Special Issue-3, 7–10.

[98] KARNOPP, D., M. J. CROSBY a R. A. HARWOOD. Vibration Control Using Semi-Active Force Generators. *Journal of Engineering for Industry*. 1974, **96**(2), 619.

[99] SAMMIER, Damien, Olivier SENAME a Luc DUGARD. Skyhook and H∞ control of semi-active suspensions: Some practical aspects. *Vehicle System Dynamics*. 2003, **39**(4), 279–308.

[100] ZINDULKA, M., Z. STRECKER a F. JENIŠ. Semiactive Seat Suspension for Agricultural Machines. *Engineering Mechanics 2020*. 2020, 26, 548–551.

[101] POUSSOT-VASSAL, Charles, Cristiano SPELTA, O. SENAME, S. M. SAVARESI a L. DUGARD. *Survey on some automotive semi-active suspension control methods: A comparative study on a single-corner model*. B.m.: IFAC, 2011.

[102] AHMADIAN, Mehdi, Fernando D. GONCALVES a Corina SANDU. An experimental analysis of suitability of various semiactive control methods for magneto-rheological vehicle suspensions. *Smart Structures and Materials 2005: Damping and Isolation*. 2005, **5760**, s. 208–216.

[103] SAVARESI, Sergio M., Enrico SILANI a Sergio BITTANTI. Acceleration-Driven-Damper (ADD): An optimal control algorithm for comfort-oriented semiactive suspensions. *Journal of Dynamic Systems, Measurement and Control, Transactions of the ASME*. 2005, **127**(2), 218–229.

[104] MORSELLI, Riccardo a Roberto ZANASI. Control of port Hamiltonian systems by dissipative devices and its application to improve the semi-active suspension behaviour. *Mechatronics*. 2008, **18**(7), 364–369.

[105] LIU, Y., T. P. WATERS a M. J. BRENNAN. A comparison of semi-active damping control strategies for vibration isolation of harmonic disturbances. *Journal of Sound and Vibration*. 2005, **280**(1–2), 21–39.

[106] RAMASASTRY, Dva, K V RAMANA, N Mohan RAO, SVR Siva KUMAR and T G L PRIYANKA. Analysis of Train Suspension System Using MR dampers. *IOP Conference Series: Materials Science and Engineering*. 2016, **149**(1), 12137.

[107] ALFI, Stefano, Stefano BRUNI, Egidio DI GIALLEONARDO a Alan FACCHINETTI. Active Control of Airspring Secondary Suspension for Improving Ride Comfort in Presence of Random Track Irregularity. *Journal of Mechanical Systems for Transportation and Logistics*. 2010, **3**(1), s. 143–153.

[108] KUBÍK, Michal, Zbyněk STRECKER, Filip JENIŠ, Ondřej MACHÁČEK, Matěj PŘIKRYL a Petr ŠPALEK. Magnetorheological Yaw Damper with Short Response Time for Rail- way Vehicle Bogie. In: *International Conference and Exhibition on New Actuator Systems and Applications 2021*. 2021, 373–376.

[109] GIORGETTI, A., N. BALDANZINI, M. BIASIOTTO a P. CITTI. Design and testing of a MRF rotational damper for vehicle applications. *Smart Materials and Structures*. 2010, **19**(6).

[110] MACHÁČEK, Ondřej, Michal KUBÍK a Petr NOVÁK. New method of magnetorheological damper quality evaluation. In: *ENGINEERING MECHANICS 2017*. 2017.

[111] STRECKER, Zbyněk, Filip JENIŠ, Michal KUBÍK, Ondřej MACHÁČEK a Seung Bok CHOI. Novel approaches to the design of an ultra-fast magnetorheological valve for semi-active control. *Materials*. 2021, **14**(10).

[112] JENIŠ, F, M KUBÍK, O MACHÁČEK, K ŠEBESTA a Z STRECKER. Insight into the response time of fail-safe magnetorheological damper. *Smart Materials and Structures*. 2021, **30**(1), 017004.

[113] JENIŠ, Filip, Michal KUBÍK, Tomáš MICHÁLEK, Zbyněk STRECKER, Jiří ŽÁČEK a Ivan MAZŮREK. Effect of the Magnetorheological Damper Dynamic Behaviour on the Rail Vehicle Comfort: Hardware-in-the-Loop Simulation. *Actuators*. 2023, **12**(2), s. 1–14.

[114] CEN. *Railway applications – Testing and Simulation for the acceptance of running characteristics of railway vehicles – Running behaviour and stationary tests, EN 14363:2016+A1*. 2020

[115] JENIŠ, Filip a Tomáš MICHÁLEK. The effect of semi-active control of bogie yaw dampers on the railway vehicle critical speed. In: *Proccedings of the 26th International Conference Current Problems in Rail Vehicles 2023*. Žilina: Scientific and Technical Society at the University of Žilina, 2023, 213–220.

[116] JENIŠ, Filip, Tomáš MICHÁLEK a Ivan MAZUREK. Benefit of a semi-actively controlled magnetorheological damper for a railway vehicle. In: *Proccedings of the 25th conference with international participation Current Problems in Rail Vehicles 2021*. Česká Třebová: Faculty of transport engineering University of Pardubice, 2021, 85–92.

10 LIST OF FIGURES AND TABLES

11 LIST OF ABBREVIATIONS AND SYMBOLS

ADD	Acceleration Driven Damping
ADD-2	two-states Acceleration Driven Damping
ADD-L	Acceleration Driven Damping linear
B-H	magnetic flux density (B) – magnetising force (H) (curve)
B-I	magnetic flux density (B) – electric current (I) (curve)
CDC	Continuously Damping Control
C.U.	control unit
DoF	degree of freedom
DCC	dynamic chassis control
FE	finite elements
FEA	finite elements analysis
FEM	finite elements method
FFT	fast fourier transform
F-v	force-velocity (curve)
F-v-I	force-velocity-current (map)
HILS	Hardware-in-the-loop simulation
LPV	linear parameter-varying (control)
LQG	linear–quadratic–Gaussian
LQR	linear-quadratic regulator
MCP	model predictive control
Mix-SH-ADD	Mix of Skyhook and ADD algorithms
MR	magnetorheological
MRF	magnetorheological fluid
PSD	power spectral density
PWM	pulse width modulation
RMS	root mean square
S/A	semi-active
SH-2	two-states Skyhook
SH-L	Skyhook linear
SJKV	simulation of a railway vehicle run
SLM	selective laser melting
SMC	Soft Magnetic Composites

2D		two dimensional
3D		three dimensional

a_2	[ms^{-2}]	sprung mass acceleration
a_1	[ms^{-2}]	excitation acceleration
$v_2 - v_1$	[ms^{-1}]	damper piston velocity
w	[m]	excitation displacement
x_1, q_1	[m]	unsprung mass displacement
x_2, q_2	[m]	sprung mass displacement
$\dot{x}_1$	[ms^{-1}]	unsprung mass velocity
$\dot{x}_2$	[ms^{-1}]	sprung mass velocity
$\ddot{x}_1$	[ms^{-2}]	unsprung mass acceleration
$\ddot{x}_2$	[ms^{-2}]	sprung mass acceleration
y_i, y_0	[m]	wheelset lateral displacement
y_t, y_1	[m]	bogie lateral displacement
y_2	[m]	carbody lateral displacement
$\dot{y}_1$, V_{bogie}	[ms^{-1}]	bogie frame lateral velocity
$\dot{y}_2$, V_{body}	[ms^{-1}]	carbody lateral velocity
V_{rel}	[ms^{-1}]	relative velocity between body and bogie
$\ddot{y}_2$	[ms^{-2}]	carbody lateral acceleration
z_i	[m]	wheelset vertical displacement
φ_i	[rad]	wheelset roll angle
ψ_i	[rad]	wheelset yaw angle
ψ_t	[rad]	bogie yaw angle
σ_{sky}	[ms^{-1}]	Skyhook part of damping force calculation
σ_{gnd}	[ms^{-1}]	Groundhook part of damping force calculation

b	[Nsm^{-1}]	damping coefficient
b_{max}	[Nsm^{-1}]	maximal damping coefficient
b_{min}	[Nsm^{-1}]	minimal damping coefficient
c_1	[Nsm^{-1}]	wheelset-bogie frame bond damping
C_{body}	[Nsm^{-1}]	damping coefficient for body-based Skyhook
C_{bogie}	[Nsm^{-1}]	damping coefficient for bogie-based Skyhook

dr, DR	[-]	damper dynamic force range
$F(v)$	[N]	damping force
F_{mr}	[N]	force of MR damper
$F_{max}(v)$	[N]	damping force at a current of I_{max}
$F_{min}(v)$	[N]	damping force at a current of I_{min}
$F_0(v)$	[N]	force at $t = 0$
$F_1(v)$	[N]	desired force for the given velocity and current
F_{tu}	[MPa]	ultimate tensile strength
k	[Nm^{-1}]	sprung stiffness
k_1	[Nm^{-1}]	wheelset-bogie frame bond stiffness
k_2	[Nm^{-1}]	bogie frame-carbody bond stiffness
m	[kg]	sprung mass weight
m_1	[kg]	half bogie frame weight
m_2	[kg]	quarter carbody weight
α	[-]	$\alpha \in [0,1]$, tuning parameter
f	[Hz]	frequency
t	[s]	time from the change of the control signal
T_c	[ms]	time of the final value of the electric current reaching
T_p	[ms]	primary response time
T_s	[ms]	secondary response time
τ	[ms]	time constant, response time, artificial current response time
τ_{63}	[ms]	time constant, primary response time for MR damper force rise
τ_{90}	[ms]	secondary response time for MR damper force rise
τ_{36}	[ms]	time constant, primary response time for damper force drop
τ_{10}	[ms]	secondary response time for MR damper force drop
B	[T]	magnetic flux density
B_{coil}	[T]	magnetic flux density caused by coil
B_{fail}	[T]	magnetic flux density in fail-safe mode
B_{mag}	[T]	magnetic flux density caused by a permanent magnet
B_{max}	[T]	maximal magnetic flux density
B_{min}	[T]	minimal magnetic flux density
B_r	[T]	remanence

H	[Am^{-1}]	magnetic field intensity
H_c	[Am^{-1}]	coercivity
I	[A]	electric current
I_{max}	[A]	maximal electric current
I_{min}	[A]	minimal electric current
I_0	[A]	electric current at t = 0
I_1	[A]	desired current
L	[mH]	coil inductance in the damper electric circuit
R	[Ω]	electrical resistance
σ	[MSm^{-1}]	electrical conductivity
ρ	[Ωm]	electrical resistivity
μ	[Hm^{-1}]	permeability
μ_r	[-]	relative permeability

www.ustavkonstruovani.cz